Japanese Journal of
Applied Physics

PROGRESS REVIEW • OPEN ACCESS

Science-based, data-driven developments in plasma processing for material synthesis and device-integration technologies

To cite this article: Makoto Kambara *et al* 2023 *Jpn. J. Appl. Phys.* **62** SA0803

View the article online for updates and enhancements.

You may also like

- Evaluation of garden functions of SMAN 2 Lubuk Basung as science-based education park
Afrinaldi and H Rifai

- The 2022 Plasma Roadmap: low temperature plasma science and technology
I Adamovich, S Agarwal, E Ahedo et al.

- Functional nitrogen science based on plasma processing: quantum devices, photocatalysts and activation of plant defense and immune systems
Toshiro Kaneko, Hiromitsu Kato, Hideaki Yamada et al.

UNITED THROUGH SCIENCE & TECHNOLOGY

ECS The Electrochemical Society
Advancing solid state & electrochemical science & technology

248th
ECS Meeting
Chicago, IL
October 12-16, 2025
Hilton Chicago

Science + Technology + YOU!

SUBMIT ABSTRACTS by March 28, 2025

SUBMIT NOW

This content was downloaded from IP address 194.95.157.29 on 23/01/2025 at 09:11

OPEN ACCESS

Japanese Journal of Applied Physics **62**, SA0803 (2023) **PROGRESS REVIEW**
https://doi.org/10.35848/1347-4065/ac9189

Science-based, data-driven developments in plasma processing for material synthesis and device-integration technologies

Makoto Kambara[1], Satoru Kawaguchi[2], Hae June Lee[3], Kazumasa Ikuse[4], Satoshi Hamaguchi[4], Takeshi Ohmori[5], and Kenji Ishikawa[6*]

[1]*Department of Materials and Manufacturing Science, Osaka University, Suita, Osaka 565-0871 Japan*
[2]*Division of Information and Electronic Engineering, Graduate School of Engineering, Muroran Institute of Technology, Muroran, Hokkaido 050-8585, Japan*
[3]*Department of Electrical Engineering, Pusan National University, Busan 46241, Republic of Korea*
[4]*Center for Atomic and Molecular Technologies, Osaka University, Suita, Osaka 565-0871 Japan*
[5]*Center for Digital Services, Research & Development Group, Hitachi, Ltd., Kokubunji, Tokyo 185-8601 Japan*
[6]*Center for Low-temperature Plasma Sciences, Nagoya University, Nagoya 464-8601 Japan*

[*]E-mail: ishikawa.kenji@nagoya-u.jp

Received June 5, 2022; revised August 17, 2022; accepted September 13, 2022; published online November 30, 2022

Low-temperature plasma-processing technologies are essential for material synthesis and device fabrication. Not only the utilization but also the development of plasma-related products and services requires an understanding of the multiscale hierarchies of complex behaviors of plasma-related phenomena, including plasma generation in physics and chemistry, transport of energy and mass through the sheath region, and morphology- and geometry-dependent surface reactions. Low-temperature plasma science and technology play a pivotal role in the exploration of new applications and in the development and control of plasma-processing methods. Presently, science-based and data-driven approaches to control systems are progressing with the state-of-the-art deep learning, machine learning, and artificial intelligence. In this review, researchers in material science and plasma processing, review and discuss the requirements and challenges of research and development in these fields. In particular, the prediction of plasma parameters and the discovery of processing recipes are asserted by outlining the emerging science-based, data-driven approaches, which are called plasma informatics. © 2022 The Author(s). Published on behalf of The Japan Society of Applied Physics by IOP Publishing Ltd

Abbreviations

0D, 1D, 2D, 3D	0, 1, 2, 3-dimensional
AC	alternative current
AI	artificial intelligence
AL	active learning
ALD	atomic layer deposition
ALE	atomic layer etching
ANN	artificial neural network
APC	advanced process control
APPJ	atmospheric pressure plasma jet
APS	atmospheric pressure spray
BE	Boltzmann equation
CCP or E-mode	capacitively coupled plasma
CD	critical dimension
CFD	computational fluid dynamics
CNN	convolutional neural networks
CVD	chemical vapor deposition
DC	direct current
DFT	density functional theory
DNN	deep neural network
DNS	direct numerical solution
EEDF	electron energy distribution function
EFR	electric field reversal
ELM	extreme learning machine
EVDF	electron velocity distribution function
FDC	fault detection classification
HAR	high-apect-ratio
HVAF	high velocity jets with air fuel
HVOF	high velocity jets with oxygen fuel
ICP or H-mode	inductively coupled plasma
MC	Monte Carlo
MD	molecular dynamics
MHD	magneto-hydro-dynamics
ML	machine learning
MPC	model predictive control
OES	optical emission spectroscopy
PDE	partial differential equation
PFI	particle flux imaging
PIC	particle-in-cell
PINN	physics-informed neural network
PVD	physical vapor deposition
R2R	run-to-run
RbR	run-by-run
RF	radio frequency
RL	reinforcement learning
RNN	recurrent neural network
SEM	scanning electron microscopy
SHAP	Shapley additive explanation value
SLFN	single hidden layer feed-forward neural network
SPC	statistical process control
SVID	status variable identification
SVM	support vector machine
Te	electron temperature
VM	virtual methodology or metrology

Content from this work may be used under the terms of the Creative Commons Attribution 4.0 license. Any further distribution of this work must maintain attribution to the author(s) and the title of the work, journal citation and DOI.
© 2022 The Author(s). Published on behalf of The Japan Society of Applied Physics by IOP Publishing Ltd

1. Introduction

Low-temperature, plasma-processing technologies are essential for material synthesis and device fabrication.[1,2] Plasma is a unique state-of matter that is ionized by the application of electromagnetic energy. Ionized fluids consist of electrons, positive and negative ions, chemically reactive atoms and molecules, radicals, and excited states. Electrons are sustained as energetic owing to the acceleration resulting from externally applied electromagnetic forces. As energetic electrons collide with neutrals, they induce electron collision reactions, such as ionization, excitation, dissociation, and attachment. When the frequency of collisions is sufficiently small, a low temperature is generated. Frequent collisions lead to a different mode of thermal arc discharges. Given the reactivity of these plasmas, their applications, particularly in plasma electronics, have been steadily increasing. Both thermal and nonthermal plasmas are useful in various technical fields (e.g. electronics, energy, environment, agriculture and aquaculture, life sciences, and medicine)[3] (Fig. 1).

Typically, low-temperature plasma is processed in a chamber used as a reactor that is isolated to control the reaction field independently in an unregulated environment. Plasma generates reactive species, which are transported towards the target substrate placed in the chamber. At the boundary or surface in contact with the plasma, material synthesis and etching fabrication are enabled through plasma-surface interactions. Problems arise in the results of these complex interactions. Discovery and optimization of the best recipe are difficult processes. Recently, the machine learning (ML) technique for data analysis enables us to optimize processing recipes and discover the best one. In future, it will be possible to achieve optimization using a virtual methodology and plasma informatics (Fig. 2).

Herein, we review the recent progress in the field of plasma processing for material synthesis, film deposition, and etching nanofabrication, focusing on science-based research and data-driven approaches (Fig. 3). Computing power has increased significantly, and informatics has developed ever since information technologies, such as ML, deep learning, and data-driven science, were first applied extensively in plasma processing.[4,5] Section 2 provides the background for this review. The plasma-processing system comprises the hierarchies of plasma, sheath, and surface of the substrate, and the problems in each region, interface, and system are highlighted. The comprehensive construction of a model that can represent the nonlinearity of the group of equations and the nonequilibrium dynamics of the behavior is underdeveloped owing to its complexity. State-of-the-art technology allows for multiscale simulations that integrate the three domains of plasma, sheath, and surface. Currently, the process is being automatically controlled using a data-driven approach, and novel controllers are being developed. In Sect. 3, we introduce the new concept of plasma informatics and briefly examine its basic concepts, such as isolation and regression of data, prediction and presumption, and kernel-based and neural networks. In Sect. 4, we discuss plasma as an electromagnetic fluid and its fundamental governing equation, the Boltzmann equation (BE). Attempts have been made to solve the complex ensembles of electrodynamic behaviors by applying various ML techniques. In Sect. 5, we review the progress in computational simulations of micro- and nano-sized particle syntheses in plasma. The complex coupling between plasma fluidity and heterogeneity related to geometric surfaces, such as particles, mists, and bubbles, are treated using multi-scale approaches. In Sect. 6, we review the progress in solving the plasma-surface interaction problem. Plasma-enhanced film deposition and plasma etching technologies are discussed in this paper. In particular, to discuss the morphology, topography, and feature profiles, we must consider the trajectories and motions of energetic particles in the sheath region, which appear between the plasma and surface. Moreover, industrial applications are reviewed with examples of image processing for plasma etching. In Sect. 7, we envision future innovations in the development of plasma processing, data-driven plasma

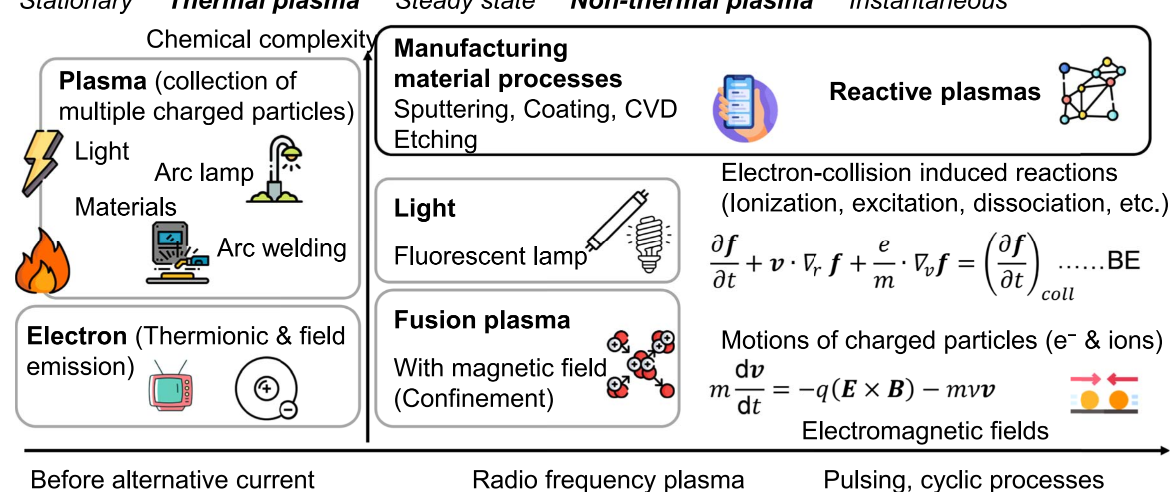

Fig. 1. (Color online) Application fields of plasma technologies. Thermionic emission generates liberated electrons from an electrode. Gaseous discharges produce sources of light and heat. Vacuum and radio frequency power technologies realized various material processing as well as fusion plasma. The major difference in reactive plasma is chemical complexity, which is caused by electron collisions and secondary processes and is recognized on long time scales.

© 2022 The Author(s). Published on behalf of The Japan Society of Applied Physics by IOP Publishing Ltd

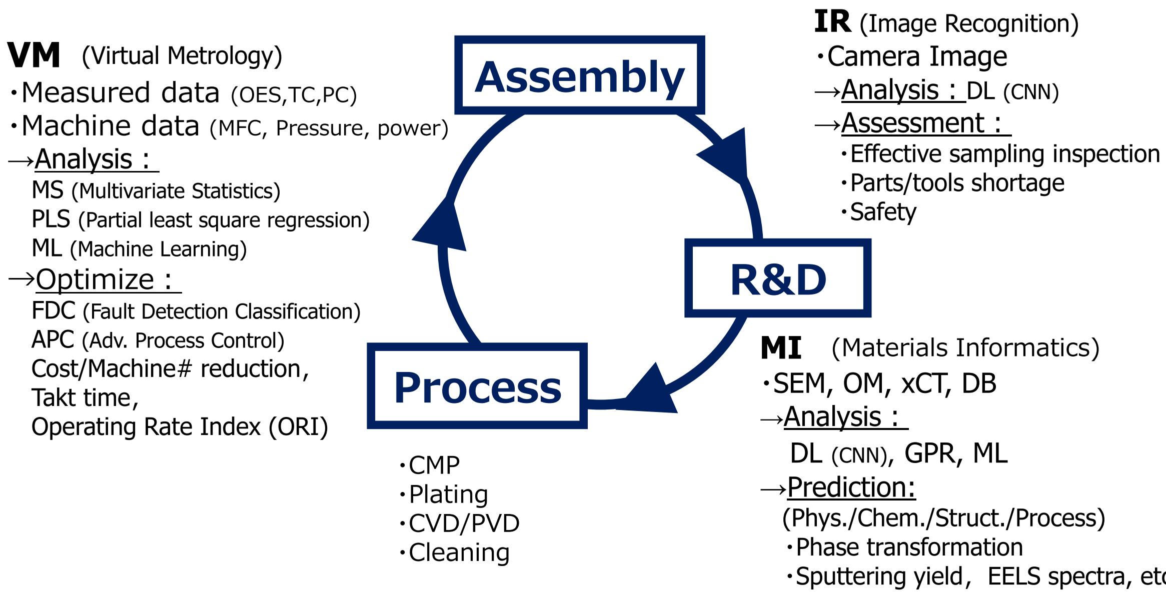

Fig. 2. (Color online) Overview of the data-driven innovation of plasma processing technologies. Research and development (R&D) is the work for creation of products and services. In the process of marketing and launching them, it needs to assemble and integrate huge number of individually and/or interrelated elemental technologies. The goal of this assembly is to optimize under a number of constraints. This complex loop of R&D, process, and assembly must be cycled with robust feedback, without arbitrary decisions. Therefore, the topical trends of smart manufacturing and digital transformation are gaining attention to solve this requirement through analysis, optimization, assessment, and prediction.

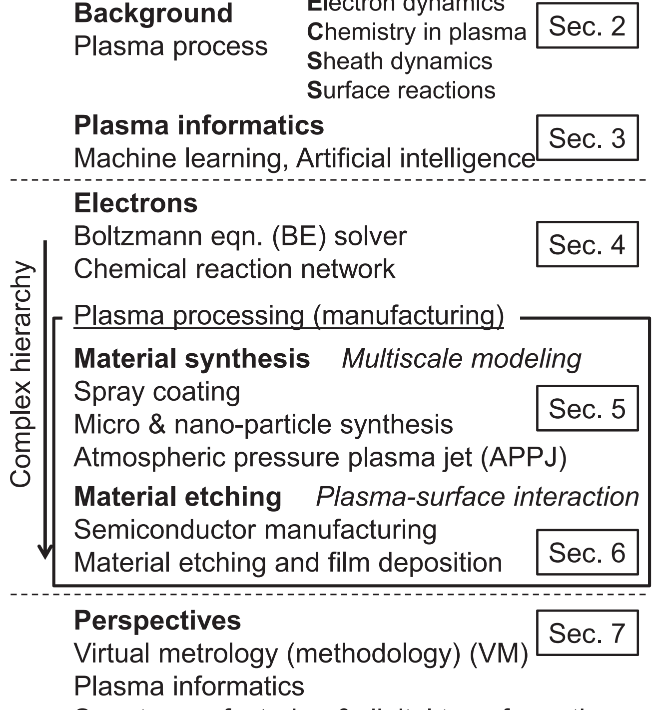

Fig. 3. Overview of this review. This review covers technological areas of low-temperature plasma processing.

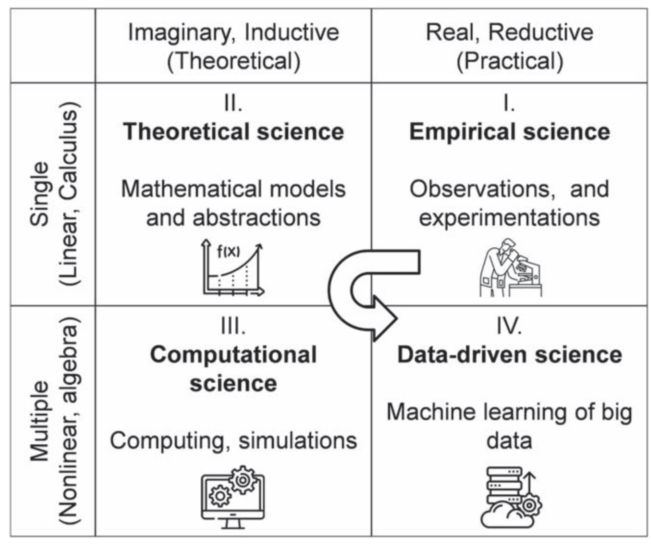

Fig. 4. Development of science over the centuries. The fourth paradigm is the data-driven science.[7]

science, and plasma informatics in all the phases of research and development, process, and assembly.

2. Background

Herein, we introduce the background of the plasma processing technology. Plasma-related phenomena have been clarified by leading-edge measurements and modeled using theoretical equations developed in the modern physics and chemistry disciplines. We attempted to solve the complexity of plasma phenomena using reductionism approaches. The rebuilding of each science field is expected to achieve success in modeling the hierarchy of plasma processes. There is room for improvement from the conclusion; thus, data-driven approaches should be considered. Before starting the main topic, we reviewed the recent developments in science-based plasma diagnostic research. This section comprises reviews on the measurement of bulk plasma properties and multiscale plasma reactor simulations. Feature profiles and plasma-induced damage are also noted.

© 2022 The Author(s). Published on behalf of The Japan Society of Applied Physics by IOP Publishing Ltd

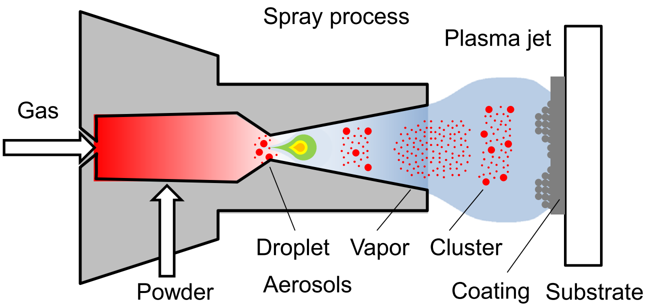

Fig. 5. (Color online) Schematic illustration of spray coating. Inert gas flows with high speed and powder accelerates toward downstream. The flowing gas is reached to temperature of up to 1000 °C. The powder is melted and vaporized and then spray particles and clusters are directed and coated on the substrate. Spray clusters passing through the De Laval nozzle are injected outward from the nozzle throat at supersonic speeds.

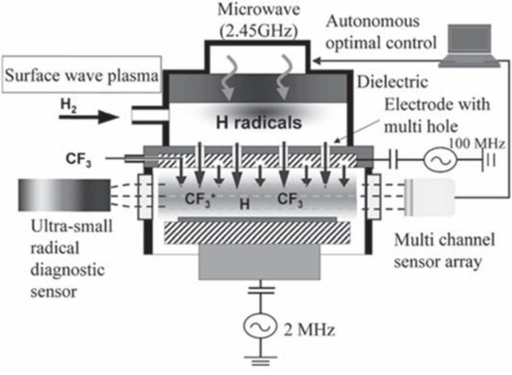

Fig. 6. Schematic diagram of autonomous nano-process system with radical injection [Reprinted from M. Hiramatsu, J. Plasma Fusion Res. 81, 669 (2005).[20]].

2.1. Brief description of development of science

In the development of science over the centuries (Fig. 4), empirical science has been developed along the lines of observations. The purely experimental approach has moved the realm of theoretical models and formulated generalizations. The laws can be described by mathematical equations. Overcoming the limitations of analytical equations, the computational approach has facilitated the simulations of complex phenomena based on theoretical models. Developing from the previous paradigms, today huge amounts of data are being generated by experiments and simulations. In response to such big data, a new approach called as data-driven science has emerged in informatics.[6] To enable the timely discovery and deployment of scientific knowledge now, we will provide an overview of the science and technology to understand and control the dynamics of plasma processes in real time.

As shown in Fig. 1, manufacturing material-processing, such as film deposition and etching materials, are now used plasma technologies. Regardless of substrate temperature, electron-collision-induced chemistry of ions and radicals enables us to coat and etch films, and to modify surface properties of fragilely functional materials. For examples, nitrogen molecule is inert and no thermal process with a use of nitrogen gas can carry out. On the contrary, electrical discharges of nitrogen gas can produce a rich chemistry. In situ plasma functionalization with the creation of ammonia and nitric acids from water nitrogen plasma has attracted much attention for building a circular economy.[8,9]

2.2. Plasma processing in spray coating

For a long period of time, conventional thermal plasma was used for all types of coating[10] (Fig. 5). Recent spray coatings has expanded from thermal spraying to cold spraying to high velocity jets with oxygen fuel (HVOF) and air fuel (HVAF).[11–13] The coating processes of deposition of powdery metals or compounds should be controlled by a total of 500 or more of all dependent variables.[14–16] Using the variables as a black box, a ML approach is used to calculate the porosity, macrostructure, and mechanical properties of the coating films as targets. There are functional coatings as well as mechanical coatings. Elementary processes are important to understand through calculations based on temperature and velocity of molten powdery particles.

2.3. Plasma processing in semiconductor manufacturing

As exemplified in semiconductor manufacturing, optimization cannot always be achieved through trial and error. Cost reduction and simplification are expected to be obtained in virtual experiments that require numerical computations based on theories and stored fundamental datasets.[17]

Automation of plasma processing has been addressed for a long time. Statistical process control (SPC) was developed in the 1980s[18] and was based on the design of experiments proposed by Taguchi.[19] In 2005, Hiramatsu and Hori argued that behaviors of radicals in plasma should be constantly monitored and controlling compositions and densities in real time[20] (Fig. 6).

The radical densities were controlled independent on source gases by the radical injection method.[21] Radical densities were monitored by optical method and substrate temperature affects radical reactions.[22] Substrate temperature is monitored by an optical interferometric method.[23] Following the monitor, feedback was applied autonomously in real time to maintain optimal plasma conditions[24] (Fig. 7). Yamamoto et al. reported that etched feature profiles were modified by a real time control of radical densities on the basis of substrate temperature change.[25] The controlling method developed that etchant radical density of H atom increased in early stage with low substrate temperature and passivation radical density of N atom increased at later stage with high substrate temperature. H and N atom densities in the H_2 and N_2 mixture plasma were monitored in real time by the vacuum ultraviolet absorption spectroscopy.[26] As reported by Suzuki et al., it was demonstrated that these densities were maintained autonomously by a feedback controller system, even when chamber wall conditions were disturbed.[27,28] To apply a plasma etching process, etched featured profiles were tailored by lateral etching amount in a trend of processing time (Fig. 8). More precise substrate temperature was controlled by feedback operated on-off sequences of plasma and bias powers.[29]

Advanced process controls (APC) have become widespread in semiconductor manufacturing. However, there is still room for improvement, and the methodology is challenging in real-time run-to-run (R2R) and run-by-run (RbR) control and in fault detection and classification (FDC). A predictive analysis can be performed through regression,

© 2022 The Author(s). Published on behalf of The Japan Society of Applied Physics by IOP Publishing Ltd

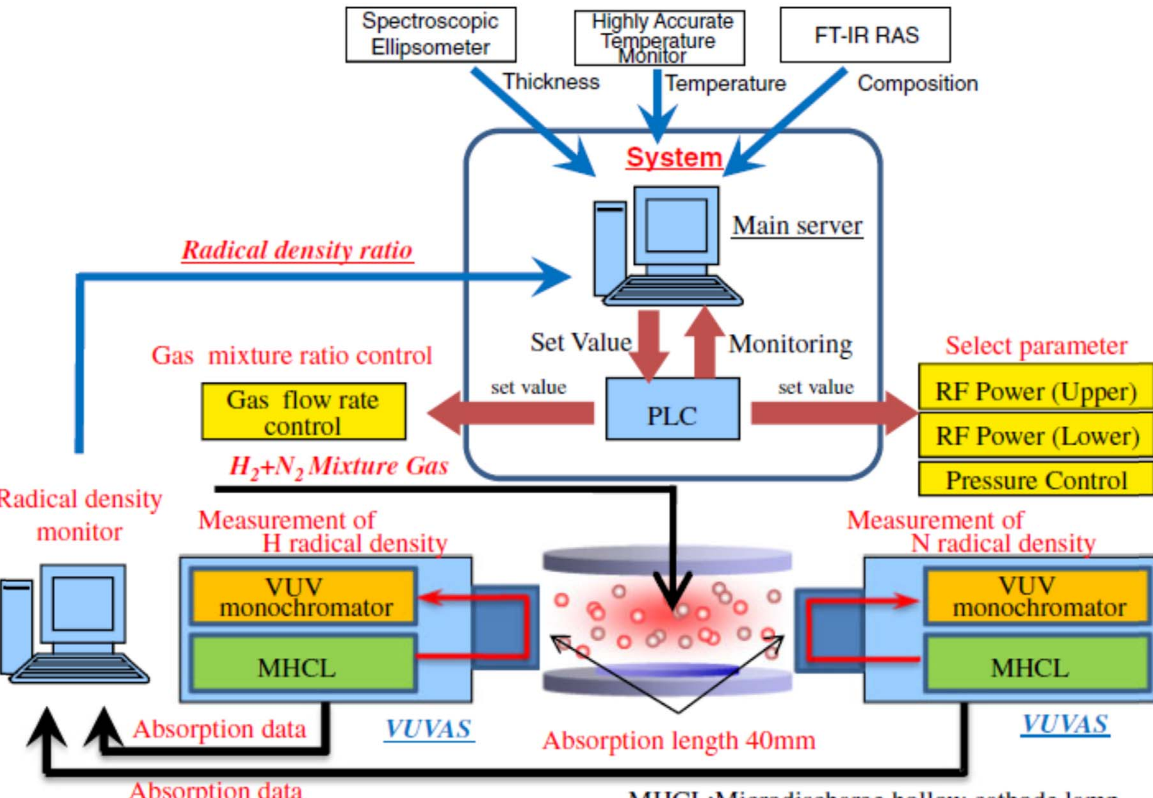

Fig. 7. (Color online) Autonomous nano-process system for plasma etching of films. Schematic diagram of feedback control system for radical density ratio H/(H + N). PLC stands for the programmable logic controller, and Fourier transformed infrared reflection absorption spectrometer (FT-IR-RAS) and vacuum ultraviolet (VUV). [Reprinted from S. Takahashi, et al. *Jpn. J. Appl. Phys.* 51, 016202 (2012).[24)]].

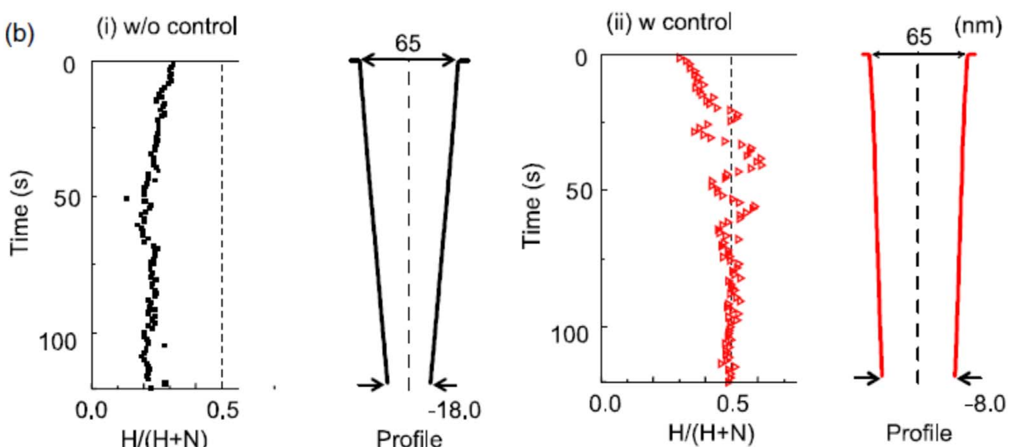

Fig. 8. (Color online) Temporal trends of measured density ratio of H and N atoms and etched feature profiles obtained with or without real time control of the radical density ratio [Reprinted from T. Suzuki et al., *J. Phys. D: Appl. Phys.* 47, 422001 (2014).[28)]].

classification, and deep learning of data for sensing and monitoring of plasma reactors (Fig. 9).

2.4. Science-based modeling hierarchies of plasma processes

To realize this, knowledge hierarchies of several levels involving areas such as plasma physics, plasma chemistry, plasma sheath, fluid dynamics, ion optics, particle-motion dynamics, surface reaction chemistry, and thermodynamics should be integrated[30)] (Fig. 10). A design of processing chamber determines structural parameters, such as processing volume and area, feeding methods of electromagnetic power, vacuum and flow of gases, temperature. First, a electromagnetic power source generates electromagnetic fields for

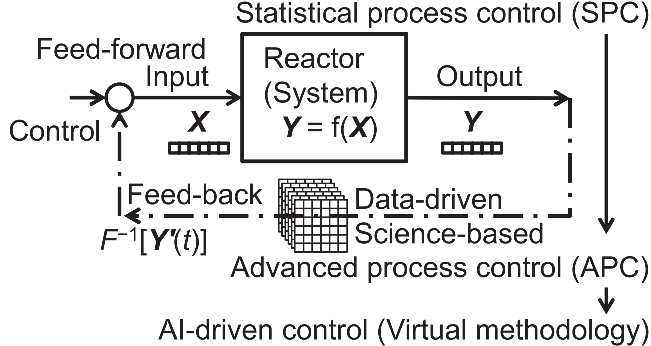

Fig. 9. The science-based, data-driven process control opens a new avenue for future innovations in low-temperature plasma processing.

© 2022 The Author(s). Published on behalf of The Japan Society of Applied Physics by IOP Publishing Ltd

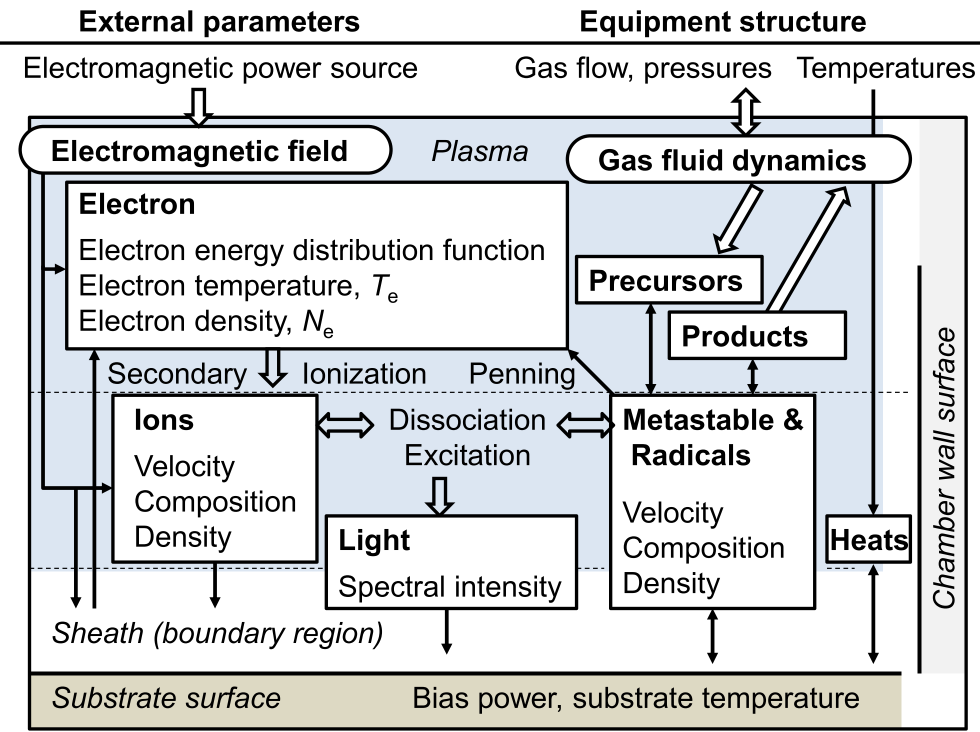

Fig. 10. (Color online) Schematic illustration of plasma processing and the equipment [Translated and modified from R. Itatani (1990).[31)]].

acceleration of electrons. The important internal parameter of a collection of electrons is electron velocity distribution function (EVDF). Second, highly energetic electron possibly induces collisional reactions with atoms and molecules, such as ionization, excitation, and dissociation. Ions, metastables, radicals, and light are produced and irradiated towards the substrate surface passing through the sheath boundary region. For positive ions, the sheath develops high electric field and then highly accelerated ions can bombard the surface with sputtering effects and secondary electron generations. Third, the by-products of precursor's reactions potentially change processing conditions. There are many key parameters for controlling processing (Fig. 11).

Plasma processes occur at the heterogeneous interface between the plasma and the surface. We consider that the "process architecture" comprises plasma, sheath, and a geometrical surface (Fig. 12).[30)] That is, the hierarchical systems of bulk plasma, sheath transport, and surface reactions are handled here.

Bulk plasma is characterized by the key parameter of the EVDF. This is formulated using the BE. However, this nonlinear equation cannot be solved analytically whenever assumptions are made regarding plasma physics and boundary conditions. More importantly, especially for low-temperature plasma, a variety of reactive species is generated from electron collision-induced reactions. Multiple particles, such as electrons, ions, and radicals in the plasma are analyzed using both plasma physics and chemistry.

The space between the plasma and surface is called plasma sheath. The sheath region also contains complex phenomena wherein plasma-generated species are transported towards the surface of the substrate, mass, and energy flow between the bulk plasma and wall boundary. In this sheath region, there is motion of the charged particles through the building electromagnetic fields.

The particles react chemically at the surface of the substrate. Electrically neutral species, such as atoms, molecules, and radicals, are adsorbed on the surface, whereas charged species (e.g. electrons, ions, and negative ions) hit the surface. The states of the surface change sequentially, and the accumulation of the adsorption and bombardment is determined recurrently in the next-stage state. That is, a nonlinear process in a nonequilibrium state occurs at the surface during contact with the plasma. Elementary surface processes are governed by physical chemistry formulations; however, no single solution can be obtained. Hence, diagnostics and monitoring of the bulk plasma, sheath, and reacting surface should be conducted in situ and in real time. In view of this hierarchy, the combinational approaches comprising the building of theory, computational modeling, and experimental monitoring play an important role in controlling the processes.

2.5. Electron behaviors in bulk plasma—Plasma physics

2.5.1. Time-averaged measurements of the parameters of bulk plasma.

The electron density in the bulk plasma can be measured using Langmuir probe.[32)] Measurement of the deposition of plasma using the Langmuir probe often fails because of the deposits on the probe surface. These deposits disturb the electrical conduction between the plasma and probe.

Invasive diagnostics of plasma properties are obtained using microwave probes.[33)] These methodologies are based on the detection of the resonant frequency of the surface-

© 2022 The Author(s). Published on behalf of The Japan Society of Applied Physics by IOP Publishing Ltd

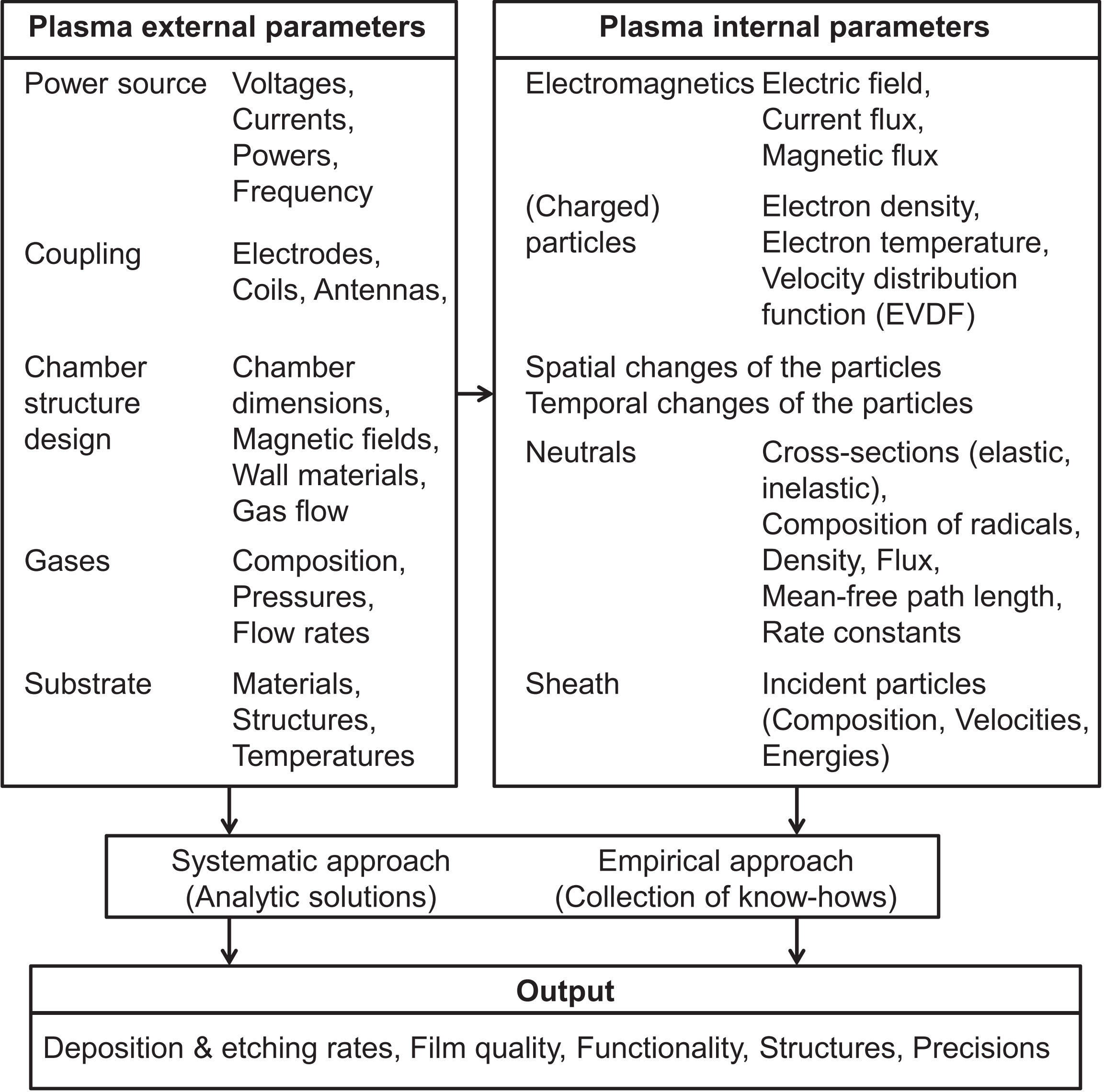

Fig. 11. Process outputs closely related with plasma external parameters and plasma internal parameters. Inelastic collisions which govern chemical reactions, such as ionization, excitation dissociation, are also coupled with behaviors of space charge potentials and charged particles. This diagram was drawn originally in the entitled article of "Well-controlled Reactive Plasma" in 1990 [Translated and modified from R. Itatani (1990).[31]].

wave component generated at the interface between the plasma and surface. Even thick micron-scale deposits are not affected to the measurements. The design of the probe has been continuously improved and is called curling probe. For instance, a double-curling probe was demonstrated[34,35] and successfully monitored in real time.[36] The curling probe was used for the measurements of the plasma thruster.[37] The hairpin resonator has also been used to measure the electron temperature.[38] The spatial distribution of plasma density in a chamber was revealed by the cutoff probe[39,40] and the surface-wave probe.[41,42]

Optical diagnostics are categorized into passive and active methodologies. The former is optical emission spectroscopy (OES), in which plasma, as a measurement target, is emitted as a light source. The latter is laser spectroscopy, in which laser light as the other light source is used for the detection of scattering and fluorescence by the excitation of species in the plasma. The electrons can be measured using laser Thomson scattering.[43] Low pressure inductively coupled plasma (ICP) discharge was measured by Thomson scattering, and its electron density was calculated using the finite element analysis method.[44] An automatic measurement of Thomson scattering was proposed.[45] The temporal variation in 2D measurements of electron density and electron temperature was reported in the case of laser-produced plasma, although it is slightly different from that in high-pressure plasma, using collective Thomson scattering with ion features.[46]

Optical emissions can be measured relatively simply and are commonly diagnosed by analysis using the collisional radiative model.[47,48] Emissions of two excitation energy levels can be drawn on an electron density and electron temperature plane; thus, a pair of density and temperature can be obtained at an intersection point on the contour plane.[49] These relationships can be stored in relation to the probe data without a physical model through ML. In actual cases, the model, as suggested by the collisional radiative model, is only an approximation. Therefore, it is more accurate to use stored data based on actual measurements, such as Thomson scattering data. Nishijima et al. reported the ML prediction of the electron density and Te of OES data acquired by a

© 2022 The Author(s). Published on behalf of The Japan Society of Applied Physics by IOP Publishing Ltd

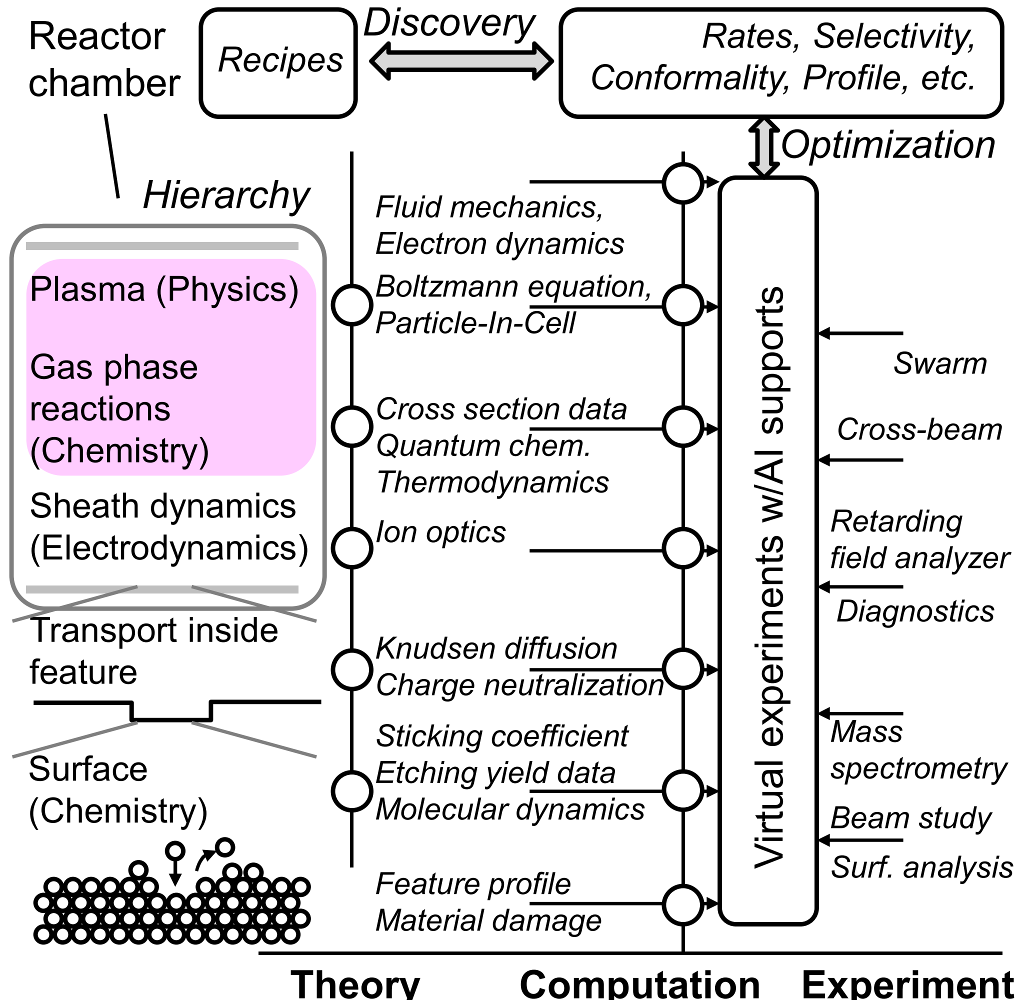

Fig. 12. (Color online) Architecture of the plasma processes and modeling hierarchies for the plasma processing reactor. Discovery of processing recipes through the combination of theory, computation, and experiments [Reprinted and modified from *Jpn. J. Appl. Phys.* (57, 06JA01, 2018).[30]].

multispectral camera.[50–53] Multiple regression of optical emissions could be applied to real-time measurements for roughing the surface during sputtering processing[54] (Fig. 13).

In past, multivariate principle component analysis and partial least squares were employed to relate the various OES signatures to etching performance, such as etch rates, uniformity, and aspect-ratio-dependent etching.[55] The highly accurate end-point detection of etching by impedance monitoring was demonstrated.[56]

2.5.2. Phase-resolved measurements of the parameters of bulk plasma. As an example of reactive plasma with electronegativity, pulsed fluorocarbon plasma is operated by turning on and off the excitation power, and a surface-wave probe was used to measure the electron density decay.[57,58] Phase-resolved OES data were analyzed by the corona model and local thermal equilibrium approximations that are satisfied by simultaneously the Boltzmann and Saha equations for to determine the plasma density and Te.[59] The plasma density in the afterglow speedily decreased within a short time of approximately 5 μs. The production of ion–ion plasmas by the effective utilization of negative ions in the afterglow phase was suggested.[59] Makabe et al. reviewed the electronegativity of reactive plasmas[60] (Fig. 14).

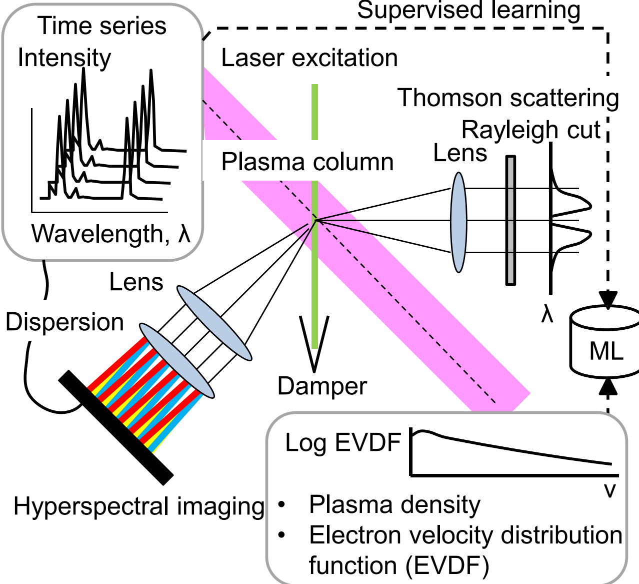

Fig. 13. (Color online) A setup of the ML prediction of electron density and temperature of optical emission spectra acquired by a hyperspectral imaging system and simultaneously the Thomson laser scattering measurement.

© 2022 The Author(s). Published on behalf of The Japan Society of Applied Physics by IOP Publishing Ltd

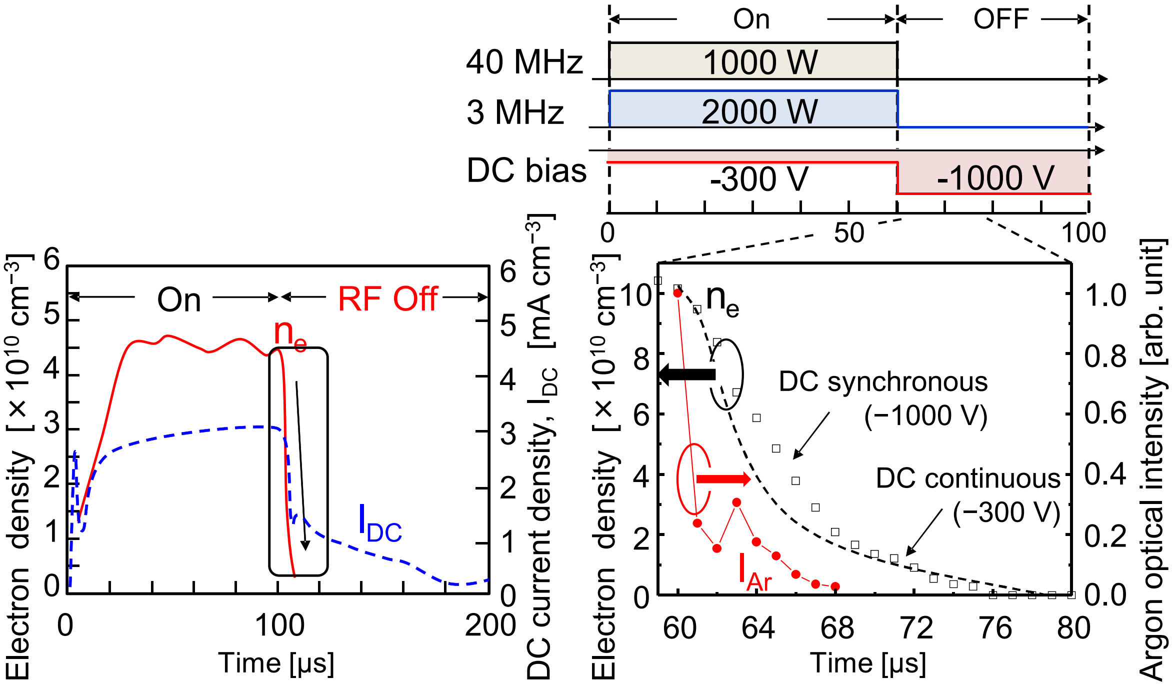

Fig. 14. (Color online) Schematic diagram of positive and negative ions from pulsed plasma with DC bias operation.[48] In pulsed plasmas, negative ions can be extracted from the bulk plasma to boundary surface applying electrical reversal potential or positive bias.[50]

In situ monitoring of plasma ignition in capacitively coupled plasma has been reported.[61] The transient behavior of pulsed electronegative plasmas has attracted considerable attention. Measurements of pulsed Ar capacitive coupled plasmas (CCPs) through phase-resolved OES showed an overshoot in the light emission intensity at the reignition of the pulsed discharge and differences in spatial emission patterns, depending on the pulse frequency. Lower frequency is exhibited in a mixture of the α heating mode and drift-ambipolar heating mode, which is ordinarily only found in electronegative discharges.[62] Electrical characteristics, such as RF current and voltage, power, and direct current (DC) bias voltage, were measured as a function of time during the reignition of pulsed Ar plasmas. The overshoot at reignition reflected the moving heating mechanisms, from stochastic heating to a combination of stochastic and ohmic heating.[63]

2.5.3. Electron heating and other mechanisms. The Te was computationally calculated when the plasma was sustained by a 5 kHz pulsed power using Ar/Cl_2 mixtures at 20 mTorr. Te spikes to a high value during a low-to-high power transition and to a low value during a high-to-low power transition, and Te reaches a quasi-steady state during both high- and low-power excitations. This is determined by the electromagnetic skin depth.[64]

The dynamics of power matching to pulsed ICPs of Ar/Cl_2 mixtures of tens of mTorr pressure using fixed-component impedance matching networks were investigated.[65] This early power coupling enables a more rapid ramp-up in the plasma density while being mismatched during the inductively coupled (H)-mode later in the pulse. The early match also produces a more energetic ion bombardment of the surfaces. Matching late in the pulse diminishes the power dissipated in the capacitively coupled (E)-mode at the cost of reducing the rate of increase in the plasma density.[65]

Another example is the measurement of microarcs by electrical detection[66] and a microwave flat cutoff probe.[67] Sensory data can be used to detect abnormalities in the plasma processing apparatus.

The ion flux uniformity and electron temperatures of the dual-antenna ICP were measured using a Langmuir probe floating by a DC blocking capacitor based on the floating harmonic method. At high pressures, electron heating occurred locally, and the ion flux uniformity was affected by the gas flow rate or gas residence time in the electron-heating region.[68]

2.6. Reactive species in bulk plasma—plasma chemistry

2.6.1. Motivation of the control of reactive species. The process results must be controlled, and the process value was controlled in a closed loop by using a sensor to maintain the set value. In the absence of a suitable sensor signal, the system is controlled based solely on independent equipment parameters in an open loop manner. At the most basic level, quality control is used by statistical process control methods to monitor and control a process.

For example, in semiconductor fabrication of ultra-large-scale integrated circuit, plasma processes are indispensable for geometrical pattern transfer and the fabrication of high-aspect-ratio (HAR) features.[69,70] For the fabrication of wires and interconnects of the device, an insulating film is deposited, and then holes and trenches are manufactured by etching uncovered areas of the film with the protection of a patterned resist mask.[71] Reactive plasma is used for etching the insulating dielectric films, such as silicon dioxide,[72] silicon nitride,[73] silicon oxyfluoride,[74] and silicon oxycarbide.[75–78] Since the late 1990s, anisotropic etching has been used for the fabrication of deep holes and trenches with dimensions narrower than 100 nm and high-aspect ratios

© 2022 The Author(s). Published on behalf of The Japan Society of Applied Physics by IOP Publishing Ltd

of more than 20.[71] In addition, the structures and functions were controlled, and material damage could be minimized.[79]

To satisfy the requirements for controlling the feature profiles and reducing damage, all levels of the plasma, sheath, and surface reactions were characterized by quantitative measurements.

2.6.2. Models of electron collision-induced reactions in bulk plasma. Reductive approaches to understand the collection of electron-collision-related reactions in plasma can be evaluated using the statistical average of all single events. Assuming the Boltzmann distribution, multivariable integration can be employed using the Monte Carlo (MC) method to solve the macroscopic behavior of the plasma system using information from microscopic elementary reactions.

The motion of an electron close to the chamber wall in a magnetized ICP was analyzed, and a counterintuitive mechanism of electron reflection was revealed.[80] Lorentz force along the RF electric field induced electron motions parallel to the sidewall. The behavior of the majority of electrons was determined by individual electrons that gained energy stochastically.[81] The azimuthal velocity of electron motion in a cylindrical chamber under an RF electric field and confronting divergent magnetic fields was simulated to evaluate the phase-resolved profiles of power deposition on electrons in a low-pressure inductively coupled magnetized plasma.[82] The average velocity of electron motion under crossed fields of alternative current (AC) electric and DC magnetic components was formulated analytically. The velocity vector draws elliptical loci with alternating electric fields. The electron transport phenomena in magnetized plasmas were explicitly described with the collision frequency, which was described as the electron collision cross-section of gases.[83] The elliptical loci for electron swarms in F_2 or Ar/CF_4 changed significantly because of the directional electron drift in inductively coupled magnetized plasmas.[84] The effects of ionization and electron attachment have shown that ionization increases the proportion of isotropic electrons and electron attachment reduces the population of scattered electrons.[85]

Breakdown data for alcohol vapors were provided by the electrical and OES data of emissions for excited OH, CH, and H atoms.[86,87] Discharges in liquid alcohol have been used in material synthesis applications, particularly of nanographene synthesis at room temperature.[88–91] The voltage and current characteristics of low-pressure, low to moderate DC current discharges in vapors of alcohols, such as methanol, ethanol, isopropanol, and n-butanol, were reported.[92] Further investigation showed that the effective ionization coefficients for the alcohol vapors were measured by breakdown voltage and emission profile measurements in low-pressure DC discharges.[93] Electron collision cross-sections of dimethyl ether (DME, C_2H_6O) were measured under a constant electric field and crossed electric and magnetic fields through the standard swarm analysis.[94]

A multiple term solution of the BE for electron noble gases, including He, Ne, Ar, Kr, and Xe, were discussed by considering the third-order transport coefficient tensor[95] and the effect of longitudinal field components on the spatial profile of electron swarms.[95,96] The third-order transport coefficients for electrons in N_2 and CF_4 were discussed.[97]

To date, 2D simulations of ICPs of $Ar/CF_4/O_2$ mixtures for etching applications showed the results of spatially and temporally plasma density and energy-resolved ion and radical fluxes towards surface.[98–100] The plasma kinetics of perfluorocyclobutane (c-C_4F_8) was modeled using a self-consistent plasma fluid simulation model.[101] Applying a high negative DC voltage to a RF biased electrode, the flux of secondary electrons and plasma uniformity were discussed with phenomena of trapping and dumping of ballistic electrons that depend on the magnitudes of overlapped voltages. High-energy secondary electrons altered the

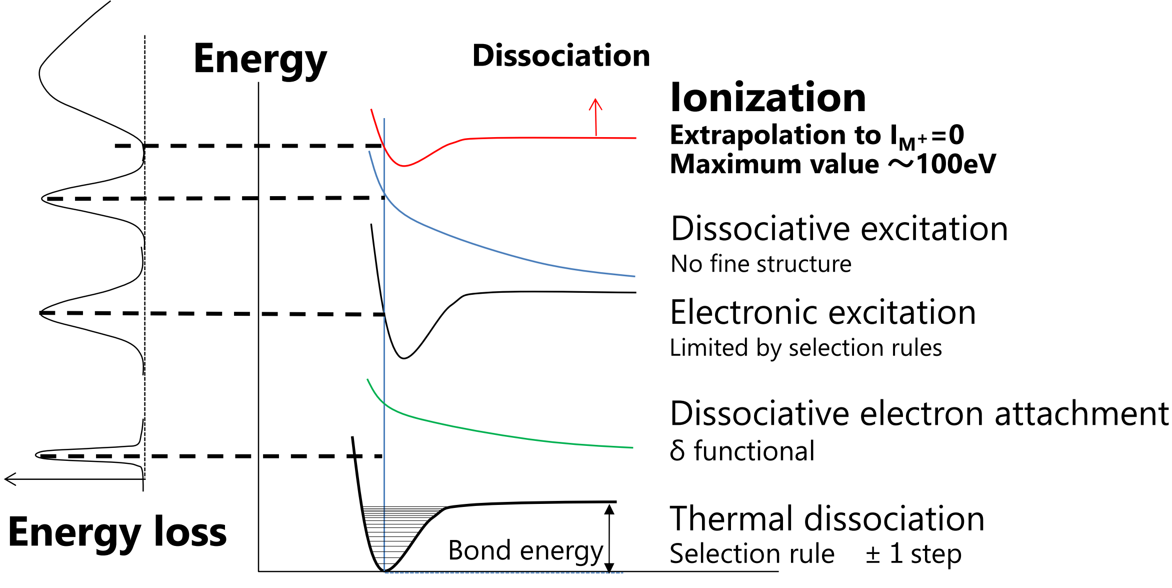

Fig. 15. (Color online) Electron collision processes in gas-phase. Computational approaches for estimation of:: reaction pathway and threshold energy of these reactions (Courtesy: Toshio Hayashi).

© 2022 The Author(s). Published on behalf of The Japan Society of Applied Physics by IOP Publishing Ltd

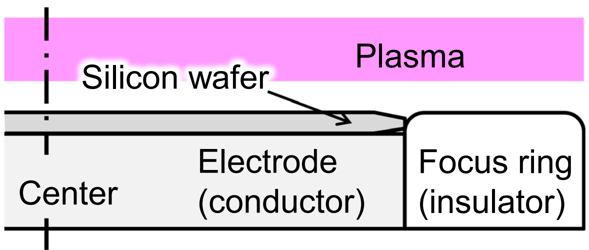

Fig. 16. (Color online) A schematic cross-section of a plasma etching reactor. A wafer edge is surrounded by a focus ring made of insulating materials. A gap between the wafer edge and the focus ring is closely related plasma uniformity at the edge of a wafer.

electron energy distribution function (EEDF) at the wafer, high-energy electron flux to the wafer and the plasma density profile.[102)]

Inelastic dissociation processes under consideration of the vibrational states were reported.[103–105)] Simulations of atmospheric pressure plasma at the nonequilibrium phase were reviewed by Tochikubo.[106)]

2.6.3. Computational chemistry for electron molecule collisions. Computational quantum chemistry approaches to electron-molecule collisions have been investigated[107)] (Fig. 15). In the semiconductor industries, film depositions used silicon precursors such as silane (SiH_4) for silicon films and carbon precursors such as methane (CH_4), and material etching used halogen etchants such as tetrafluoromethane (CF_4).

Electron-molecule collision cross-sections for polyatomic molecules have been studied for fluorocarbon and hydrofluorocarbon etchants used in the semiconductor industry.[108,109)] Electron impact dissociation cross-sections for C_2F_6 have been reported.[110)] Meanwhile, electron impact ionization cross-sections for C_2F_6 and C_3F_8 have been reported.[111)] The total ionization cross-sections for perfluorocarbons, such as C_4F_6 and C_4F_8, were calculated using the binary-encounter Bethe method.[112)] Various types of analyses of C_4F_8 plasma were performed, and the dissociation of CF_2 via C_2F_4 was presumed based on the analysis of the results.[113)] Thereafter, the electronic excited states of C_4F_8 were calculated.[114)] Furthermore, the dissociation channels for C_4F_8 into CF_2 and $C_3F_5{}^+$ ions were assigned to the ab initio molecular orbitals.[115,116)] The electron impact elastic and excitation cross-sections of C_4F_6 isomers have been reported.[117)] The electron impact dissociation channels for C_5F_8 and C_5HF_7 have been studied.[118)] The electron impact ionization process of C_3F_6O has been reported.[119)]

The primary dissociation channels of hydrofluoro compounds were predicted through quantum chemical calculations,[120–123)] including fluoromethane compounds (e.g. CF_4, CF_3, CHF_3, CH_2F_2, and CH_3F),[120)] fluoroethane compounds,[121)] and 1,1,1,2-tetrafluoroethane (HFC-134a).[122)] Among these, 1,1,2-trifluoroethane (CH_2FCHF_2) was examined for the generation of CH_2F and CHF_2 radicals and ions by quadrupole mass spectrometry. In addition, the etch selectivity of silicon nitride (SiN), silicon dioxide (SiO_2), and poly-Si films using CH_2FCHF_2 plasma mixed with O_2 and Ar was explained with respect to the CH_2FCHF_2 and O_2 mixed gas-phase using quantum chemical calculations.[123)]

2.7. Sheath-related phenomena—dynamics in transports of mass and energy

2.7.1. Ion trajectories at sheath and feature levels. Ion trajectories are issued to control the feature profiles. Wafer-scale simulations have been reported for this purpose. The formation of DC self-bias voltage in CCP RF plasmas driven by multi-frequency waveforms has been reported.[124)] Electron-induced secondary electron emission (γ-electrons) strongly affects the ionization dynamics and plasma density.[125)] The focus ring skews the difference in sheath thickness above the wafer and focus ring.[126)] The plasma discharge is concentrated over the focus ring, not being in the center of the reactor. A large potential difference and a high capacitive power deposition appears at the surface area between the substrate and focus ring[127)] (Fig. 16). Multiscale modeling with a sheath was applied to predict ion fluxes around a gap between a wafer and a focus ring in a dual-frequency (40 MHz + 3.2 MHz).[128)] The uniformity across the large area of wafer has been attracted attention in plasma sheath formation around the edge and gap of focus ring.[129–132)]

Electric field reversals (EFRs) in the sheath and pre-sheath, the electronegative nature, and increasing mole fractions of O_2 impede electron transport to the surface, which further increases EFR.[133–135)] The 2D axisymmetric plasma sheath model predicted ion trajectory deviations at the plasma–wafer interface for actual chamber geometries and etch conditions.[136)] The plasma sheath was deformed, and the ion trajectories tilted from the normal to the surface in the vicinity of the wafer edge. The feature-scale kinetic MC etch model determines the asymmetries in the post-etched feature profiles.[137)] The topographic simulation platform simultaneously considers 3D surface movement, neutral and ion transport, and surface reactions in plasma HAR oxide etching.[137)] The stochastic charging of the inside surfaces of features resulted in tilting of the HAR features in random directions.[138)] The ion energy and angular distribution functions (IED and IAD) of ions and fast neutrals were estimated computationally by a hybrid model of fluid and particles and they were validated across a range of operating conditions of experiments.[139)] The IED were measured by a retarding field energy analyzer and the IED function varies over a pulse period. The results were shown that the ion energy increased and energy spread from single peaked to bi-modal with the decrease of RF power duty cycle.[140)] During transitions of plasma in a pulsed period from a plasma ignition stage to a stable glow stage and to an afterglow period, the ion energy and ion flux were tailored by pulsing waveforms.[141)]

2.7.2. Measurement of transport in the interior of HAR features. Inside the HAR features, the entrance of electrons is shaded, and the feature bottom will have electrostatic charges built up owing to the unbalanced entrance of electrons and positive ions (Fig. 17). Noda et al. reported that the ions that penetrated real contact holes with a diameter of 0.2 μm fabricated on a micro-capillary plate were directly measured by using an electrically floated quadruple mass spectrometer.[142)] The charge density at the bottom was monitored using the capillary-hole method.[143,144)] The angular distributions of energetic neutrals and ions were analyzed.[145)]

2.8. Plasma-induced surface reactions—Surface chemistry

2.8.1. Molecular simulations of plasma-induced surface reactions. The cyclic process of deposition and etching is

© 2022 The Author(s). Published on behalf of The Japan Society of Applied Physics by IOP Publishing Ltd

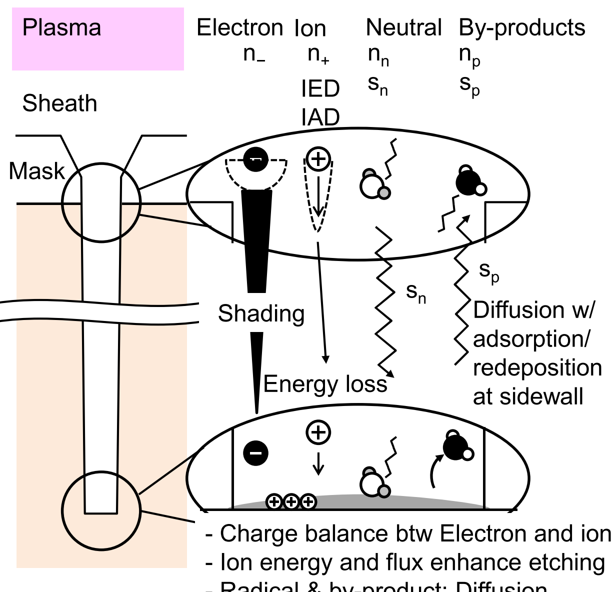

Fig. 17. (Color online) A diagram of schematics of transports inside high-aspect-ratio features. Neutral transport rate is obtained by molecular diffusion and the surface sticking coefficient. The sticking of neutrals determines the neutral flux towards the bottom of feature during the transport. Ion energy and angular distribution determines global sheath field and local charge-built up surface (Reprinted from *Jpn. J. Appl. Phys.* 57, 06JA01 (2018).[30]

called (quasi) atomic layer etching (ALE). The computational results of the ALE of SiO_2 on flat surfaces and in short trenches using capacitively coupled plasmas comprising a deposition step (fluorocarbon plasma) and an etch step (argon plasma) showed a delicate balance between the deposition of the polymer during the first half cycle and etching (with polymer removal) during the second half cycle.[146] The thermal ALE process of crystalline HfO_2 and ZrO_2 using a hydrogen fluoride (HF) pulse was calculated using a computational model.[147)]

2.8.2. Minimization of plasma-induced damages. Plasma-induced damage has been recently characterized by various methods, such as the combination of quantum chemical computation[148] and electrical conductance measurements.[149,150] It is caused by bombardment of energetic ions, penetration of chemically active atoms, and radiation of high-energy photons.[151] The effects of ion bombardment on the surface were analyzed experimentally and numerically.[152] On-wafer monitoring of the ion bombardment energy has been reported.[153]

2.9. Science-based modeling hierarchies of plasma processing reactors

2.9.1. Simulation of multiscale modeling of plasma processes in a reactor. The previous section reviewed the recent progress in the measurement of bulk plasma. At the next level, multiscale modeling of plasma processing should be developed, including particle transport and surface reactions inside the reactors. That is, plasma processing has been modeled using multiscale simulations for equipment-scale plasma and feature-scale profiles (Fig. 18).

In plasma etching, multiscale models have been developed to simulate both the gas-phase reactions and transportation phenomena in Cl_2/Ar plasma chambers, as reported by Osano and Ono,[154–158] Kushner et al.,[159–162] Chang and Sawin,[163–165] Graves, et al.,[166,167] Hamaguchi et al.,[168–170] and Tinck and Bogaerts.[171–173]

Kuboi et al. modeled the surface reactions and plasma-induced damage on SiO_2 and Si_3N_4 with fluorocarbon plasma using the voxel-slab model developed by Kuboi.[174–178] Vanraes reviewed the standardized computational methods to be used for multiscale modeling in a case study of Si and SiO_2 etching by fluorocarbon plasmas.[179]

In plasma film deposition, Depoh et al. reported plasma and feature profile simulations of plasma-enhanced chemical vapor deposition (PECVD) of a titanium film.[180] Numerical simulations were also performed for physical vapor deposition (PVD), such as ionized magnetron sputter deposition.[181–184]

The etching properties of $C_6F_6/Ar/O_2$ in ICP and CCP systems were compared.[185] Pulse-modulated plasma for SiO_2 etching characteristics was reviewed.[186]

2.9.2. Monitor and control of substrate temperature. Noncontact measurements of the substrate temperature have been reported by low-coherence interferometry.[187] The uniformity of the substrate temperature was controlled using a multizone heating system.[188–191]

The temperature of the electrostatic chuck, used as a wafer susceptor, was monitored using a wireless-type on-wafer temperature monitoring system.[189] To understand the temperature results, the heat transfer characteristics of the ceramic puck for the electrostatic chuck, and the effects of different types of heating zones, such as multi-zone/single-zone heaters,[190] and the temperature uniformity of the ceramic puck[191,192] were investigated.

3. Toward plasma informatics—basics of data-driven approaches

Data-driven approaches have been taken into account also in plasma science recently,[5,193] which may be called "plasma informatics."[6,194] Accordingly, the plasma informatics is defined as applications of techniques based on informatics and data-driven sciences to plasma science (Fig. 19). Recent significant improvements in the information processing capabilities of computers and the development of sensor technology have facilitated the collection of large amounts of data, and the high-speed processing of big data has allowed for qualitatively different and useful results to be obtained.[6] The emphasis that informatics and data-driven science are merely statistical methods of regression and sorting of data without physics, it is meaningless without combination of theory, computation, and experiments.

Historically, the first paradigm is empirical science-based on observation; the second one is model-based theoretical science; the third one is computational science, which comprises simulations; and the fourth one is evolutionarily big data-driven science.[195,196] In the research and development phase, data-driven approaches have emerged.[7] In fact, a large dataset contributes to the discovery of complex plasma.[197,198]

Predictive analysis is possible in the regression of data. The quality in the production of the materials and fabrication of the devices must be controlled by informatics. Simply stated, it is to explore relationship between inputs and outputs through computation. There are three such learning

© 2022 The Author(s). Published on behalf of
The Japan Society of Applied Physics by IOP Publishing Ltd

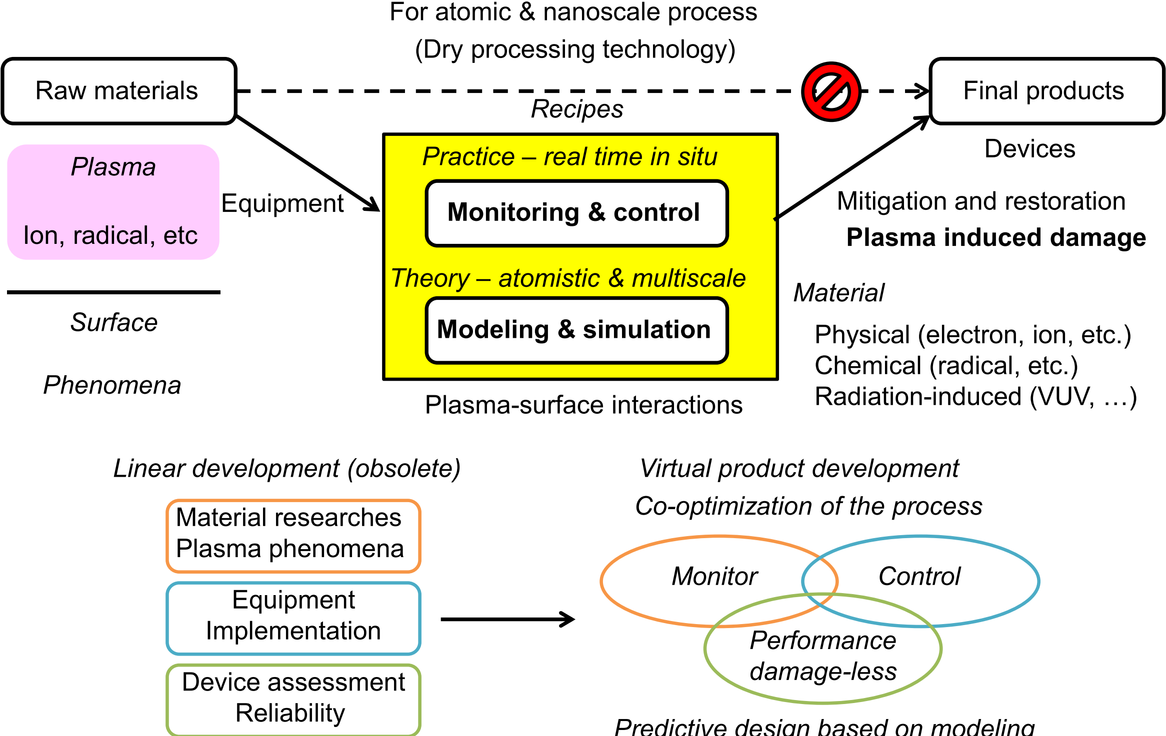

Fig. 18. (Color online) Schematic diagram of process development, including (i) modeling and simulation and (ii) monitoring and control, for nanoscale dry processing without damage. (Reprinted from *Jpn. J. Appl. Phys.* 58, SE0804 (2019).[17])

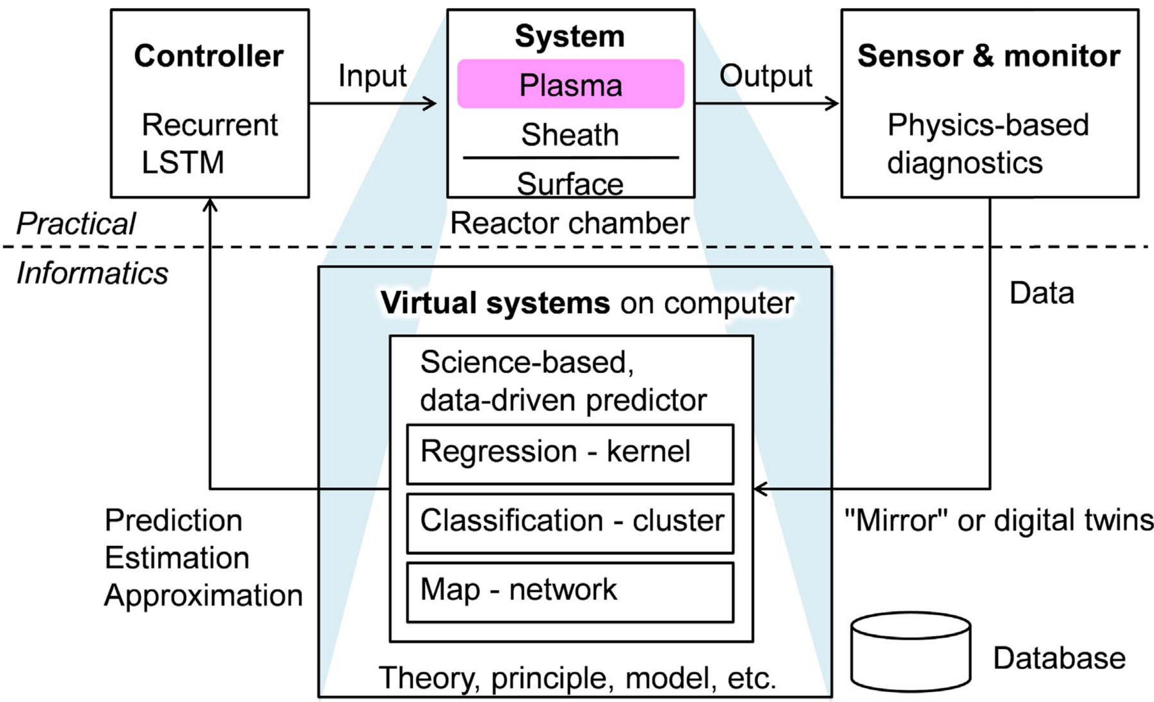

Fig. 19. (Color online) Diagram of science-based, data-driven approaches called as plasma informatics. LSTM stands for long short-term memory.

approaches: supervised learning, unsupervised learning and network modeling based on the Graph theory using a collection of nodes and edges. This review provides an overview of these advances, focusing on plasma processing researches and not fusion plasma. Consequently, smart manufacturing and an understanding of the mechanisms and properties of complex systems are topics in plasma informatics.

3.1. Basics of machine learning

Deep learning is defined as a subset of ML methods for prediction and classification to learn the underlying features in data using deep neural networks (DNN), such as

© 2022 The Author(s). Published on behalf of
The Japan Society of Applied Physics by IOP Publishing Ltd

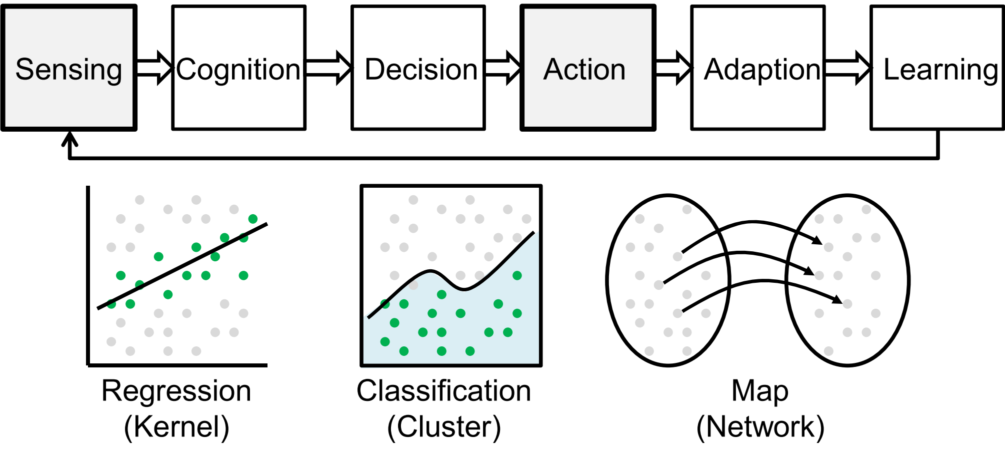

Fig. 20. (Color online) A diagram of cognitive system with artificial intelligence technology.

convolutional neural networks (CNN). Autonomous control can be built on two different architectures: a reactive system based on a simple loop of sensing and action. Another is a cognitive system based on a complex loop of sensing, cognition, decision, action, adaption, and learning (Fig. 20). In these systems, data are collected and processed to achieve an environmental state under specific time and space constraints. Perception comprehensively integrates information to create awareness in the decision-making process. To extend this perception, artificial intelligence can be built by mimicking or reversing the engineering of biological intelligence.[199]

3.2. Overview of data regression

Regression using ML has two advantages in obtaining accurate predictions. First, a regressor is obtained without assuming the exact regression functions. Better regression functions can be obtained by optimizing the hyperparameters to adjust the coefficients in a regression function. A parameter search method using a grid search or gradient method was used to optimize the hyperparameters. Second, unacquired data can be predicted with a high generalization performance. That is, a regressor that avoids overfitting can be obtained through regularization.

Table I lists the typical methods that can be used as regressors. There are a wide variety of methods, such as kernel-, decision tree-, and neural network-based. However, no method can be appropriate for all task types. Each method has its weaknesses and strengths. For example, a DNN has universal approximation ability. However, it requires a large amount of learning data to determine its coefficients. Therefore, it is better to select methods that are well-suited to a target task.

3.3. Kernel-based models—gaussian process regression and support vector machine (SVM)

Gaussian process regression, a statistical ML method, can be applied to spectroscopy measurement data and crystal growth data, which can accelerate material research by reducing the experimental time and cost. It is important to design and use appropriate evaluation functions for the exploitation and exploration of experimental data using ML. The prediction accuracy of unknown experimental data varies significantly depending on the adequacy of the evaluation functions. Therefore, it is necessary to evaluate the accuracy of the model and check whether overfitting has occurred using test data that are not included in the training data. Cross-validation during training or validation with test-specific training is used for the check.

3.4. Decision tree-based models—random forest

In the decision tree, the explanatory variables are split into intervals. A cost function is used to determine the range and number of intervals. The split constitutes a tree structure that branches step-by-step from the root node. Therefore, it is easy to explain the reason for obtaining an inference result by following the branch nodes. In recent years, more advanced methods, such as extreme gradient boosting (XGBoost)[200] and light gradient boosting machine (LightGBM),[201] which apply a boosting technique to decision trees, have been developed and used for various problems.

3.5. Network-based models—deep neural networks (DNNs)

Deep learning with neural networks has emerged in various fields, such as regression, classification, computer vision, and natural language processing. A neural network has input and output layers and middle layers. A network with a large

Table I. List of regressors using machine learning.

Model		Data size availability
Kernel based		
Gaussian process regression	Bayesian optimization	High dimensions
Support vector regression (SVM)	Sparse model	High dimensions
Decision tree-based		
Random forest	Few hyperparameters, but overfitting	Large dataset
Extreme gradient boosting	Many hyperparameters	Small dataset
Network-based		
Deep neural network (DNN)	Universal approximation	Large dataset

© 2022 The Author(s). Published on behalf of The Japan Society of Applied Physics by IOP Publishing Ltd

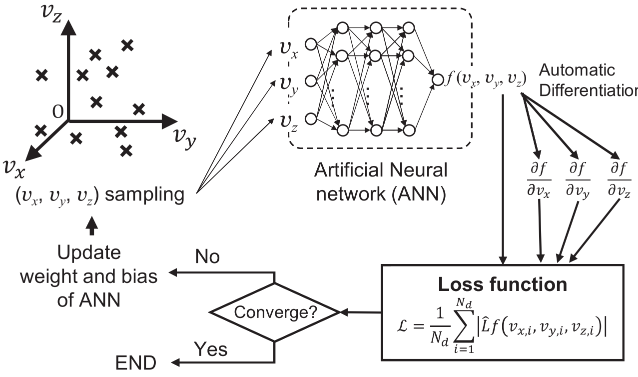

Fig. 21. Diagram of the PINN approach for calculating the EVDF.

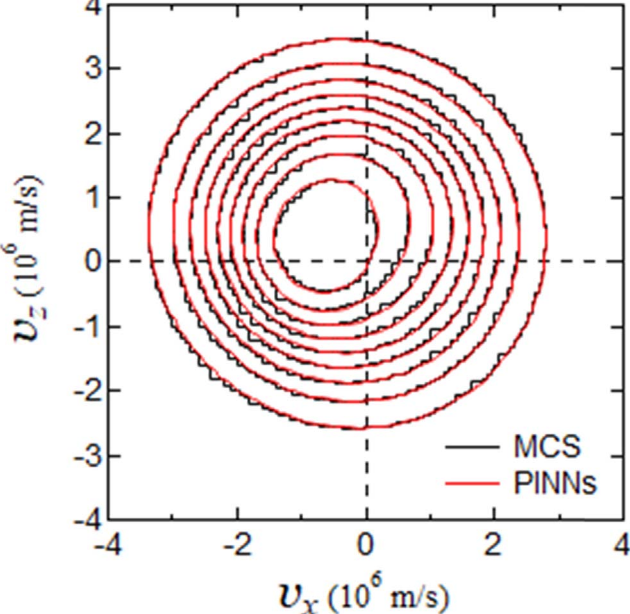

Fig. 22. (Color online) Electron velocity distribution function $f(v_x, v_z)$ in SF_6 at $E/N = 2000$ Td (1 Td $= 10^{-21}$ Vm^2) and $B/N = 2000$ Hx (1 Hx $= 10^{-27}$ Tm^2). Here, E denotes the electric field strength, B denotes the magnetic flux density, and N denotes the number density of gas molecules. $f(v_x, v_z)$ is calculated by taking a projection of $f(v_x, v_y, v_z)$ to the v_x–v_z plane. The contours of $f(v_x, v_z)$ are plotted from 0.0025 to 0.0225 in steps of 0.0025.

number of middle layers is called a DNN. Overfitting has long been a problem in the training of neural networks. However, methods that can avoid overfitting, such as dropout,[202] have been developed in recent years, and the application of neural networks has expanded significantly. Various models have been proposed depending on the network structure, such as the number of layers and nodes, function and interconnection of layers, and recursion of inputs and outputs. Typical examples are CNNs, which capture features by convolutional layers and are often used for image recognition, and recurrent neural networks (RNNs), which are excellent for processing time-series data, such as sensor logs and sounds.

4. Recent progress in bulk plasma research—machine learning of plasma parameters

4.1. EVDF and BE solver

The EVDF provides basic information on electron transport and reactions in plasma. The electron transport coefficients

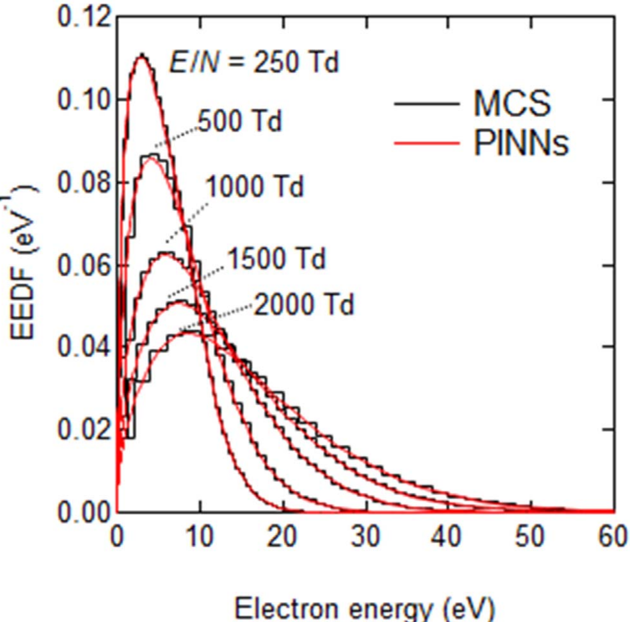

Fig. 23. (Color online) Electron energy distribution function (EEDF) in SF_6. The value of B/N is fixed at 2000 Hx.

and rate coefficients for electron collision-induced reactions can be calculated using the EVDF. These coefficients are required for the plasma simulation. The EVDF can be obtained as a solution to the electron BE, and various numerical methods have been developed for solving the BE.[203] The direct numerical solution (DNS), where no expansion of the EVDF is required, is the best method to calculate the EVDF exactly.[204–206] However, the calculation of the 3D or higher-dimensional EVDF by DNS has still been restricted owing to the high memory capacity required for storing the EVDF. Recently, the physics-informed neural network (PINN) approach has attracted significant attention as a mesh-free approach for solving partial differential equations (PDEs).[207] In this approach, an artificial neural network (ANN) is employed as a function approximator and is trained to satisfy both PDEs and boundary conditions. The trained ANN represents the solution function of the PDE. The partial derivatives of the function represented by the ANN can be calculated analytically using automatic differentiation,[208] making the PINN approach mesh-free. The PINN approach allows us to address high-dimensional problems while saving the memory capacity required for the calculation. The applicability of the PINN approach for solving the BE was demonstrated in the calculation of the 2D equilibrium EVDF under DC uniform electric fields[209] and the 3D equilibrium EVDF under DC uniform electric and magnetic fields.[210]

Figure 21 shows a diagram of the PINN approach for calculating the 3D EVDF $f(v_x, v_y, v_z)$. The inputs of the ANN are the components of the electron velocities v_x, v_y, and v_z. The output of the ANN is the value of the function $f(v_x, v_y, v_z)$. The ANN was constructed in accordance with the architecture presented by Wang et al.,[211] and it has four hidden layers and 100 units per layer. All BE terms are transferred to the left-hand side, and the BE is represented as $\hat{L}f(v_x, v_y, v_z) = 0$. How well the ANN respects the BE is measured by the loss function defined as the mean absolute value of $\hat{L}f(v_x, v_y, v_z)$. We sampled points in the velocity

© 2022 The Author(s). Published on behalf of The Japan Society of Applied Physics by IOP Publishing Ltd

space, calculated the output of the ANN at the sampling points and the value of the loss function, and then trained the ANN to minimize the value of the loss function via a gradient-based optimizer, such as Adam.[212] The training of the ANN was continued until the value of the loss function converged.

The equilibrium EVDF and EEDF calculated from the PINN approach in SF_6 under DC uniform electric and magnetic fields are shown in Figs. 22 and 23. The MC simulation results are shown in these figures. The applied electric and magnetic fields are parallel to $-v_z$ and $-v_y$, respectively, making the EVDF anisotropic. The PINN approach can obtain a smooth distribution and properly reproduce the anisotropic EVDF. The EEDF calculated by the PINN approach reproduces the MC similation (MCS) results excellently over a wide range of E/N values.

The 3D EVDF was represented by an ANN with 41 700 parameters. The EVDF in the same condition was also calculated by DNS[206] and was stored in a 3D array with a size of $10\,000 \times 45 \times 720$. Given that the precision of the floating point used in the calculation is the same, the PINN approach allows us to represent the 3D EVDF properly, with approximately 0.01% of the memory capacity required in the conventional DNS.

4.2. Plasma density profile in a reactor and surrogate model of particle-in-cell simulations

In surrogate models of plasma discharge, a large amount of work has been conducted on plasma discharge simulations based on fluid-based models, particle-based models, and their combinations (hybrid models) (Fig. 24). A recent study[213] presented surrogate models based on ML techniques, mostly neural networks, using simulation data of Ar plasmas. The basic concept is to perform numerical simulations with a variety of system parameters, such as the applied voltage and gas pressure, and to use the resulting profiles of, for example, the electron density, electrical potential, and electron temperature, as learning data.

A surrogate model is constructed as an appropriate interpolation of these data, from which approximate plasma properties can be instantly predicted for arbitrary combinations of system parameters; thus, the surrogate model can be used as a real-time simulator. Figure 25 shows an example of a surrogate model-based on a 1D fluid-based simulation of Ar plasmas.

A surrogate model-based on relatively simple simulations can be used as a reference for the development of a more complex model via transfer learning. For example, particle-in-cell/Monte Carlo Collision (PIC/MCC) models can handle non-Maxwellian electron distributions and typically provide more accurate predictions of plasma dynamics than that of fluid-based models. PIC/MCC simulation is far more time-consuming and, thus, more expensive than the corresponding simulation with fluid-based models. A surrogate model for 1D plasma simulation that can handle non-Maxwellian electron distributions was created using PIC simulation data via transfer learning from a fluid-based ML model of 1D plasmas.

Plasma processing involves complex physical and chemical systems under nonthermal equilibrium conditions. Therefore, the numerical simulation of plasma processing often requires multi-scale modeling of complex physical systems. A data science-based approach to such problems

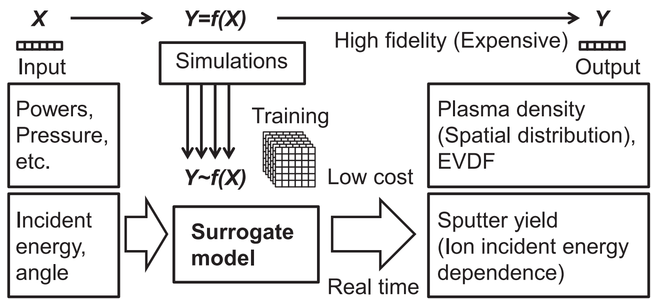

Fig. 24. Surrogate models based on ML techniques accelerate simulation-based analyses using high-fidelity, time-consuming calculations.

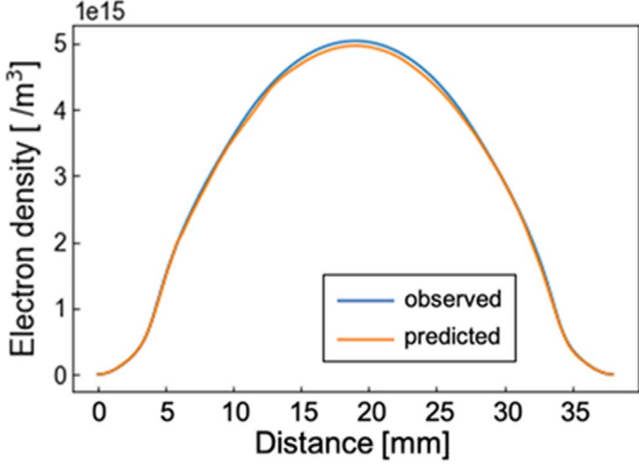

Fig. 25. (Color online) Comparison of the electron density profiles (blue curve) obtained from 1D fluid-based simulation of Ar plasmas with that from the neural network-based prediction (brown curve). The modeled plasma is a parallel-plate CCP driven by 13.54 MHz RF power without bias voltage. The peak-to-peak voltage was 300V and Ar gas pressure was 60 Pa.[213]

may provide a different insight into the underlying physical mechanisms of the observed phenomena and some practical solutions to technical problems.

4.3. Network in plasma chemistry using the graph theory

Plasma chemistry consists of a complex system of tremendous chemical reactions of large variance lifetime species, such as electrons, positive and negative ions, excited neutrals, and radicals. Besides, researchers have studied some significant reactions among these species and the selected reactions with rate coefficients are listed in database. To understand overall reactions, scientific modeling through network analysis based on graph theory is necessary. Sakai et al. demonstrated a web-like network analysis of chemical reactions of methane plasma. For examples, electron impact dissociation of CH_4 takes place with generation of CH_3 radical and H atom. These species of CH_4, CH_3, and H are represented as nodes and the reaction is also represented by a graph representation of directed edges which are connected to the nodes. Decomposition and/or synthesis of species in the plasma are linked with intermediate species, such as atoms, molecules, and radicals.[214] From this network, Mizui et al. reported that the centrality of species reveals in the network structure in plasma chemistry.[215] The presented graph of reactions in silane plasma[216] and methane plasma[217] included the diagram which showed a relationship between betweenness and closeness centralities. These values indicate

© 2022 The Author(s). Published on behalf of The Japan Society of Applied Physics by IOP Publishing Ltd

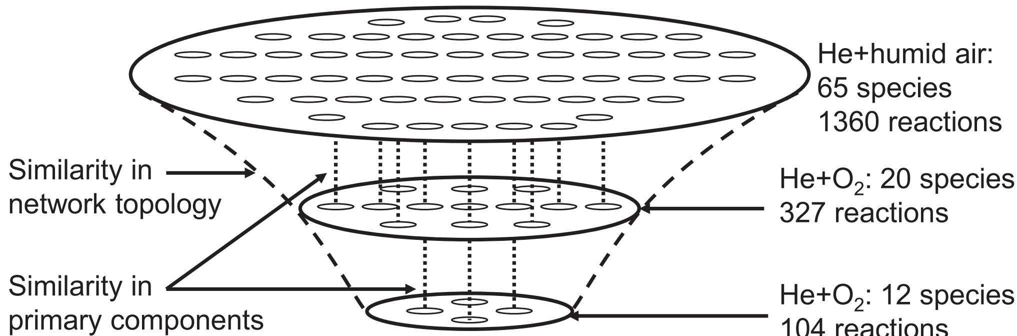

Fig. 26. The initial reaction set allows the reaction network to be reduced while preserving network similarity [Modified from Murakami and Sakai, *Plasma Sources Sci. Technol.* 29, 115018 (2020).[218]].

mathematical notation of dependencies of each reactions. They pointed out that the plasma-enhanced chemical reactions takes place tens of chemical reactions in parallel.[216,217]

Murakami et al. reported a graph representation of reactions for the He and O_2 mixed plasma chemistry and extracted inherent information from the network. Scalability of the network was also discussed. They assumed that the network can rescale with criteria: (1) maintain the scale-freeness and self-similarity in the network topology and (2) select the primary species considering its topological centrality. The unique scale-freeness of plasma-induced chemistry allows a robust rescaling of the chemical network. From this, the complex network as the initial set with 65 species and 1360 reactions was able to be compressed and reduced the reaction set with 12 species and 104 reactions, which retains the network topology and reduces similar network[218] (Fig. 26).

Holmes et al. studied graph visualization for atmospheric chemistry reactions using the graph theory for exploring engineering of plasma chemical reactions with temperature dependent rate coefficients. The Dijkstra's shortest path algorithm[219] can probe significant reaction pathways, applying a open-source graph visualization software (Gephi).[220] The optimal condition approaching via reaction-in-network analysis was used for a graph analysis of ozone production in humid air plasma discharge. Time dependent 0D simulations calculated formation for O and O_3.[221]

Very recently, Sakai et al. addressed that plasma processing reactions occurred not in a uniquely determinant pathway. Always there is a possibility for determining one in multiple pathways that meant microscopic causal relationships are not established. Direct application of ML methods is not always possible, since levels of complexities are very high in comparison with other scientific research targets, considering causalities in the plasma processing's complexities. Therefore, they proposed that sophisticated plasma diagnostics and data acquisition systems were required for the use of predictively computational deduction of experiments. It is required to handle a large number of data obtained from visualization, acquisition, and analysis methods for development of intellectual design in industrial plasma processes.[222]

5. Recent progress in material synthesis and real time control

5.1. Spray coating

The atmospheric plasma (thermal) spray is a method for metal or non-metallic coatings.[223] In the thermal spray processing, there are at least essentially forty processing parameters that define the overall coating quality and these must be selected in an optimized fashion to manufacture a coating that exhibits desirable properties. The proper combination of processing variables is critical since these influence the cost as well as the coating characteristics. The in-flight

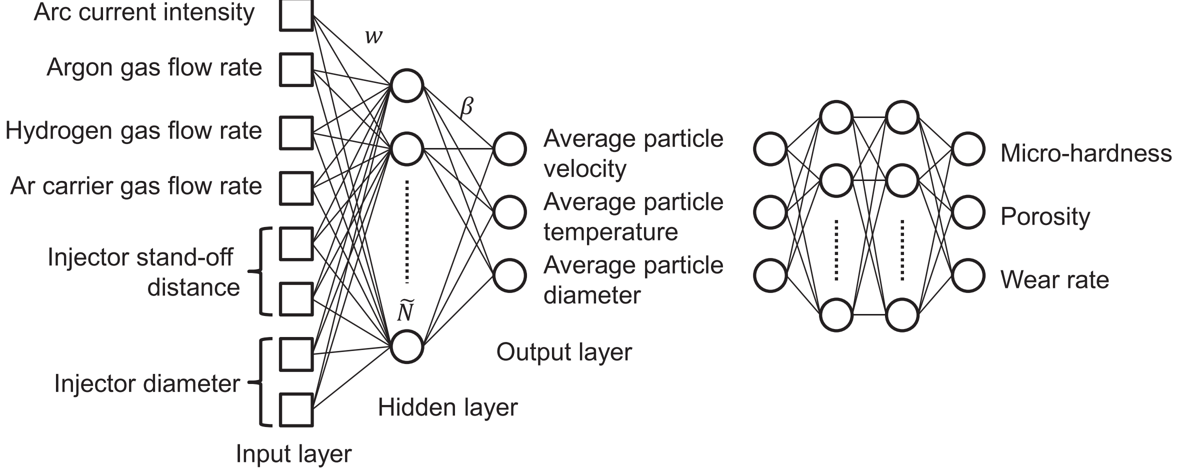

Fig. 27. Example of architectures of single layer feed-forward network (SLFN)[225] and artificial neural network (ANN) for spray coating.[227]

© 2022 The Author(s). Published on behalf of The Japan Society of Applied Physics by IOP Publishing Ltd

particle characteristics have significant influence on the in-service coating properties. Choudhury et al. studied optimization procedures that were demonstrated to predict the output of the in-flight particle, based on the ANN method.[224] They demonstrated that modeling of the in-flight particle characteristics of the atmospheric plasma spray (APS) process. The single hidden layer feed-forward neural network (SLFN) and an extreme learning machine (ELM) algorithm, instead of traditional back propagation algorithms, were used for rapid prediction of the in-flight particle characteristics.[225] To train and optimize the thermal spray processing, they demonstrated an effective way of making subsets of the input and output relationship and applying a modular ANNs structure. For example, the spray process divided into sub-tasks such as the in-flight particle temperature, diameter, velocity and then the trained databases were built for ANN modular components[226] (Fig. 27).

Based on the fact that a disturbance of the coating process results in a change of the properties of the spray particle stream, this change of properties can be recorded using the diagnostic system particle flux imaging (PFI) which characterizes the particle stream on the basis of ellipsoidal shapes. Deviations from a reference ellipse defined for optimal coating parameters means a deviation from the optimal process. Based on this, an ANN-based control was implemented using PFI ellipse numbers as input values.[228]

Batra and Taetragool calculated numerically mean particles' temperature and mean particle velocity parameterized flow rates of argon and hydrogen, powder feed rate, and discharge current in APS processing conditions using the LAVA-P-3D code.[229,230] The spray process was monitored through the least squares regression and the response surface methodology of the gaseous synthesized particles arrived at the substrate to be coated.[231]

The CNN was used to optimize synthesized parameters of in-flight particle characteristics of the spraying process. First, the experimental datasets were trained and predicted by analysis through the CNN models.[232] The relationship between process control parameters and in-flight particle behavior was modeled by implementation of the parameter-transfer learning method. Zhu et al. conducted the simulation of the plasma spraying with various parameters such as arc currents and voltages, process gases and flow rates, spray distance, and average injection velocity using simulation outputs running on the LAVA3D-P code.[229,230] The CNN model was trained prior to the targeted particle synthesis and the pre-trained CNN model can predict the designed target parameters.[233]

In the thermal spray coating, an ANN model was used to predict the HVOF sprayed chromium-nickel alloy (nichrome) coatings.[227] Liu et al. demonstrated that an ANN modeling predicted complex 3D shapes in cold spray additive manufacturing which is a solid state deposition onto a flat substrate and a curved substrate. A large set of profile data for the deposition process was trained by the ANN model involving the number of neurons in hidden layers.[234]

Up to now, feed-forward ANNs with back propagation algorithm has been popular for modeling the spray process. The ANNs has a merit of solving intricate nonlinear processes of the plasma spray coating with a number of controllable parameters. They reviewed the processing with ANNs which can control coating thicknesses, hardness, microstructure and particles, tribological properties, roughness, amphiphobic surface properties, and so on.[235]

The perspective visions written by Mauer and Moreau are that monitoring and controlling thermal spray processes are extremely challenging since these processes involve a large number of variables, some of them not being well-controlled such as the electrode wear. From this view, future thermal spray production units could comprise a series of process diagnostic tools for monitoring on-line key extrinsic and intrinsic spray parameters. Therefore, further development of sensors, testing, modeling, and ML techniques are found in concerted action with other activities to improve the design and control of thermal spray processes.[236]

Malamousi et al. reviewed the readily available digital tools and methods for coating deposition optimization, equipment health monitoring, process control and metallographic analysis in the thermal spray technologies. The most promising ML methods are discussed for thermal and cold spray. The transient kinetic models have been developed for coating on topological surface. The tribological and mechanical properties of the coating can be predicted from the spray parameters. This enables us to evolve in a virtual environment and digital post examination of coating properties. CNNs can be also used for the classification of spray process images and real-time videos.[237]

Properties such as hardness, bonding strength, and porosity of the coatings of Ni-based alloy were optimized by the Back Propagation ANNs model, although there were unmelted particles on the surface of the coating, the overall spreading was good and the compactness was high.[238]

Particle deposition behavior was modeled by a 3D multi-particle random deposition model-based on the coupled Eulerian and Lagrangian (CEL) method. Mechanical strain and stress fields affected to the pore defects and random grain distribution.[239] Composite coatings by APS are reported.[240]

The transfer learning-based error control method was proposed by Liu et al. The error mechanism modeling is conducted to demonstrate the memory behavior of thermal errors, and the applicability of a long short-term memory network (LSTMN) for the error prediction was proven. The improved least mean square (ILMS) filtered the high-frequency noises and removed singular values. The differential spotted hyenas optimization algorithm was proposed based on the chaos initialization strategy, differential mutation operator, and nonlinear control factor to optimize the hyperparameters of the LSTMN.[241]

In the spray process, temperature of a droplet is one of the key elements that controls the microstructure and properties of the coating so deposited. Bobzin et al. have attempted the methods, residual neural network and SVM, to estimate the averaged in-flight particle properties, together with CFD simulation results, central composite design and latin hypercube sampling to cover the representative process parameters. They have demonstrated that the trends of particle properties are estimated to be extremely faster than the averaged plasma jet simulation (from 3 h to less than 5 s).[242]

By technological outcomes, this field is becoming a hot topic for controlling using the ML and AI techniques without physical understanding of the significant parameters. We emphasize the importance of understanding the physics of the

© 2022 The Author(s). Published on behalf of
The Japan Society of Applied Physics by IOP Publishing Ltd

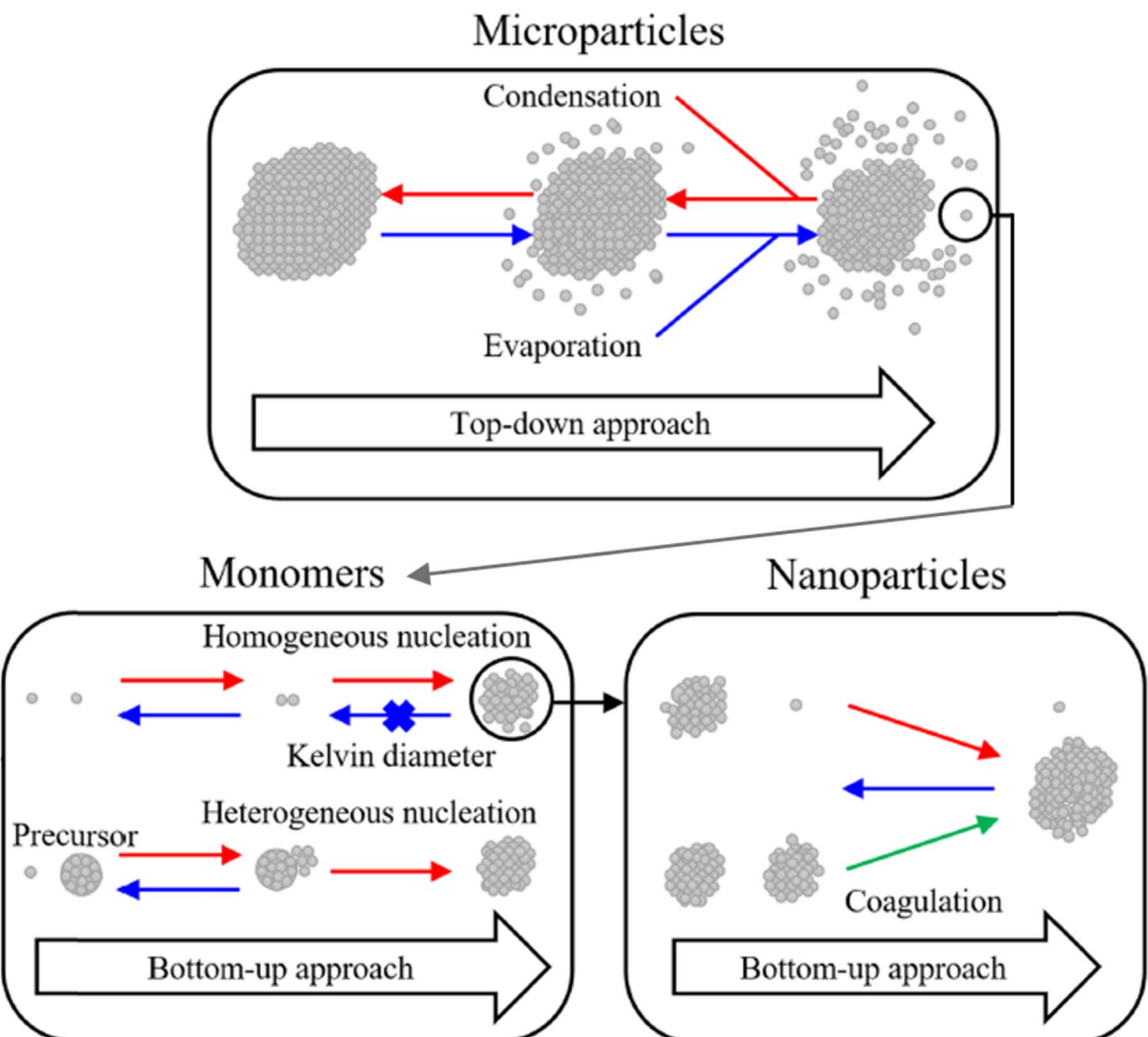

Fig. 28. (Color online) Schematic illustration of the growth process of nanoparticles from microparticles.

Table II. The species property data for the considered metal.

Particle species	Melting temperature (T_m)	Boiling temperature (T_b)	Latent heat at T_m (H_m) [kJ kg^{-1}]	Latent heat at T_b (H_b) [kJ kg^{-1}]
Silver	1235 K	2435 K	105	2390
Gold	1337 K	3129 K	63.7	1645
Copper	1357 K	2835 K	209	4730
Iron	1811 K	3134 K	247	6090
Tin	504 K	2875 K	59.2	2490

system in order to achieve comprehensive control of critical parameters.

5.2. Multiscale simulation for plasma synthesis of micro and nanoparticles

Nanoparticles are utilized in many applications of electronics, optics, chemical engineering, and biomedical engineering. As an example of a specific application, the generation of hybrid micro-nanopowders are required for metal injection molding using in situ one-step processes via RF thermal plasma treatment.[243] One of the nanopowder generators is to utilize thermal plasmas generated by a RF-ICP torch. Figure 28 shows the growth process of the nanoparticles from micro-scale macroparticles. The injected microparticles undergo evaporation in the high-temperature region and condensation in the low-temperature region. The ICP torch simulation calculates the temperature profiles at the steady state, as referred material properties shown in Table II. The evaporated particles from monomers, homogeneous and heterogeneous nucleation processes are the dominant source of nanoparticle formation. The nanoparticles interact by the Coulomb force or coagulate to form large-size particles again.

In order to understand the reaction mechanisms of metal nanoparticle synthesis by a thermal plasma torch, we introduced a computer simulation model. A combined simulation method merges the ICP torch simulation and the particle dynamics calculation, as shown in Fig. 29. The inductively coupled RF plasma torch is simulated with a 2D MHD fluid equation with a k-ε turbulence model.[244,245] The reaction data for the conservation equations for the ICP torch are calculated from the local thermodynamic equilibrium assumptions. For the particle dynamics, the Lagrangian scheme for microparticles and the nodal method for the nanoparticles are combined. The microparticles are simulated using a particle method to calculate Newton's equation of motion following the Coulomb force and charging effect. For the nanoparticles, the total number of particles gets very large. Thus, a nodal method is utilized to include nucleation,

© 2022 The Author(s). Published on behalf of The Japan Society of Applied Physics by IOP Publishing Ltd

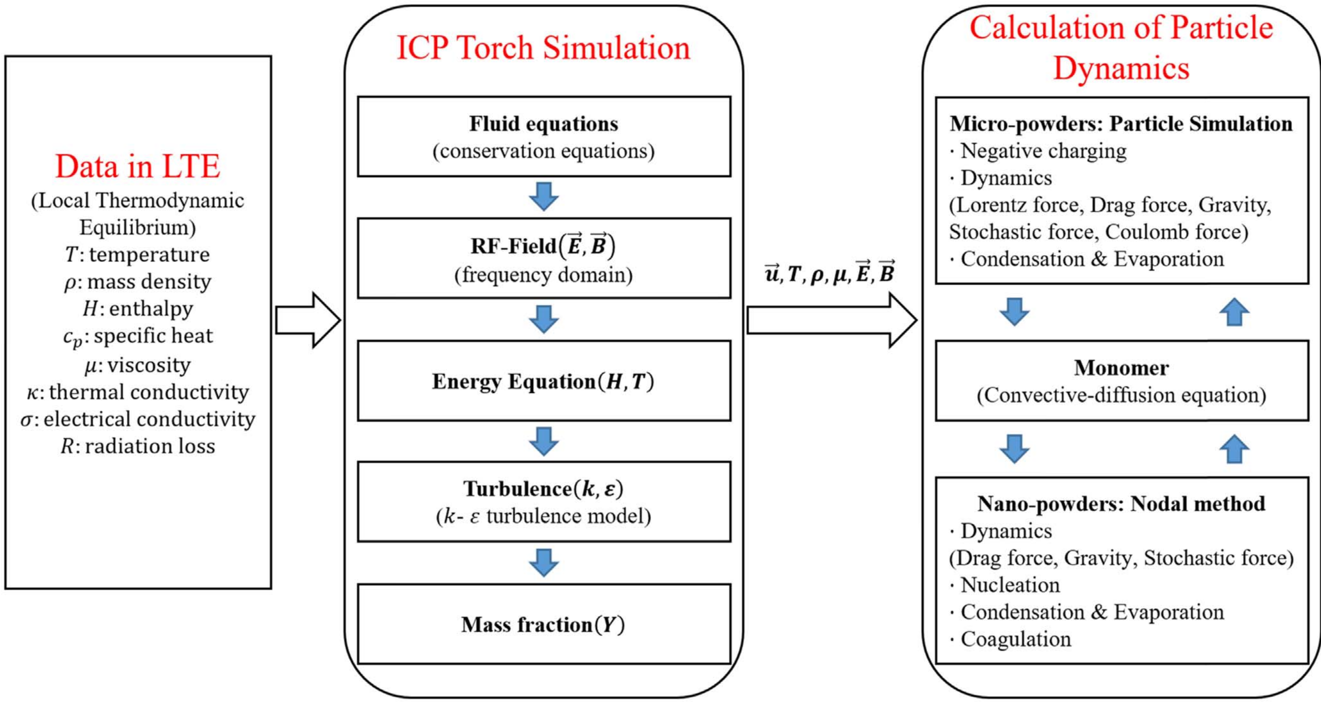

Fig. 29. (Color online) Numerical computation schemes for combining the plasma simulation and the dynamics of particles.

condensation, evaporation, and coagulations in Eulerian scheme. As the number of nanoparticles is larger than that of microparticles, this method is beneficial in reducing the calculation time.

Lee et al. simulated an RF plasma torch, as shown in Fig. 30, obtaining the spatial temperature profiles for three different feeding nozzle locations. They obtain a higher temperature as the nozzle location is near the ICP antenna. When particles are injected at the nozzle end, evaporation occurs actively in the hot region of the ICP torch and generates the monomer source. As a result, monomers are consumed for the nucleation and the condensation of microparticles and nanoparticles. It is possible to control the size distributions of the synthesized nanoparticles and microparticles by changing the location of the evaporation and condensation reactions by the variation of the control parameters, such as the driving power and frequencies, the quenching gas flow rate, and the structure design.

Figures 31 and 32 show the distributions of the microparticle diameter in the axial direction for a long and an intermediate nozzle length, respectively. Four different metal species of silver, gold, iron, and tin are considered in the system with an initial size of 5 mm. The melting point is shown in black color, and the other three colors mean the temperature ranges. As shown in Table II, the boiling temperature is lowest for silver and then followed by copper, tin, gold, and iron. For this reason, the vapor pressure is most elevated for Ag followed by Cu, Au, Sn, and Fe for a temperature larger than 2000 K. Because of the easy evaporation, the size of silver microparticles decreases rapidly from the injection position shown in Fig. 31(d).

As seen in Fig. 32, the shorter nozzle length results in a higher gas temperature at the injection position, and the evaporation happens much faster to reduce the size of the precursors in a very short length. Finally, the change of the nozzle location results in the size distributions of nano and microparticles.

5.3. Unsupervised learning, real time control of experiments

Recently, there were increased situations in which atmospheric pressure plasma jets (APPJs) are used in biomedical application as well as materials processing. The APPJ distanced from the target surface and its plasma characteristics varied sensitively independent on exogenous disturbances. For examples, to reduce the variability, a feedback control of the target surface temperature with regard to the thermal effect was conducted using a proportional-integral (PI) control strategy and a model predictive control (MPC) strategy based on OES intensities of the helium APPJ. The existence of most living organisms is limited to a temperature range and thus Yoshimura et al. successfully controlled gas temperature of helium APPJ by considering a balance among energy input and energy losses in open system.[246] A data-driven model of the APPJ was developed for a linear operating range using the subspace identification method. The MPC strategy successfully regulated the multivariable dynamics of the APPJ in real-time and was able to track the set-point in facing of disturbances and constraint handling[247] (Fig. 33).

Gidon et al. demonstrated that real-time diagnostics of APPJ and data analytics of ML methods. OES and electroacoustic emission were used and they showed effective means for estimation of operation-relevant parameters such as rotational and vibrational temperature and substrate characteristic in real time.[248] Easy-to-use and open-source software such as TensorFlow,[249] and scikit-learn[250] are available to use ML for plasma processing applications. Note that training data depends on (i) systematic validation and cross-validation on independent datasets to avoid overfitting a model; (ii) use of some level of system knowledge or

© 2022 The Author(s). Published on behalf of The Japan Society of Applied Physics by IOP Publishing Ltd

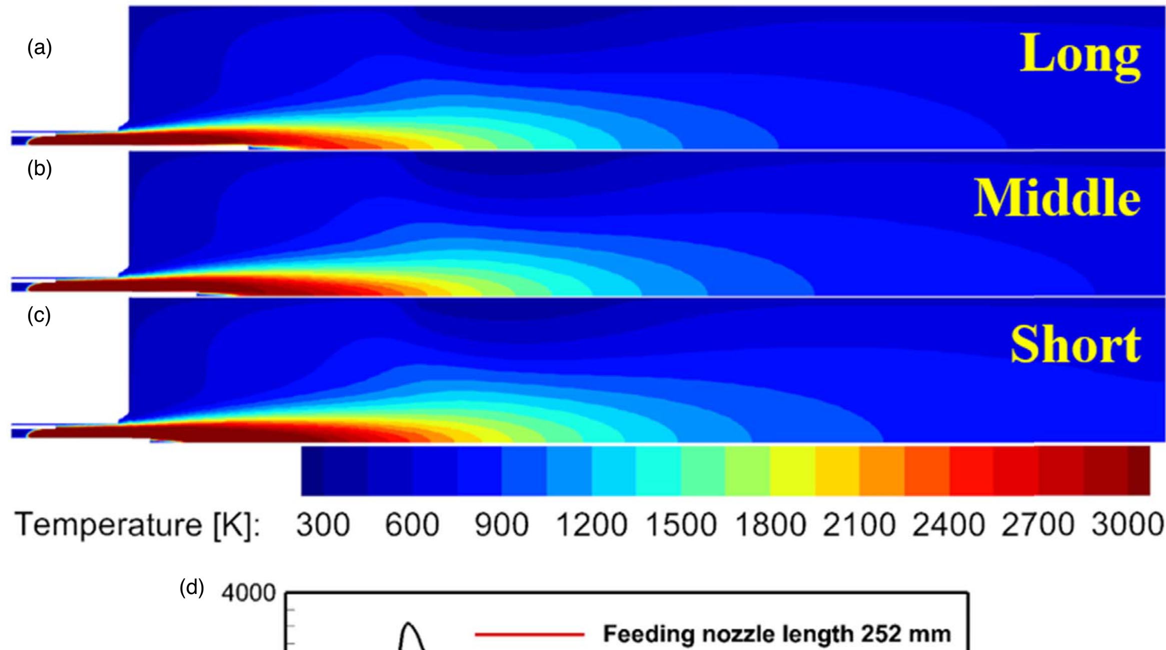

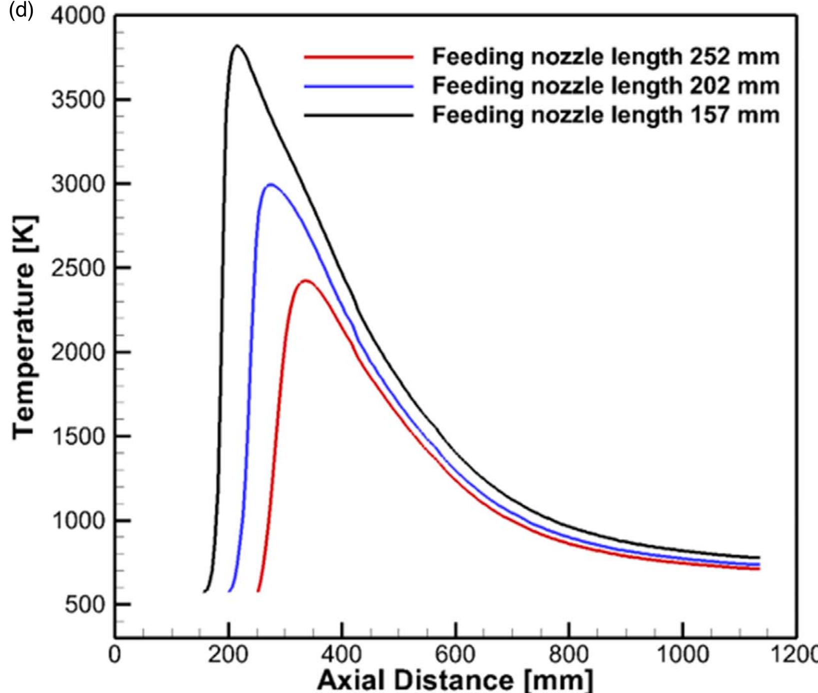

Fig. 30. (Color online) Spatial profiles of the gas temperature with the variation of the feeding nozzle locations at (a) 252 mm, (b) 202 mm, and (c) 157 nm from the ICP antenna. (d) the temperature profile along the axis is shown together.

assumptions to improve the generalizability of a model beyond training data; (iii) selection of relevant input features to improve prediction accuracy and reduce computational cost of a model; and (iv) training and testing model ensembles, instead of a single model, to enhance reliability of predictions.[251] However, Mesbah and Graves addressed that ML can use applications of predictive modeling, diagnostics, and process control with supervised, unsupervised, and reinforced learnings. The supervised leanings are regression, neural networks, kriging, SVMs. The unsupervised learnings are clustering, dimension reduction.[251]

Ghahramani et al. pointed out that the paradigm of probabilistic or Bayesian ML enables quantifying and manipulating uncertainty about models and predictions.[252] Bayesian inference indicates predisposition of rare cases. Probability of the rare cases can be represented by the Bayes sum rule $P(x) = \text{Sum } P(x, y)$ of y in Y and product rule $P(x, y) = P(x)P(x|y)$. A target can be treated by the Dicrete Marcov process, Wiener process, and Gaussian process. Posterior probability distribution can be calculated after receipt of current observation. Then the Bayesian optimization method can be applied to the reinforcement learning (RL).[252]

As example for controlling, local thermal effects of APPJ was considered, cumulative received heats can be accounted by thermal dose as an indicator. The cumulative, nonlinear thermal effects of plasma were able to be quantified from translation of the cumulative dose over a dielectric substrate. An optimization-based feedback control strategy was proposed for real-time regulation of thermal dose delivery using spatial measurements of substrate temperature and OES.[253,254]

The APPJ treatment conditions were optimized for reducing cancer cell viability of less than a prescribed goal while

© 2022 The Author(s). Published on behalf of
The Japan Society of Applied Physics by IOP Publishing Ltd

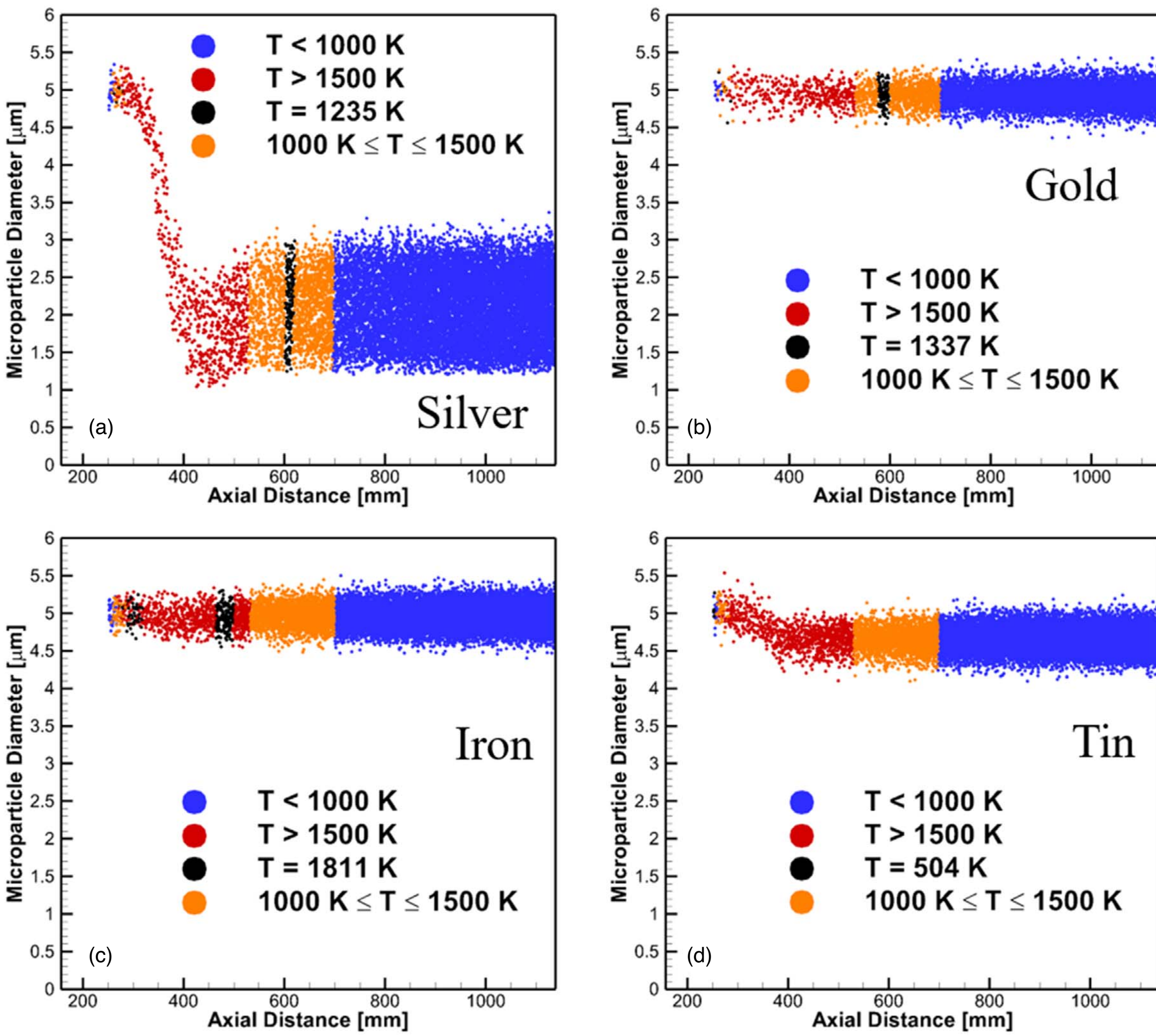

Fig. 31. (Color online) Particle distributions in the axial direction for different metal species of (a) silver, (b) gold, (c) iron, and (d) tin with a long nozzle length of 252 nm from the ICP.

minimizing a weighted sum of the treatment duration and the discharge voltage. The MPC framework for the actual cancer cell response and the efficacy of the proposed approach were illustrated by numerical simulations based on experimental data.[255] Surface charging determines from current voltage waveforms. The streamers inception and propagation inside the dielectric channel and outside of plasma device were calculated by 2D fluid model. Recombination was considered and streamer propagation through volumetric plasma.[256]

A time-varying or non-uniform characteristic of APPJ applications was controlled by the RL methods. The use of a deep RL method regulated thermal properties of variant APPJs on many kinds of substrates. Using simulated data from an experimentally-validated, physics-based model of the thermal dynamics of the plasma-substrate interactions, an RL agent was trained to perform temperature set-point tracking. The training the RL agent using a wide range of simulated thermal dynamics of the plasma-substrate interactions allowed for capturing the diverse temperature responses of different substrates. The proposed RL agent for the APPJ treatments enabled effective temperature control over a wide variety of substrates with drastically different thermal and electrical properties.[257]

The MPC of APPJ requires highly computational costs for solving theoretical plasma models. Simple, physics-based models were able to be adapted to an optimal control approach for controlling the nonlinear and cumulative effects. Through parsimonious input parameterization, a data-driven adaptive algorithm based on modifier adaptation was dealt with the structural plant-model mismatch by estimating the mismatch in the cost and constraints of the optimization. The adaptive approach converged to a Karush–Kuhn–Tucker point of the optimization for the true system.[258]

An active learning (AL) approach for exploring the multi-variable and highly nonlinear parameter space was effective for optimization of the low temperature, air plasmas produce NO_x for nitrogen fixation. A data-driven optimization method, Bayesian optimization, was demonstrated in automated and efficient exploration of the high-dimensional parameter space of the complex behaviors.[259]

The following three challenges are stated: (1) data-driven modeling of hard-to-model plasma-surface interactions and plasma treatment outcomes; (2) learning data analytics for plasma and surface diagnostics in real time; and (3) developing predictive controllers that enable reliable and effective APPJ treatments.[260]

© 2022 The Author(s). Published on behalf of The Japan Society of Applied Physics by IOP Publishing Ltd

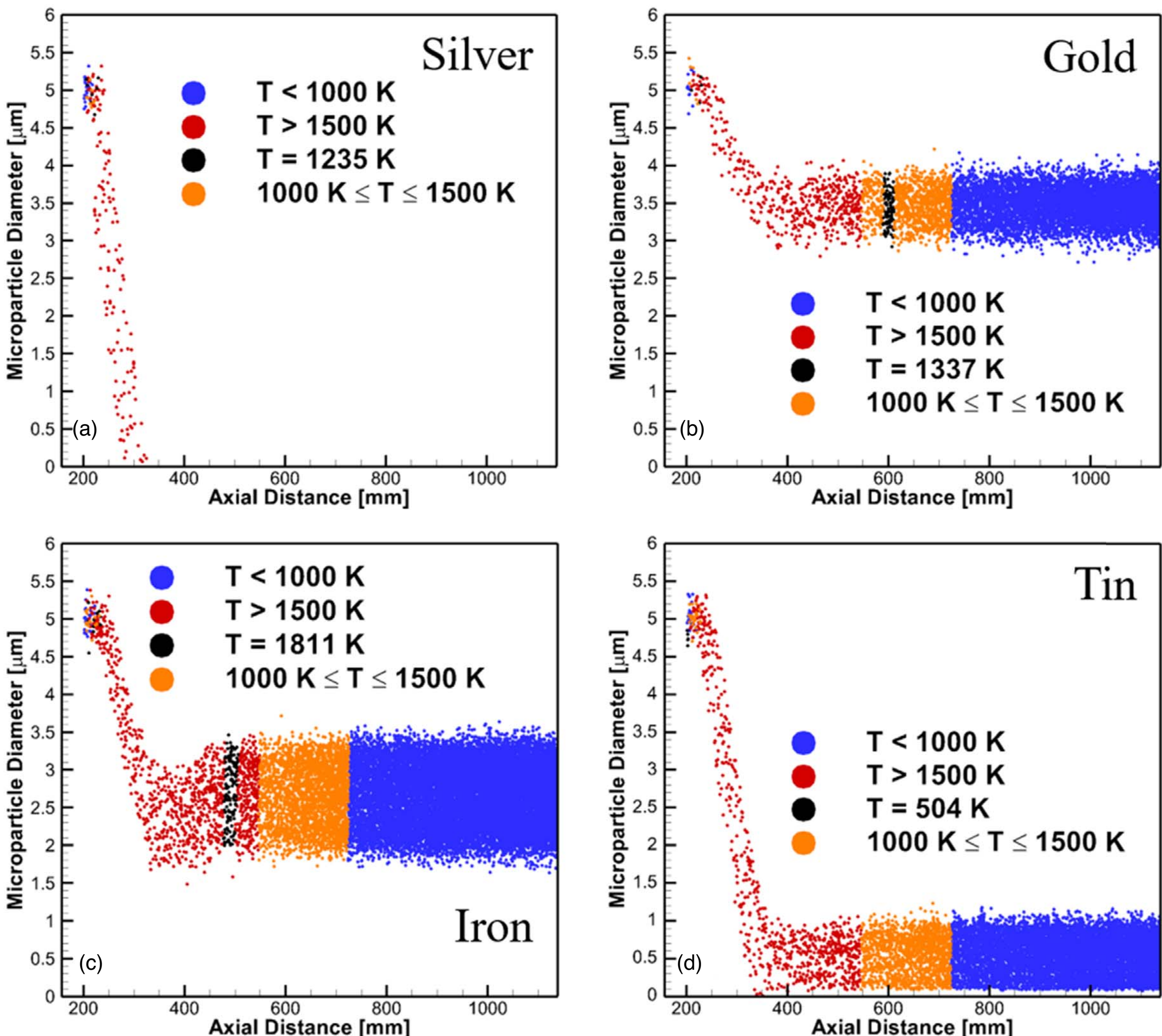

Fig. 32. (Color online) Particle distributions in the axial direction for different metal species of (a) silver, (b) gold, (c) iron, and (d) tin with a nozzle length of 202 nm from the ICP.

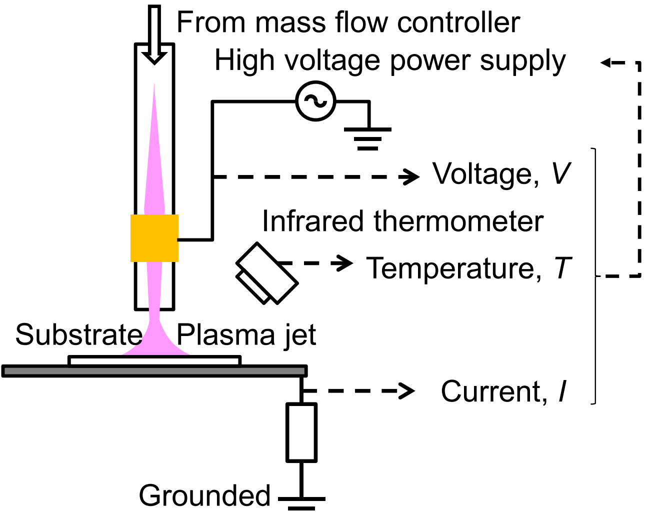

Fig. 33. (Color online) Setup of the APPJ irradiation system. The applied voltage is manipulated by the controller. The MPC is applied by the real-time measurement of voltage, current and substrate temperature.

Closed loop simulations and real time control using a low memory fast approximate nonlinear model predictive control (NMPC) strategy for an APPJ, handles nonlinear control at fast sampling time and DNN approximate an implicit NMPC law with an explicit control law.[261] The increasing complexity of modern technical systems can exacerbate model uncertainty in MPC. Real-time learning of model improved control performance by reducing plant-model mismatch. A learning-based stochastic model predictive control (LB-SMPC) strategy for reference tracking of stochastic linear systems with additive state-dependent uncertainty was demonstrated. Standard reachability and statistical tools were leveraged along with the state-dependent uncertainty model to develop a chance constraint-tightening approach, which ensured state constraint satisfaction in probability. The stability and recursive feasibility of the LB-SMPC strategy were established for tracking time-varying targets.[262]

6. Recent progress in surface chemistry for semiconductor fabrication

6.1. Prediction of sputtering rates—a data-driven scientific approach

The dimensions of advanced semiconductor devices are now approaching the sizes of atoms, and further improvements in performance have been achieved using complex 3D device structures and new materials. Plasma processing, which is widely used in semiconductor manufacturing, is a key technology for forming complex device structures on

© 2022 The Author(s). Published on behalf of
The Japan Society of Applied Physics by IOP Publishing Ltd

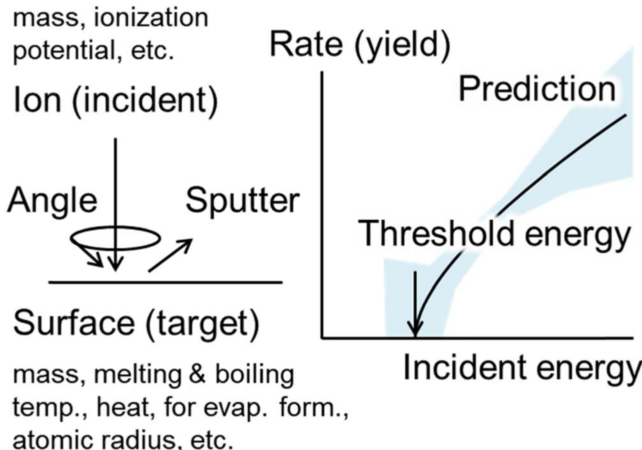

Fig. 34. (Color online) A scheme of sputtering process and typical representation of incident energy-dependence of sputtering yields. Lower energies than the threshold are negligible of the sputtering and an increase in the incident energy yields the rate dependent on a squared root of incident energy.

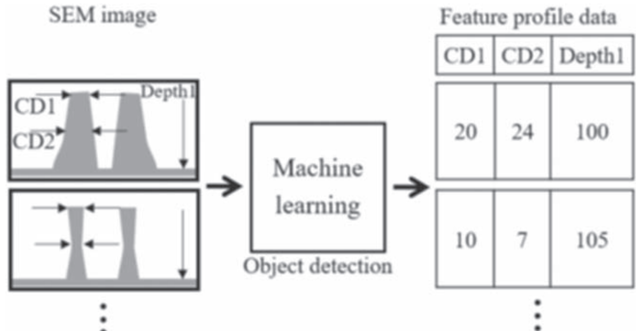

Fig. 35. Schematic illustration of the extraction of feature profile values using ML. Critical dimensions (CD1 and CD2) and etched depth (Depth1) are used for feature extraction variables.

material surfaces with atomic-scale accuracy. For various non-conventional materials used in micro/nanoelectronic devices, such as ferromagnetic metals for magnetoresistive random-access memories and perovskite-type oxides for resistive random-access memories, new etching and deposition process techniques often need to be developed for better process control and efficiency. In most cases, the interactions between the newly introduced material surfaces and the conventional or newly introduced gaseous species of plasma processing are not well understood, making the process development highly challenging and costly. Furthermore, having a variety of choices for surface materials and process conditions increases the complexity of process development, and an exhaustive search for process optimization by experiments becomes prohibitively expensive. One of the possible ways to tackle these challenges is to use ML to predict the gas-phase and surface reactions of plasma processing based on the existing knowledge of such systems.

In the development of classical interatomic potential models, plasma-surface interactions can be modeled using classical molecular dynamics (MD) simulations for a large number of atoms representing a surface material and incident species (e.g. ions and radicals).[263] One of the major challenges in such simulations is the development of new potential functions for new materials.[264–266] Data on the total potential energies of multi-atom systems obtained from density functional theory (DFT) calculations can be used to construct interatomic potential models using ML techniques.[267,268] The development of interatomic potential functions that can represent both small molecules and large solids with reasonable accuracy is a significant challenge.

To predict the sputtering yields, experimental and simulation data of the physical sputtering yields of single-element materials under single-species ion bombardment obtained as functions of the ion incident energy for normal injection by the mid-90s are summarized in Ref. 269 (Fig. 34). It has been found that the sputtering yield generally depends strongly only on a relatively small number of physical parameters, such as the masses of the material and incident atoms, and the melting temperature of the material.[270] Based on Gaussian process regression, the sputtering yield was predicted for various combinations of materials and incident ion species for which experimental data was lacking.[271]

6.2. Autonomous image processing of plasma-processed micro- and nano-features

Next, as shown in Fig. 12 for the plasma processing hierarchy, plasma etching can remove materials from unmasked area where it uncovered a resist mask. After the plasma etching, cross-sections of etched features are checked by microscopic techniques. From the observation, images of the cross-sections are analyzed in quality check control of the manufacturing. The smallest dimension of the open area of etched features is called critical dimension. As well as the dimensions, profile shapes of the etched features are important for the control, because the shape abnormality may cause electrical opening or shortage of device interconnects, and so on.

Selecting the appropriate CD and depth as feature profile parameters and the exact values of the feature parameters in the etching results of scanning electron microscope (SEM) images are required to evaluate the etching profile. The prediction accuracy of the ML model also depends on the quality of the feature parameters and values. In addition, the feature parameters change; therefore, the parameters must be measured again because better measurement points can be found by repeating the etching experiments. Therefore, the measurement of feature values in SEM images is as time-consuming as etching experiments. Figure 35 shows a schematic illustration of object detection using ML, which can be used for auto-measuring feature values. The object detection model learns the relationship between the SEM images and the positions of each feature profile parameter in the images which can improve the measurement speed and quality.[272]

Region-based CNN (R-CNN)[273,274] can be applied to recognize and crop a unit pattern, such as a line and space pattern, for which the width, depth, and thickness are measured in SEM images. Semantic segmentation can be applied to identify materials or vacuum areas, such as masks, etched trenches or holes, and substrates in SEM images. Typical CNN and generative adversarial networks are applied to the quality enhancement of CD-SEM (a top view of a sample piece or wafer) images.[275]

6.3. Advanced process control in plasma etching

Controls of plasma processing are issued on problems. To date, no fully closed loop control has been achieved because of its complexity. Statistics of process results are used for

© 2022 The Author(s). Published on behalf of The Japan Society of Applied Physics by IOP Publishing Ltd

checking and controlling each process. A semi-closed loop control can be used. Recurrently, a monitor of the process results, updates to modify parameters of a process recipe by feedback.

The development of a RNN-based model predictive controller for a plasma etching process on a 3D substrate was reported by Xiao et al.[276] Time-series data obtained by a spatial-temporal discrete method were computed by the fluid model and kinetic MC (kMC) model concurrently. A neural network was used to reduce computational resources and optimize the model-based feedback control using proportion integral (PI) loops.[277,278]

The feed-forward ANN model was used to determine the optimal operating conditions for the thermal ALE process of aluminum oxide, as reported by Yu et al.[279] The kMC algorithm was based on the calculated activation energies of half cycles of kinetic mechanisms for hydrofluoric acid (HF) and tri-methyl aluminum (TMA) using the DFT.

6.4. Advanced process control of chemical vapor and atomic layer depositions

Process controllers are generalized in a class of nonlinear dynamic systems. If nonlinear PDEs are linearized by taking the component of a Taylor series expansion, the stability of the systems can be analyzed using the Lyupanov function. It was reported that the closed loop stability analysis failed, and the slow and fast variables in the system were separated.[280] In addition to identifying the fast and slow process state variables,[281] the development of a Lyupanov-based model predictive controller using the feed-forward neural network model was reported by Dodhia et al.[282] The model predictive controller systems for nonlinear processes could be utilized to predict nonlinear dynamics by RNN models in open-loop simulations.[283,284]

The multiscale data-driven model from a first-principles-based multiscale CFD model was utilized for a single-wafer process of thermal atomic layer deposition (ALD) for SiO_2 thin-film deposition using bis(tertiary-butylamino)silane (BTBAS) and ozone as the precursors,[285–287] for a vertical industrial-scale furnace ALD reactor[288] and for plasma-enhanced atomic layer deposition (PEALD) of SiO_2 using BTBAS and Ar/O_2 plasmas.[289]

Multiscale CFD simulations of PEALD of hafnium dioxide (HfO_2) were reported by Yun et al.[290,291] Closed loop results under a feedback controller and integration of feedback and R2R control were demonstrated.[292]

The feed-forward Bayesian regularized ANN model was also used to determine the feasible operating region and to identify the optimal process conditions, as reported by Ding et al.[293]

A CFD model of the ALD reactor for ZnO deposition inside porous Al_2O_3 was constructed, and the prediction of optimal conditions was performed using the data-driven model, as reported by Zhyang et al.[294,295]

Dallaev reported the amount of hydrogen impurities in ALD aluminum nitride (AlN) films deposited by PEALD using TMA and $N_2 + H_2$ plasma and analyzed them using elastic recoil detection analysis, nuclear reaction analysis, and secondary-ion mass spectrometry.[296]

Sharma et al. reviewed the science-guided ML approach for nonlinear chemical processes.[297] The dynamic behavior of complex, nonlinear chemical processes is captured from operational data and learned by ML techniques using RNNs and feed-forward neural networks.[298] Paulson et al. compared optimization methods for simulated ALD processes, including random optimization, Bayesian optimization, and expert system optimization.[299]

Cheimarios et al. reviewed a multiscale process at the reactor scale and atomic-scale based on kMC models of physicochemical surface phenomena in deposition processes compared with molecular mechanics or MD.[300,301] Albao reported that a combined DFT and kMC simulation of epitaxial growth and surface diffusion was conducted under far-from-equilibrium conditions, however different kinetics with pinning effect of diffusing atoms appear, and not equal surface mobility.[302,303]

The radial and azimuthal uniformities of hydrogenated amorphous silicon (a-Si:H) film deposition were controlled combining R2R and CFD models.[304,305]

The growth of amorphous carbon films by PECVD using H_2, CH_4, and C_3H_6 mixture was systematically and quantitatively analyzed by using appearance mass spectrometry and spectroscopic ellipsometry (Fig. 36). The acquired data was classified into levels of contribution of film deposition and obtained a correlation model between process conditions and film properties by a random forest regression model of ML. Further, the representative oxygen etching rates for the films could be predicted by the mass spectroscopic data through the learning model. The prediction accuracy was improved by the use of Shapley additive explanation value (SHAP) in ML.[306]

6.5. Fault detection and classification

Process fault detection was demonstrated using OES data. Abnormal equipment conditions were detected using the extended isolation forest approach to demonstrate the ICP of SF_6, O_2, and Ar mixtures.[307] A non-invasive in situ plasma monitoring sensor was installed in the main chamber with a small chamber to generate self-plasma OES to show the chemical species residing inside the chamber.[308,309]

It has been reported that the end-point detection technique is improved by the CNN-based classifier as compared with the third-order SVM and adaptive boosting (Adaboost) ensemble classifiers.[310]

Fault detection and classification of silicon etching in $SF_6/O_2/Ar$ plasma were performed using ML of OES data for advanced equipment control in real time. Parameters such as the electron temperature and Te density were derived from the SHAP for fault detection and control from the OES data. By combining the isolation forest algorithm for finding plasma abnormalities in real time and the Adaboost algorithm for classifying the root causes of faults, the DeepSHAP algorithm identified critical parameters.[311] It has been reported that fault detection using a one-class SVM determines anomalies and fault classification using XGBoost.[312]

ML-based virtual metrology (VM) predicted the etch profile and depth in deep silicon trench etching with $SF_6/O_2/Ar$ plasma by using random forest and XGBoost algorithms, recipe-based equipment status variable identification (SVID) data, and OES data.[313] The etching profiles of Si were estimated from the ratio of the intensities of the oxygen emission to the fluorine lines in the OES data for the $SF_6/C_4F_8/O_2$ plasma.[314]

To monitor the condition of the equipment and examine the potential cause of the fault, SVID was identified from

© 2022 The Author(s). Published on behalf of The Japan Society of Applied Physics by IOP Publishing Ltd

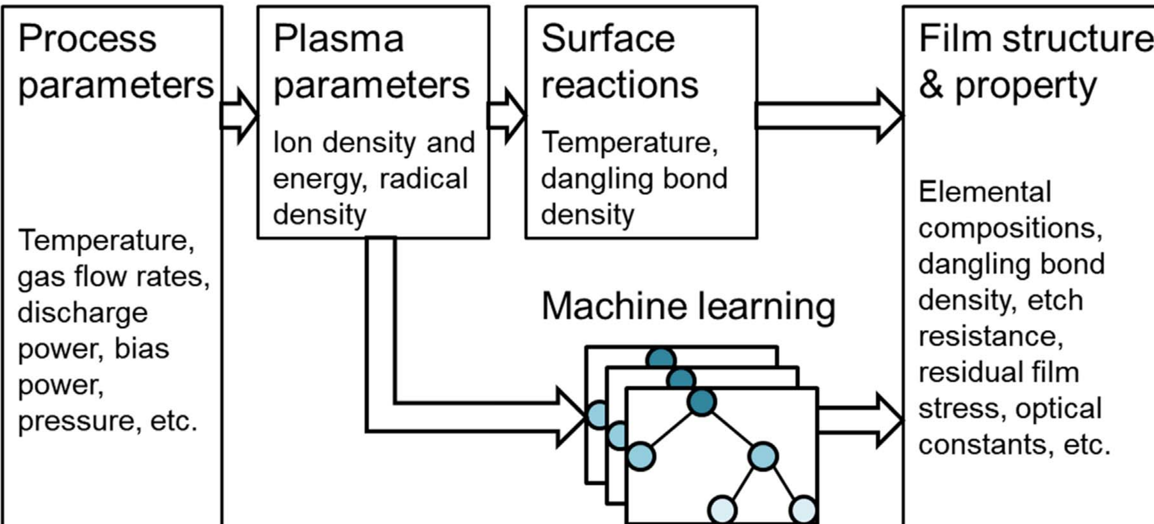

Fig. 36. (Color online) A direct, fast predicting method of film structure and property of the deposited films by using mass spectrometric detection of chemical species in gas-phase plasma and in situ spectroscopic ellipsometry of film quality.

sensor data using k-means and ML methods, k-nearest neighbors (kNNs algorithms),[315] and naive Bayes classifiers. Multidimensional SVID are graphically depicted using t-distributed stochastic neighbor embedding.[316]

ANNs have been reported to provide accurate real-time fault detection of overhead transport systems, which consist of a rail network and vehicles in 300 mm semiconductor factories.[317] The sheet resistance of sputter-deposited thin indium-doped zinc oxide films was predicted by deep learning of the ANN of the spectral data of plasma emission.[318]

A data-driven method of AdaBoost was implemented to identify the key features of process monitoring and for fault detection of natural variation in wafer-to-wafer in semiconductor manufacturing.[319]

The plasma density of the etch equipment was predicted using a regression method of multilayer perceptron employing a pre-trained variational auto-encoder of the OES data.[320] The real-time end-point of SiO_2 plasma etching using OES data was improved by using a Gaussian mixture model as compared with the clustering method of the modified k-means cluster analysis.[321] An integrated algorithm of regression and clustering of wafer defects in the semiconductor manufacturing process was improved by prescreening of degradation in the yield at early evaluation, which was processed sequentially.[322] Abnormal discharge in the aluminum sputtering chamber was detected by using equivalent electrical circuits.[323]

Tsuda et al. developed the equipment monitoring system that handles the data in a superior method in high speed and in real time. They developed a system which can stop automatically when the equipment was detected as fault condition and extract immediately key data. The high-speed and high-accuracy process control system was developed and implemented virtual metrology and the R2R function for the purpose to reduce process variation.[324] Big data challenges in semiconductor manufacturing are solved effectively in advanced process control, predictive maintenance, virtual metrology, and yield prediction.[325] Furthermore, the state-of-the-art metrology in semiconductor industry has advanced significantly. Nanoscale roughness and atomical defects are evaluated by CD scanning electron microscopy (CD-SEM), scatterometry, atomic force microscopy (AFM), small angle scattering X-ray (SAXS), and transmission electron microscopy (TEM).[326] No single method solves adequate measurements. The advanced data would be able to meet the future demands and increase performance of modeling and simulations.

7. Perspectives

7.1. Virtual metrology (VM)

Typically, research in physics explores a universal theory that can explain the data by deriving first-principles. We believe that these theoretical representations correspond to the experimental data. Considering statistics, fitting the data with a theoretical curve can guarantee the correctness of the physical theory. Conversely, it destroys any theory for data fitting, and only using informatics approaches is criticized as non-scientific. This review and recent trends show that the research of effective methods to solve problems that are too costly to reproduce is worthwhile, even if they can be solved as a complete theory.[327] In this review, it has already been discussed that ML techniques can effectively handle the BE solver. Currently, only time and space equilibrium (flow) velocity distribution functions are being handled. In future, time- and space-dependent calculations will be performed. In addition to the velocity space, the position space and time scale will be considered to address higher-dimensional computational domains. Consequently, the proposed method is expected to reduce memory usage in the future.

As mentioned in Sect. 2, plasma processes behave in a nonlinear manner in a nonequilibrium state. The plasma processing architecture is complex to construct by stacking blocks of the elementary reactions. Its complexity is solved using data assimilation methods in modeling hierarchies. That is, real-time monitoring feeds forward and back into the predictive computations. Thus, plasma processing as a target can be reproduced in a virtual environment using data-driven simulations with science-based modeling. Consequently, the

© 2022 The Author(s). Published on behalf of The Japan Society of Applied Physics by IOP Publishing Ltd

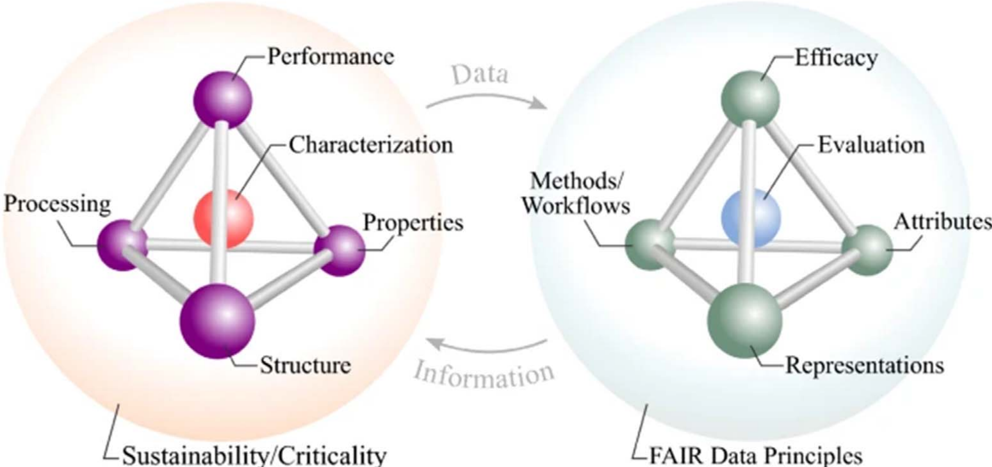

Fig. 37. (Color online) Materials-information twin tetrahedra of process-structure-property-performance (PSPP) reciprocity [Reprinted from M. E. Deagen, et al., *MRS Bull.* 47, 38 (2022).[344]].

virtual methodology for the plasma process will be able to realize effective development of plasma processes.

7.2. Material informatics and plasma informatics

In the development phase of new materials, material informatics is progressing as an experimental technique to explore new materials using high-throughput screening (HTS). Wakabayashi et al. demonstrated Bayesian optimization of the molecular beam epitaxy of ternary compounds, such as $SrRuO_3$.[328–340] HTS techniques can reduce the number of trials and reach a goal using predictive conditions obtained from the data of previous runs.[341] Predictive RbR control has enabled the efficient development of a processing method for new materials.

In practice, material design is a process of developing material functionality in three stages.[342] The stages contain "process", "structure", and "property". The properties in the third stage determine the total performance of the new material. Thus, this representation of the process-structure-property-performance (PSPP) reciprocity gives knowledge in the form of relationships among these factors.[343] The framework expands into materials and informatics and this is called as materials-information twin tetrahedral (MITT)[344] (Fig. 37).

In the case of plasma processing research, the time evolution of processing should be further considered when compared with materials informatics. In this review, RNN approaches are introduced as examples. Informatics techniques rely on each discipline and problem. In the past, plasma science has developed in its own manner and its original concepts are characteristic, even when compared with ordinary disciplines, such as fluid dynamics and material sciences. The theory and instrumentation in plasma science, that is, in plasma informatics, are expected to develop in their own ways. Similarly, the data-driven scientific approaches in plasma science will be unique and different from those in condensed matter physics and fluid mechanics.[327]

Materials are stationary and it is sufficient to consider their static phases. Plasma processes as manufacturing technologies must take into account the interactions among the excited plasma phases, the transports of reactive species in the sheath regions, and the activated surface reactions. In other words, all the plasma processes occur instantaneously. Therefore, sequences and dynamic behaviors in plasma processes must be considered, and differentiation of state variables for the plasma processes plays an important role in understanding and controlling plasma-based stimulations to systems, where the physical action (the impulse) catalyzes chemical relaxations.[8]

Analogous to the PSPP chain, a plasma processing-information relationship has a tetrahedron framework involving four edges, such as electron dynamics, chemical kinetics, sheath boundary transport, and surface reactions (ECSS) (Fig. 38). In the context on "how should we know the best recipe for plasma process?", it is important to recall the science-based explanation of electron-dynamics and chemical kinetics, serving to quantum chemistry and statistical analysis with the Boltzmann equation. These give knowledge for complex and heterogeneous reactive species. Instead, processing performance have to be known transport and reactions of these species at targeted surface. In this aspect, the ECSS relationship may explain the process performance.

In the other fields, supervised ML can derive models automatically from labeled training data. However the method is only good as the quality of the data.[345,346] In other words, good quality data is required to progress in the field. We emphasize that science-based approaches involving diagnostics and first principle computation are becoming more important. The informatics is supported by scientific data of the plasma processing. Repeatedly the ML method can actually help development and establishment of principles. The data-driven science facilitates a sort of knowledge, thus an importance of that approaches can be found in seamless integration of theory, computation, and experiments. At least, the data science can accelerate the development and also guide future directions.

7.3. Smart manufacturing (SM) and digital transformation (DX)

In manufacturing processes using plasma, monitoring and controlling processes are important for improving productivity and yields.

© 2022 The Author(s). Published on behalf of The Japan Society of Applied Physics by IOP Publishing Ltd

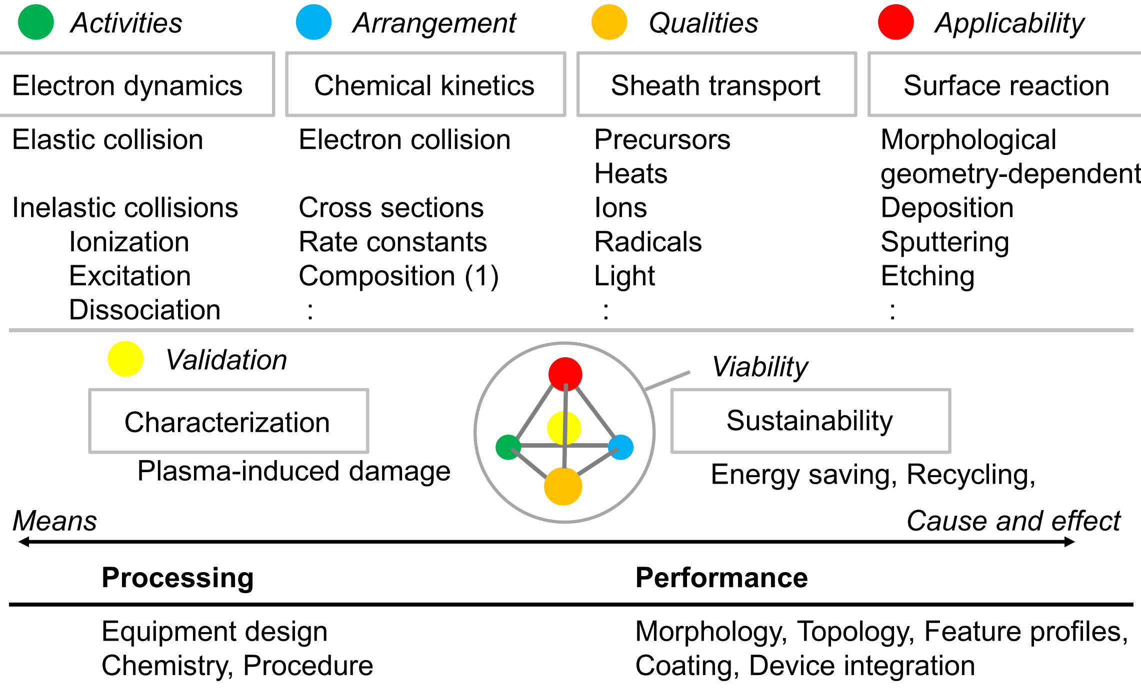

Fig. 38. (Color online) A plasma processing-information relationship of electron dynamics, chemical kinetics, sheath boundary transport, and surface reactions (ECSS) through consideration of activities, applicability, validation, and viability. Plasma informatics is developing with the framework that considers both plasma science and technology with informatics side by side.

While the core of plasma processes is studied by science, collective behaviors of the chemical species ensembles are controlled by data-driven science and network science. The emerging science uses digital space to create smarter and more digitalized artificial control environments for manufacturing and industrial applications. In the previous Sects. 4–6, with the increase in computational power, combinations among theory, computation, and experiments have been progressing and all the data are fused and considered. There are unquestionable outcomes of the strategy of maximizing the use of fully computational power with the supports of data-driven science and informatics. However, no progress will stop somewhere in absence of physics, if only mathematical conclusions are drawn.

Revisiting the fundamentals and principles of reactive plasma processing, electromagnetic power converts of electron dynamics and the chemical reactions of electrons and reactants take place including transports of species generated in plasma toward the reacted boundaries. It is desirable to know the control knobs of the inputs to achieve the outputs such as morphological shapes and material properties. In other words, electron collision processes are indispensable for determination the processing outputs. In this view, the most important point begins with the selection of precursor, that is, chemistry. Therefore elemental reactions in electron-molecule collisions must be taken into account for controlling the plasma processing based on the physics-based approach. For this purpose, we stressed to attract quantum chemical calculation-based data. In near future, the computational prediction helps in development of an emerging precursor.

If a virtual environment for experiments will be available, researches will be able to conduct a process development. Stolterman and Fors wrote that “the digital transformation can be understood as the changes that the digital technology causes or influences in all aspects of human life. The research challenge has to be accepted on behalf of humans, not in their role as users, customers, leaders, or any other role, but as humanity living a life.”[347] As a result, it is expected to reduce trial and errors during the development phase and promotes energy-saving development. Furthermore, experimental data should be stored in database (Fig. 39). Processing recipes are provided for a specific condition of processing. Processing results can be classified by software technique. During the processing, operational variables can also be monitored and sensed by sophisticated diagnostic methods. A set of time-series data is stored in the database. The development of such datasets is becoming more possible than ever imagined. Discoveries that could not be reached by conventional methodologies or human cognitive abilities are expected. The power of informatics to analyze diverse and vast datasets will lead to the discovery of unconscious phenomena and their laws. Consequently, we believe that the integrated fusion of informatics and engineering is an indispensable way to realize the digitalization—digital transformation—of the research environment and to open a new avenue of plasma informatics.

8. Conclusion

The science-based and data-driven approaches to control the low-temperature plasma processing systems are progressing with the state-of-the-art machine learning, etc. The science-based diagnostics of the plasma processes are reviewed and the multiscale modeling of plasma hierarchies are developed in advanced simulation methods. Especially for complex plasma etching processing, it is recognized significant developments for fabrication of high-aspect-ratio features at atomic-scale precision. The data-driven scientific approaches are also emerging for the purposes of understanding system

© 2022 The Author(s). Published on behalf of The Japan Society of Applied Physics by IOP Publishing Ltd

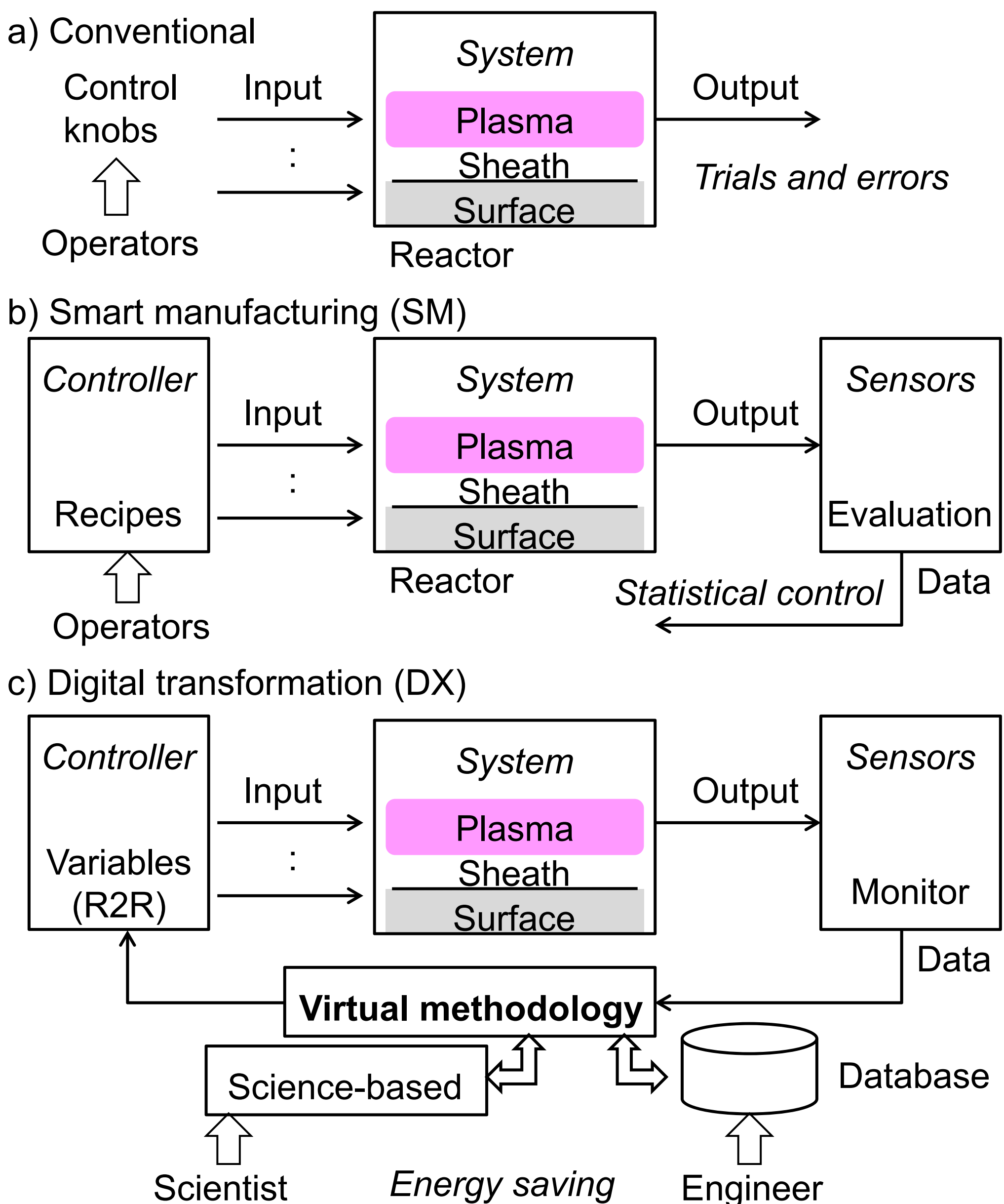

Fig. 39. (Color online) Development of optimization and control of plasma processing. The conventional optimization is carried out by trials and errors. The smart manufacturing level allows the use of real-time sensing data and a statistical control can reduce a number of trials. The digital transformation automatically controls the processing controller applying virtual methodology techniques.

behaviors effectively. Physics-based modeling of a set of nonlinear equations, even if accurate, is often computationally intensive or solution-less. The machine learning approaches can solve these problems. Herein the demonstrations of EVDF and spatial distribution of plasma density are reviewed. Currently, the goal of developments to control complex plasma processing is to create a virtual methodological field that combines theory, computation and experiment. Accordingly a level of advanced process control has been reached and improved. In the next future, the virtual methodology and plasma informatics is continuing to develop for comprehensive control of plasma processing and for creation of industrial applications based on low-temperature plasma sciences.

Acknowledgments

The authors would like to thank Dr. Yuki Wakabayashi and Dr. Daisuke Nishijima for the fruitful discussions; professors Dr. Noriyasu Ohno, Dr. Hirotaka Toyoda, Dr. Shin Kajita, Dr. Yoshihiro Kangawa, and Dr. Shinya Kumagai; and all the members of the program committee of the 14th International Symposium on Advanced Plasma Science and Its Applications for Nitrides and Nanomaterials and the 15th International Conference on Plasma-Nanotechnology and Science (ISPlasma2022/IC-PLANTS2022). SH is grateful to Prof. Jong-Shinn Wu, Dr. Kuan-Lin Chen of National Yang Ming Chiao Tung University, Taiwan, and Dr. Zoltan Donko of the Wigner Research Centre for Physics, Hungary, for providing simulation data as well as Prof. Ryo Yoshida and Dr. Stephen Wu of the Institute of Statistical Mathematics, Japan, Prof. Sadruddin Benkadda of Aix-Marseille University, France, and Prof. Ikutaro Hamada of Osaka University for the helpful discussions. SH acknowledges that this work was partially supported by Tokyo Electron Ltd., the Japan Society of the Promotion of Science (JSPS) Grants-in-Aid for Scientific Research (S)

© 2022 The Author(s). Published on behalf of The Japan Society of Applied Physics by IOP Publishing Ltd

15H05736, (A) 21H04453, Challenging Research (Exploratory) 18K18753, JSPS Core-to-Core Program JPJSCCA2019002, and Osaka University International Joint Research Promotion Programs 406 (Type A). KI thank professors Dr. Masaru Hori, Dr. Makoto Sekine, Dr. Masaharu Shiratani, Dr. Kazunori Koga, and Dr. Toshiro Kaneko for their encouragement and the Hori-Ishikawa laboratory members for technical assistances in this review. KI acknowledges that this work was partially supported by JSPS KAKENHI Nos. 20H00142, 21H01073, and 21H04451.

ORCID iDs

Satoru Kawaguchi https://orcid.org/0000-0003-3115-8719
Hae June Lee https://orcid.org/0000-0003-3401-3355
Kazumasa Ikuse https://orcid.org/0000-0003-1648-628X
Satoshi Hamaguchi https://orcid.org/0000-0001-6580-8797
Kenji Ishikawa https://orcid.org/0000-0002-8288-6620

1) M. A. Lieberman and A. J. Lichtenberg, *Principles of Plasma Discharges and Materials Processing* (Wiley-Interscience, New York, 2005) 2nd ed.
2) A. Fridman, *Plasma Chemistry* (Cambridge University Press, Cambridge, 2008).
3) I. Adamovich et al., "The plasma roadmap: low temperature plasma science and technology," J. Phys. D: Appl. Phys. **50**, 323001 (2017).
4) I. Adamovich et al., "The 2022 plasma roadmap: low-temperature plasma science and technology," J. Phys. D; Appl. Phys. **55**, 373001 (2022).
5) R. Anirudh et al., "2022 review of data-driven plasma science," (2022), arXiv:2205.15832.
6) S. Hamaguchi, "Plasma informatics—application of data-driven science to plasma science," J. Institute Electrostat. Japan **43**, 198 (2019).
7) T. Hey and J. Gray, *The Fourth Paradigm: Data-Intensive Scientific Discovery* (Microsoft Press, Redmond, WA, 2009).
8) K. Ishikawa, "Perspectives on functional nitrogen science and plasma-based in situ functionalization," Jpn. J. Appl. Phys. **61**, SA0802 (2022).
9) T. Kaneko et al., "Functional nitrogen science based on plasma processing: quantum devices, photocatalysts and activation of plant defense and immune systems," Jpn. J. Appl. Phys. **61**, SA0805 (2022).
10) A. Vardell et al., "The 2016 thermal spray roadmap," J. Thermal Spray Technol. **25**, 1376 (2016).
11) P. Fauchais, M. Vardelle, and S. Goutier, "Atmospheric plasma spraying evolution since the sixties through modeling, measurements and sensors," Plasma Chem. Plasma Process. **37**, 601 (2017).
12) T. Yoshida, "Toward a new era of plasma spray processing," Pure Appl. Chem. **78**, 1093 (2006).
13) K. Homma, M. Kambara, and T. Yoshida, "High throughput production of nanocomposite SiOx powders by plasma spray physical vapor deposition for negative electrode of lithium ion batteries," Sci. Technol. Adv. Mater. **15**, 025006 (2014).
14) N. Branland, E. Meillot, P. Fauchais, A. Vardelle, F. Gitzhofer, and M. Boulos, "Relationships between microstructure and electrical properties of RF and DC plasma-sprayed titania coatings," J. Thermal Spray Technol. **15**, 53 (2006).
15) J. P. Trelles, E. Pfender, and J. V. R. Heberlein, "Multiscale finite element modeling of arc dynamics in a DC plasma torch," Plasma Chem. Plasma Process. **26**, 557 (2006).
16) J. P. Trelles, E. Pfender, and J. V. R. Heberlein, "Thermal none-quilibrium simulation of an arc plasma jet," IEEE Trans. Plasma Sci. **36**, 1026 (2008).
17) T. Iwase et al., "Progress and perspectives in dry processes for leading-edge manufacturing of devices: toward intelligent processes and virtual product development," Jpn. J. Appl. Phys. **58**, SE0804 (2019).
18) G. S. May and C. J. Spanos, *Fundamentals of Semiconductor Manufacturing and Process Control* (Wiley, New York, 2006).
19) G. Taguchi, "Quality engineering in Japan," Communication of Statistics—Theory and methods **14**, 2785 (1985).
20) M. Hiramatsu and M. Hori, "Synthesis of aligned carbon nanowalls using radio-frequency plasma enhanced chemical vapor deposition," Jpn. Plasma Fusion Res. **81**, 669 (2005).
21) T. Goto and M. Hori, "Radical behavior in fluorocarbon plasma and control of silicon oxide etching by injection of radicals," Jpn. J. Appl. Phys. **35**, 6521 (1996).
22) M. Hori and T. Goto, "Insights into sticking of radicals on surfaces for smart plasma nano-processing," Appl. Surf. Sci. **253**, 6657 (2007).
23) T. Tsutsumi, T. Ohta, K. Ishikawa, K. Takeda, H. Kondo, M. Sekine, M. Hori, and M. Ito, "Robust characteristics of semiconductor-substrate temperature measurement by autocorrelation-type frequency-domain low-coherence interferometry," Jpn. J. Appl. Phys. **54**, 01AB03 (2015).
24) S. Takahashi et al., "An autonomously controllable plasma etching system based on radical monitoring," Jpn. J. Appl. Phys. **51**, 076502 (2012).
25) H. Yamamoto, H. Kuroda, M. Ito, T. Ohta, K. Takeda, K. Ishikawa, H. Kondo, M. Sekine, and M. Hori, "Feature profiles on plasma etch of organic films by a temporal control of radical densities and real-time monitoring of substrate temperature," Jpn. J. Appl. Phys. **51**, 016202 (2012).
26) K. Takeda, K. Ishikawa, and M. Hori, "Wide range applications of process plasma diagnostics using vacuum ultraviolet absorption spectroscopy," Rev. Mod. Plasma Phys. **6**, 13 (2022).
27) T. Suzuki, K. Takeda, H. Kondo, K. Ishikawa, M. Sekine, and M. Hori, "Temporal changes in absolute atom densities in H_2 and N_2 mixture gas plasmas by surface modifications of reactor wall," Jpn. J. Appl. Phys. **53**, 050301 (2014).
28) T. Suzuki, K. Ishikawa, K. Takeda, H. Kondo, M. Sekine, and M. Hori, "Recovery of atom density drift caused by change in reactor wall conditions by real-time autonomous control," J. Phys. D: Appl. Phys. **47**, 422002 (2014).
29) Y. Fukunaga, T. Tsutsumi, H. Kondo, K. Ishikawa, M. Sekine, and M. Hori, "Narrow free-standing features fabricated by top-down self-limited trimming of organic materials using precisely temperature-controlled plasma etching system," Jpn. J. Appl. Phys. **58**, 020906 (2019).
30) K. Ishikawa et al., "Progress in nanoscale dry processes for fabrication of high-aspect-ratio features: how can we control critical dimension uniformity at the bottom?" Jpn. J. Appl. Phys. **57**, 06JA01 (2018).
31) R. Itatani, "The present situation and future prospects," In "Control of reactive plasmas, what and how," Denki Gakkai-shi **110**, 167 (1990) [In Japanese].
32) B. B. Sahu, J. G. Han, H. R. Kim, K. Ishikawa, and M. Hori, "Experimental evidence of warm electron populations in magnetron sputtering plasmas," J. Appl. Phys. **117**, 033301 (2015).
33) H. Sugai and K. Nakamura, "Recent innovations in microwave probes for reactive plasma diagnostics," Jpn. J. Appl. Phys. **58** (2019).
34) D. Ogawa, K. Nakamura, and H. Sugai, "A novel technique for in-situ simultaneous measurement of thickness of deposited film and electron density with two curling probes," Plasma Source. Sci. Technol. **29**, 075009 (2020).
35) D. Ogawa, K. Nakamura, and H. Sugai, "Experimental validity of double-curling probe method in film-depositing plasma," Plasma Sources Sci. Technol. **30**, 085009 (2021).
36) M. Hotta, D. Ogawa, and H. Sugai, "Real-time curling probe monitoring of dielectric layer deposited on plasma chamber wall," Jpn. J. Appl. Phys. **57**, 046201 (2018).
37) F. Boni, J. Jarrige, V. Desangles, and T. Minea, "The curling probe: a numerical and experimental study. Application to the electron density measurements in an ECR plasma thruster," Rev. Sci. Instrum. **92**, 033507 (2021).
38) D. Peterson, Y. Xiao, K. Ford, P. Kraus, and S. Shannon, "Electron temperature measurements with a hairpin resonator probe in a pulsed low pressure capacitively coupled plasma," Plasma Source. Sci. Technol. **30**, 065018 (2021).
39) S. J. Kim, J. J. Lee, Y. S. Lee, D. W. Kim, and S. J. You, "Effect of an inhomogeneous electron density profile on the transmission microwave frequency spectrum of the cutoff probe," Plasma Source. Sci. Technol. **29**, 125014 (2020).
40) S. J. Kim, J. J. Lee, Y. S. Lee, C. H. Cho, and S. J. You, "Crossing frequency method applicable to intermediate pressure plasma diagnostics using the cutoff probe," Sensors **22**, 1291 (2022).
41) T. Yamaguchi, T. Komuro, C. Koshimizu, S. Takashima, K. Takeda, H. Kondo, K. Ishikawa, M. Sekine, and M. Hori, "Direct current superposed dual-frequency capacitively coupled plasmas in selective etching of SiOCH over SiC," J. Phys. D: Appl. Phys. **45**, 025303 (2012).
42) Y. Ohya, K. Ishikawa, T. Komuro, T. Yamaguchi, K. Takeda, H. Kondo, M. Sekine, and M. Hori, "Spatial profiles of interelectrode electron density in direct current superposed dual-frequency capacitively coupled plasmas," J. Phys. D: Appl. Phys. **50**, 155201 (2017).
43) K. Muraoka and A. Kono, "Laser Thomson scattering for low-temperature plasmas," J. Phys. D: Appl. Phys. **44**, 0403001 (2011).

© 2022 The Author(s). Published on behalf of The Japan Society of Applied Physics by IOP Publishing Ltd

44) J. Sun et al., "Local pressure calibration method of inductively coupled plasma generator based on laser Thomson scattering measurement," Sci. Rep. **12**, 4655 (2022).
45) Y. Wang, J. Shi, Y. Li, Y. Zhao, C. Li, C. Feng, and H. Ding, "High resolution laser Thomson scattering system with automatic data analysis software platform for diagnosis of the low-temperature plasmas," Rev. Sci. Instrum. **92**, 123508 (2021).
46) Y. Pan, K. Tomita, K. Uchino, A. Sunahara, and K. Nishihara, "Time-resolved two-dimensional measurements of the electron density, electron temperature, and drift velocity of laser-produced carbon plasmas using the ion feature of collective laser Thomson scattering," Appl. Phys. Express **14**, 066001 (2021).
47) D. L. Crintea, U. Czarnetzki, S. Iordanova, I. Koleva, and D. Luggenholscher, "Plasma diagnostics by optical emission spectroscopy on argon and comparison with Thomson scattering," J. Phys. D: Appl. Phys. **42**, 045208 (2009).
48) Y. Yamashita, F. Yamazaki, and H. Akatsuka, "Diagnostics of low-pressure discharge argon plasma by multi-optical emission line analysis based on the collisional-radiative model," Jpn. J. Appl. Phys. **58**, 016004 (2019).
49) H. Horita, D. Kuwahara, H. Akatsuka, and S. Shinohara, "Estimating electron temperature and density using improved collisional-radiative model in high-density RF argon plasma," AIP Adv. **11**, 075226 (2021).
50) D. Nishijima, M. I. Patino, and R. P. Doerner, "New application of hyperspectral imaging to steady-state plasma observations," Rev. Sci. Instrum. **91**, 083501 (2020).
51) D. Nishijima, S. Kajita, and G. R. Tynan, "Machine learning prediction of electron density and temperature from He I line ratios," Rev. Sci. Instrum. **92**, 023505 (2021).
52) S. Kajita, D. Nishijima, K. Fujii, G. Akkermans, and H. van der Meiden, "Application of multiple regression for sensitivity analysis of helium line emissions to the electron density and temperature in Magnum-PSI," Plasma Phys. Control. Fusion **63**, 055018 (2021).
53) Specim, Spectral imaging, Ltd., (2022), last accessed on September https://specim.fi/iq/.
54) F. J. Chang, D. Nishijima, and G. R. Tynan, "Rough-surface effect on sputtering of Cr bombarded by low-energy He plasma," Nucl. Mater. Energy **29**, 101077 (2021).
55) R. Chen, H. Huang, C. Spanos, and M. Gatto, "Plasma etch modeling using optical emission spectroscopy," J. Vac. Sci. Technol. **14**, 1901 (1996).
56) M. Kanoh, M. Yamage, and H. Takada, "End-point detection of reactive ion etching by plasma impedance monitoring," Jpn. J. Appl. Phys. **40**, 1457 (2001).
57) Y. Ohya, M. Iwata, K. Ishikawa, M. Sekine, M. Hori, and H. Sugai, "Rapid electron density decay observed by surface-wave probe in afterglow of pulsed fluorocarbon-based plasma," Jpn. J. Appl. Phys. **55**, 080309 (2016).
58) T. Ueyama et al., "Electron behaviors in afterglow of synchronized dc-imposed pulsed fluorocarbon-based plasmas," Jpn. J. Appl. Phys. **56**, 06HC03 (2017).
59) B. B. Sahu, K. Nakane, K. Ishikawa, M. Sekine, T. Tsutsumi, T. Gohira, Y. Ohya, N. Ohno, and M. Hori, "Study of optical emission spectroscopy using modified Boltzmann plot in dual frequency synchronized pulsed capacitively coupled discharges with DC bias at low-pressure in $Ar/O_2/C_4F_8$ plasma etching process," Phys. Chem. Chem. Phys. **24**, 13883 (2022).
60) T. Makabe, "Current status and nature of high-frequency electronegative plasmas: basis for material processing in device manufacturing," Jpn. J. Appl. Phys. **58**, 110101 (2019).
61) Y. Lee, W. Song, and S. J. Hong, "In situ monitoring of plasma ignition step in capacitively coupled plasma systems," Jpn. J. Appl. Phys. **59**, SJJD02 (2020).
62) K. Hernandez, L. J. Overzet, and M. J. Goeckner, "Electron dynamics during the reignition of pulsed capacitively-coupled radio-frequency discharges," J. Vac. Sci. Technol. B **38**, 034005 (2020).
63) K. Hernandez, A. Press, M. J. Goeckner, and L. J. Overzet, "Optical emission intensity overshoot and electron heating mechanisms during the re-ignition of pulsed capacitively coupled Ar plasmas," J. Vac. Sci. Technol. B **39**, 024003 (2021).
64) C. H. Qu, S. K. Nam, and M. J. Kushner, "Transients using low-high pulsed power in inductively coupled plasmas," Plasma Source, Sci. Technol. **29**, 085006 (2020).
65) C. H. Qu, S. J. Lanham, S. C. Shannon, S. K. Nam, and M. J. Kushner, "Power matching to pulsed inductively coupled plasmas," J. Appl. Phys. **127**, 133302 (2020).
66) Y. Kasashima, "Easy-to-use detection method for micro-arc discharge in plasma etching equipment by measuring current flowing to ground," Jpn. J. Appl. Phys. **57**, 098002 (2018).
67) H. J. Yeom, K. H. You, J.-H. Kim, and H.-C. Lee, "Circuit model for flat cut-off probes with coplanar capacitance," Plasma Source Sci. Technol. **30**, 065012 (2021).
68) S.-W. Cho, J.-H. Moon, A. Zhang, and C.-W. Chung, "Control of the spatial distribution of ion flux in dual inductively coupled plasmas," J. Appl. Phys. **129**, 103305 (2021).
69) H. Abe, M. Yoneda, and N. Fujiwara, "Developments of plasma etching technology for fabricating semiconductor devices," Jpn. J. Appl. Phys. **47**, 1435 (2008).
70) T. Lill and O. Joubert, "The cutting edge of plasma etching," Science **319**, 1050 (2008).
71) T. Iwase et al., "Progress and perspectives in dry processes for nanoscale feature fabrication: fine pattern transfer and high-aspect-ratio feature formation," Jpn. J. Appl. Phys. **58**, SE0802 (2019).
72) M. Sekine, "Dielectric film etching in semiconductor device manufacturing: Development of SiO_2 etching and the next generation plasma reactor," Appl. Surf. Sci. **192**, 270 (2002).
73) K. Ishikawa et al., "Rethinking surface reactions in nanoscale dry processes toward atomic precision and beyond: a physics and chemistry perspective," Jpn. J. Appl. Phys. **58**, SE0801 (2019).
74) H. Miyajima, K. Ishikawa, M. Sekine, and M. Hori, "Review of methods for the mitigation of plasma-induced damage to low-dielectric-constant interlayer dielectrics used for semiconductor logic device interconnects," Plasma Process Polym. **16**, 1900039 (2019).
75) H. Miyajima, K. Ishikawa, M. Sekine, and M. Hori, "Chemical bond structures of porous SiOC Film ($k < 2.4$) for resistance of plasma induced damages," Micro Nano Eng. **3**, 1 (2019).
76) H. Miyajima, K. Watanbe, K. Ishikawa, M. Sekine, and M. Hori, "Adhesion enhancement and amine reduction using film redeposited at the interface of a stack of plasma-enhanced CVD dielectrics for Cu/low-k interconnects," Jpn. J. Appl. Phys. **58**, 020908 (2019).
77) H. Yamamoto, H. Kuroda, M. Ito, T. Ohta, K. Takeda, K. Ishikawa, H. Kondo, M. Sekine, and M. Hori, "Feature profiles on plasma etch of organic films by a temporal control of radical densities and real-time monitoring of substrate temperature," Jpn. J. Appl. Phys. **51**, 016202 (2012).
78) T. Tatsumi, "Quantitative control of plasma and surface reactions for dielectric film etching," Jpn. J. Appl. Phys. **61**, SA0804 (2022).
79) K. Eriguchi, "Characterization techniques of ion bombardment damage on electronic devices during plasma processing-plasma process-induced damage," Jpn. J. Appl. Phys. **60**, 040101 (2021).
80) H. Takahashi, K. Nakashima, T. Yamamoto, and H. Sugawara, "Stochastic electron energy gain in inductively coupled magnetized plasmas accompanying electron reflection at chamber wall," Jpn. J. Appl. Phys. **57**, 126101 (2018).
81) H. Takahashi and H. Sugawara, "Stochastic electron energy gain under sheath electric field near sidewall of chamber to drive inductively coupled magnetized plasmas," Jpn. J. Appl. Phys. **59**, 036001 (2020).
82) K. Nakashima, H. Takahashi, and H. Sugawara, "Phase-resolved profiles of electron energy deposition in inductively coupled radio-frequency plasmas driven under confronting divergent magnetic fields," Jpn. J. Appl. Phys. **58**, 116001 (2019).
83) H. Sugawara, "Derivation of the electron drift velocity vector in gas under crossed ac electric and dc magnetic fields assuming constant-collision-frequency models," Jpn. J. Appl. Phys. **58**, 108002 (2019).
84) Y. Nakata, T. Sato, and H. Sugawara, "Elliptic vector loci of average electron velocity in real gases under ac electric and dc magnetic fields," IEEE Trans. Plasma Sci. **49**, 83 (2021).
85) H. Sugawa and Y. Nakata, "Elliptic vector loci of average electron velocity of electron swarm in constant-collision-frequency model gas under ac electric and dc magnetic fields crossed at arbitrary angles," Eur. Phys. J. D **76**, 32 (2022).
86) J. Sivoš, D. Marić, N. Škoro, G. Malović, and Z. L. Petrović, "DC discharge in low-pressure ethanol vapour," Plasma Source Sci. Technol. **28**, 055011 (2019).
87) J. Sivoš, D. Marić, G. Malović, and Z. L. Petrović, "Low-pressure DC breakdown in alcohol vapours," Eur. Phys. J. D **74**, 64 (2020).
88) T. Hagino, H. Kondo, K. Ishikawa, H. Kano, M. Sekine, and M. Hori, "Ultrahigh-speed synthesis of nanographene using alcohol in-liquid plasma," Appl. Phys. Express **5**, 035101 (2012).
89) A. Ando, K. Ishikawa, H. Kondo, T. Tsutsumi, K. Takeda, T. Ohta, M. Ito, M. Hiramatsu, M. Sekine, and M. Hori, "Nanographene synthesis employing in-liquid plasmas with alcohols or hydrocarbons," Jpn. J. Appl. Phys. **57**, 026201 (2018).
90) A. Ando, K. Ishikawa, K. Takeda, T. Ohta, M. Ito, M. Hiramatsu, H. Kondo, M. Sekine, and M. Hori, "In-liquid plasma synthesis of

© 2022 The Author(s). Published on behalf of The Japan Society of Applied Physics by IOP Publishing Ltd

nanographene with a mixture of methanol and 1-butanol," ChemNanoMat **6**, 604 (2020).
91) T. Amano, H. Kondo, K. Ishikawa, T. Tsutsumi, K. Takeda, M. Hiramatsu, M. Sekine, and M. Hori, "Rapid growth of micron-sized graphene flakes using in-liquid plasma employing iron phthalocyanine-added ethanol," Appl. Phys. Express **11**, 015102 (2018).
92) J. Marjanović, D. Marić, G. Malović, and Z. L. Petrović, "Voltage–current characteristics of low-pressure discharges in vapors of several alcohols," J. Appl. Phys. **129**, 143303 (2021).
93) J. Marjanović, D. Marić, G. Malović, and Z. L. Petrović, "Effective ionization coefficients for low current dc discharges in alcohol vapours at low pressure," Eur. Phys. J. D **75**, 191 (2021).
94) Z. L. Petrovic et al., "Cross sections and transport coefficients for electrons in C_2H_6O and its mixtures with Ar and Ne," Eur. Phys. J. D **76**, 25 (2022).
95) I. Simonović, D. Bošnjaković, Z. L. Petrović, R. D. White, and S. Dujko, "Third-order transport coefficient tensor of electron swarms in noble gases," Eur. Phys. J. D **74**, 63 (2020).
96) I. Simonović, D. Bošnjaković, Z. Lj. Petrović, P. Stokes, R. D. White, and S. Dujko, "Third-order transport coefficient tensor of charged-particle swarms in electric and magnetic fields," Phys. Rev. E **101**, 023203 (2020).
97) I. Simonović, D. Bošnjaković, Z. L. Petrović, R. D. White, and S. Dujko, "Third-order transport coefficients for electrons in N_2 and CF_4: effects of non-conservative collisions, concurrence with diffusion coefficients and contribution to the spatial profile of the swarm," Plasma Source. Sci. Technol. **31**, 015003 (2022).
98) P. L. G. Ventzek, R. J. Hoekstra, and M. J. Kushner, "2-dimensional modeling of high plasma-density inductively-coupled sources for materials processing," J. Vac. Sci. Technol. B **12**, 461 (1994).
99) P. L. G. Ventzek, M. Grapperhaus, and M. J. Kushner, "Investigation of electron source and ion flux uniformity in high plasma-density inductively-coupled etching tools using 2-dimensional modeling," J. Vac. Sci. Technol. **12**, 3118 (1994).
100) P. L. G. Ventzek, T. J. Sommerer, R. J. Hoekstra, and M. J. Kushner, "2-dimensional hybrid model of inductively-coupled plasma sources for etching," Appl. Phys. Lett. **63**, 605 (1993).
101) D. Levko, C. Shukla, K. Suzuki, and L. L. Raja, "Plasma kinetics of c-C_4F_8 inductively coupled plasma revisited," J. Vac. Sci. Technol. B **40**, 022203 (2022).
102) A. Ranjan and P. L. G. Ventzek, "Simulations of hybrid direct current radiofrequency (dc/rf) capacitively coupled plasmas," Jpn. J. Appl. Phys. **58**, 036001 (2019).
103) I. Armenise and F. Esposito, "N + O_2(v) collisions: reactive, inelastic and dissociation rates for state-to-state vibrational kinetic models," Chem. Phys. **551**, 111325 (2021).
104) F. Rsposito and I. Armenise, "Reactive, inelastic, and dissociation processes in collisions of atomic nitrogen with molecular oxygen," J. Phys. Chem. A **125**, 3953 (2021).
105) E. Martines, "Interaction of cold atmospheric plasmas with cell membranes in plasma medicine studies," Jpn. J. Appl. Phys. **59**, SA0803 (2020).
106) F. Tochikubo and A. Komuro, "Review of numerical simulation of atmospheric-pressure non-equilibrium plasmas: streamer discharges and glow discharges," Jpn. J. Appl. Phys. **60**, 040501 (2021).
107) C. Winstead and V. McKoy, "Parallel computational studies of electron-molecule collisions," Comp. Phys. Comm. **128**, 386 (2000).
108) C. Winstead and V. McKoy, "Developing cross section sets for fluorocarbon etchants," AIP Conf. Proc. **636**, 241 (2002).
109) M. H. F. Bettega, S. J. Buckman, M. A. Khakoo, P. Limão-Vieira, and M. T. do N. Varella, "Molecular collisions, photoionization and dynamics: honouring Professor Vincent McKoy," Eur. Phys. J. D **76**, 65 (2022).
110) D. W. Flaherty, M. A. Kasper, J. E. Baio, D. B. Graves, H. F. Winters, C. Winstead, and V. McKoy, "Electron impact dissociation cross sections for C_2F_6," J. Phys. D: Appl. Phys. **39**, 4393 (2006).
111) D. Gupta, H. Choi, M.-Y. Song, G. P. Karwasz, and J.-S. Yoon, "Electron impact ionization cross section studies of C_2F_x ($x = 1-6$) and C_3F_x ($x = 1-8$) fluorocarbon species," Eur. Phys. J. D **71**, 88 (2017).
112) D. Gupta, H. Choi, D.-C. Kwon, J.-S. Yoon, and M.-Y. Song, "Electron induced ionization of plasma processing gases: C_4F_x ($x = 1$–8) and the isomers of C_4F_6 and C_4F_8," J. Phys. D: Appl. Phys. **51**, 155203 (2019).
113) H. Hayashi, S. Morishita, T. Tatsumi, Y. Hikosaka, S. Noda, H. Nakagawa, S. Kobayashi, and M. Inoue, "Mechanism of C_4F_8 dissociation in parallel-plate-type plasma," J. Vac. Sci. Technol. A **17**, 2557 (1999).
114) T. Nakamura, H. Motomura, and K. Tachibana, "Quantum chemical study on decomposition and polymer deposition in perfluorocarbon plasmas: molecular orbital calculations of excited states of perfluorocarbons," Jpn. J. Appl. Phys. **40**, 847 (2001).
115) T. Hayashi, K. Ishikawa, M. Sekine, M. Hori, A. Kono, and K. Suu, "Dissociation channels of c-C_4F_8 to CF_2 radical in reactive plasma," Jpn. J. Appl. Phys. **50**, 036203 (2011).
116) T. Hayashi, K. Ishikawa, M. Sekine, and M. Hori, "Dissociation channels of c-C_4F_8 to C_2F_4 in reactive plasma," Jpn. J. Appl. Phys. **61**, 106006 (2022).
117) D. Gupta, M.-Y. Song, K. L. Baluja, H. Choi, and J.-S. Yoon, "Electron impact elastic and excitation cross-sections of the isomers of C_4F_6 molecule for plasma modeling," Phys. Plasma **25**, 063504 (2018).
118) T. Hayashi, K. Ishikawa, M. Sekine, and M. Hori, "Dissociations of C_5F_8 and C_5HF_7 in etching plasma," Jpn. J. Appl. Phys. **52**, 05EB02 (2013).
119) Y. Kondo, K. Ishikawa, T. Hayashi, M. Sekine, and M. Hori, "Electron impact ionization of perfluoro-methyl-vinyl-ether C_3F_6O," Plasma Source Sci. Technol. **27**, 015009 (2018).
120) T. Hayashi, K. Ishikawa, M. Sekine, and M. Hori, "Electronic properties and primary dissociation channels of fluoromethane compounds," Jpn. J. Appl. Phys. **59**, SJJE02 (2020).
121) T. Hayashi, K. Ishikawa, M. Sekine, and M. Hori, "Electronic properties and primarily dissociation channels of fluoroethane compounds," Jpn. J. Appl. Phys. **58**, SEEF01 (2019).
122) T. Hayashi, K. Ishikawa, M. Sekine, and M. Hori, "Dissociative properties of 1,1,1,2-tetrafluoroethane obtained by computational chemistry," Jpn. J. Appl. Phys. **57**, 06JC02 (2018).
123) S.-N. Hsiao, K. Ishikawa, T. Hayashi, J. Ni, T. Tsutsumi, M. Sekine, and M. Hori, "Selective etching of SiN against SiO_2 and poly-Si films in hydrofluoroethane chemistry with a mixture of CH_2FCHF_2, O_2, and Ar," Appl. Surf. Sci. **541**, 148439 (2021).
124) R. U. Masheyeva, K. N. Dzhumagulova, M. Myrzaly, J. Schulze, and Z. Donko, "Self-bias voltage formation and charged particle dynamics in multi-frequency capacitively coupled plasmas," AIP Adv. **11**, 075024 (2021).
125) P. Hartmann et al., "Charged particle dynamics and distribution functions in low pressure dual-frequency capacitively coupled plasmas operated at low frequencies and high voltages," Plasma Source Sci. Technol. **29**, 075014 (2020).
126) X. F. Wang, H. Lee, S. K. Nam, and M. J. Kushner, "Erosion of focus rings in capacitively coupled plasma etching reactors," J. Vac. Sci. Technol. A **39**, 063002 (2021).
127) L. Z. Tong, "Effects of gas composition, focus ring and blocking capacitor on capacitively coupled RF Ar/H_2 plasmas," Jpn. J. Appl. Phys. **54**, 06GA01 (2015).
128) K. Denpoh and T. Shirafuji, "Modification of semianalytical finite element model for radio frequency sheaths in single- and dual-frequency capacitively coupled plasmas: incorporating ion density oscillation at low frequency," Jpn. J. Appl. Phys. **49**, 056202 (2010).
129) Y. Cui et al., "Uniformity improvement of deep silicon cavities fabricated by plasma etching with 12-inch wafer level," J. Micromech. Microeng. **29**, 105010 (2019).
130) X. Tang, H. Zhang, Y. Lin, Y. Cui, Z. Dong, Z. Lian, Y. Zhao, A. Ming, and C. Wang, "Towards tilt-free in plasma etching," J. Micromech. Microeng. **31**, 115007 (2021).
131) D. Kim and D. J. Economou, "Simulation of a two-dimensional sheath over a flat insulator-conductor interface on a radio-frequency biased electrode in a high-density plasma," J. Appl. Phys. **95**, 3311 (2004).
132) J. S. Kim, M. Y. Hur, H. J. Kim, and H. J. Lee, "The ion kinetics at the wafer edge by the variation of geometry and permittivity of the focus ring in capacitively coupled discharges," J. Appl. Phys. **126** (2019).
133) N. Y. Babaeva and M. J. Kushner, "Penetration of plasma into the wafer-focus ring gap in capacitively coupled plasmas," J. Appl. Phys. **101**, 113307 (2007).
134) N. Y. Babaeva and M. J. Kushner, "Ion energy and angular distributions into the wafer-focus ring gap in capacitively coupled discharges," J. Phys. D: Appl. Phys. **41**, 062004 (2008).
135) F. Kruger, H. Lee, S. K. Nam, and M. J. Kushner, "Electric field reversals resulting from voltage waveform tailoring in Ar/O_2 capacitively coupled plasmas sustained in asymmetric systems," Plasma Source, Sci. Technol. **30**, 085002 (2021).
136) H. Dzafic, M. R. Kamali, and S. P. Venugopalan, "Plasma sheath modelling to predict etch-induced overlay," J. Phys. D: Appl. Phys. **55**, 075201 (2022).
137) Y. G. Yook, H. S. You, J. H. Park, W. S. Chang, D. C. Kwon, J. S. Yoon, K. H. Yoon, S. S. Shin, D. H. Yu, and Y. H. Im, "Fast and realistic 3D feature profile simulation platform for plasma etching process," J. Appl. Phys. D **55**, 255202 (2022).
138) S. Huang, S. Shim, S. K. Nam, and M. J. Kushner, "Pattern dependent profile distortion during plasma etching of high aspect ratio features in SiO_2," J. Vac. Sci. Technol. A **38**, 023001 (2020).

© 2022 The Author(s). Published on behalf of The Japan Society of Applied Physics by IOP Publishing Ltd

139) R. R. Upaphyay, K. Suzuki, L. L. Raja, P. L. G. Ventzek, and A. Ranjan, "Experimentally validated computations of simultaneous ion and fast neutral energy and angular distributions in a capacitively coupled plasma reactor," J. Phys. D: Appl. Phys. **53**, 435209 (2020).
140) Z. Y. Chen, R. C. Longo, M. Hummel, M. Carruth, J. Blakeney, P. Ventzek, and A. Ranjan, "Factors influencing ion energy distributions in pulsed inductively coupled argon plasmas," J. Phys. D: Appl. Phys. **53**, 335202 (2020).
141) Z. Y. Chen, J. Blakeney, M. Carruth, P. Ventzek, and A. Ranjan, "Time-resolved ion energy distribution in pulsed inductively coupled argon plasma with/without DC bias," J. Vac. Sci. Technol. B **40**, 033601 (2022).
142) S. Noda, N. Ozawa, T. Kinoshita, H. Tsuboi, K. Kawashima, Y. Hikosaka, K. Kinoshita, and M. Sekine, "Investigation of ion transportation in high-aspect-ratio holes from fluorocarbon plasma for SiO_2 etching," Thin Solid Film **374**, 181 (2000).
143) M. Moriyama, N. Nakahara, A. Mitsuya, H. Suzuki, K. Kurihara, D. Iino, H. Fukumizu, and H. Toyoda, "Evaluation of absolute charge density at the bottom of high aspect capillary holes exposed to a pulsed very high frequency plasma," Jpn. J. Appl. Phys. **59**, SJJB03 (2020).
144) M. Moriyama, N. Nakahara, K. Kurihara, D. Iino, H. Fukumizu, H. Suzuki, and H. Toyoda, "Time-dependent measurement of charge density on the bottom of high aspect capillary hole in pulse-modulated VHF capacitively coupled Ar plasma," Jpn. J. Appl. Phys. **60**, 016001 (2021).
145) K. Ichikawa, M. H. Chu, M. Moriyama, N. Nakahara, H. Suzuki, D. Iino, H. Fukumizu, K. Kurihara, and H. Toyoda, "Angular distribution measurement of high-energy argon neutral and ion in a 13.56 MHz capacitively-coupled plasma," Appl. Phys. Express **14**, 126001 (2021).
146) X. F. Wang, M. M. Wang, P. Biolsi, and M. J. Kushner, "Scaling of atomic layer etching of SiO_2 in fluorocarbon plasmas: transient etching and surface roughness," J. Vac. Sci. Technol. A **39**, 033003 (2021).
147) R. Mullins, J. J. G. Moreno, and M. Nolan, "Origin of enhanced thermal atomic layer etching of amorphous HfO_2," J. Vac. Sci. Technol. A **40**, 022604 (2022).
148) Y. Yoshikawa and K. Eriguchi, "First-principles predictions of electronic structure change in plasma-damaged materials," Jpn. J. Appl. Phys. **57**, 06JD04 (2018).
149) T. Kuyama, K. Urabe, M. Fukawsawa, T. Tatsumi, and K. Eriguchi, "Characterization of dynamic behaviors of defects in Si substrates created by H_2 plasma using conductance method," Jpn. J. Appl. Phys. **59**, SJJC02 (2019).
150) T. Hamano, K. Urabe, and K. Eriguchi, "Investigation of spatial and energy profiles of plasma process-induced latent defects in Si substrate using capacitance-voltage characteristics," Jpn. J. Appl. Phys. **59**, 455102 (2019).
151) K. Eriguchi, T. Hamano, and K. Urabe, "Improvement of the plasma-induced defect generation model in Si substrates and the optimization design framework," Plasma Process Polym. **16**, 1900058 (2019).
152) H. Li, T. Ito, K. Karahashi, M. Kagaya, T. Moriya, M. Matsukuma, and S. Hamaguchi, "Experimental and numerical analysis of the effects of ion bombardment in silicon oxide (SiO_2) plasma enhanced atomic layer deposition (PEALD) processes," Jpn. J. Appl. Phys. **59**, SJJA01 (2020).
153) A. Hirata, M. Fukasawa, K. Kugimiya, K. Nagaoka, K. Karahashi, S. Hamaguchi, and H. Iwamoto, "On-wafer monitoring and control of ion energy distribution for damage minimization in atomic layer etching processes," Jpn. J. Appl. Phys. **59**, SJJC01 (2020).
154) Y. Osano and K. Ono, "An atomic scale model of multilayer surface reactions and the feature profile evolution during plasma etching," Jpn. J. Appl. Phys. **44**, 8650 (2005).
155) Y. Osano, M. Mori, and K. Ono, "A model analysis of feature profile evolution and microscopic uniformity during polysilicon gate etching in Cl_2/O_2 plasmas," Jpn. J. Appl. Phys. **45**, 8157 (2006).
156) Y. Osano and K. Ono, "Atomic-scale cellular model and profile simulation of poly-Si gate etching in high-density chlorine-based plasmas: effects of passivation layer formation on evolution of feature profiles," J. Vac. Sci. Technol. B **26**, 1425 (2008).
157) M. Mori, Y. Oasno, and K. Ono, "Formation mechanisms of etched feature profiles during Si etching in Cl_2/O_2 plasmas," J. Vac. Sci. Technol. A **37**, 051301 (2019).
158) M. Mori, S. Irie, and K. Ono, "Model analysis of the feature profile evolution during Si etching in HBr-containing plasmas," J. Vac. Sci. Technol. A **39**, 043002 (2021).
159) T. J. Sommerer and M. J. Kushner, "Monte-Carlo-fluid model of chlorine atom production in Cl_2, HCl, and CCl_4 radio-frequency discharges for plasma-etching," J. Vac. Sci. Technol. B **10**, 2179 (1992).
160) P. Subramonium and M. J. Kushner, "Pulsed inductively coupled chlorine plasmas in the presence of a substrate bias," Appl. Phys. Lett. **79**, 2145 (2001).
161) P. Subramonium and M. J. Kushner, "Two-dimensional modeling of long-term transients in inductively coupled plasmas using moderate computational parallelism. I. Ar pulsed plasmas," J. Vac. Sci. Technol. A **20**, 313 (2002).
162) P. Subramonium and M. J. Kushner, "Two-dimensional modeling of long-term transients in inductively coupled plasmas using moderate computational parallelism. II. Ar/Cl_2 pulsed plasmas," J. Vac. Sci. Technol. A **20**, 325 (2002).
163) J. P. Chang, A. P. Mahorowala, and H. H. Sawin, "Plasma-surface kinetics and feature profile evolution in chlorine etching of polysilicon," J. Vac. Sci. Technol. **16**, 217 (1998).
164) J. P. Chang, J. C. Arnold, and H. H. Sawin, "Kinetic study of low energy argon ion-enhanced plasma etching of polysilicon with atomic/molecular chlorine," J. Vac. Sci. Technol. **15**, 1853 (1997).
165) J. P. Chang and H. H. Sawin, "Kinetic study of low energy ion-enhanced polysilicon etching using Cl, Cl_2, and Cl^+ beam scattering," J. Vac. Sci. Technol. **15**, 610 (1997).
166) M. E. Barone and D. B. Graves, "Molecular-dynamics simulations of direct reactive ion etching of silicon by fluorine and chlorine," J. Appl. Phys. **78**, 6604 (1995).
167) B. A. Helmer and D. B. Graves, "Molecular dynamics simulations of Cl_2^+ onto a chlorinated silicon surface: energies and angles of the reflected Cl_2 and Cl fragments," J. Vac. Sci. Technol. A **17**, 2759 (1999).
168) H. Ohta and S. Hamaguchi, "Molecular dynamics simulation of silicon and silicon dioxide etching by energetic halogen beams," J. Vac. Sci. Technol. A **19**, 2373 (2001).
169) T. Ito, K. Karahashi, S. Y. Kang, and S. Hamaguchi, "Characteristics of silicon etching by silicon chloride ions," J. Vac. Sci. Technol. A **31**, 031301 (2013).
170) E. J. C. Tinacba, M. Isobe, and S. Hamaguchi, "Surface damage formation during atomic layer etching of silicon with chlorine adsorption," J. Vac. Sci. Technol. A **39**, 042603 (2021).
171) S. Tinck, A. Bogaerts, and D. Shamiryan, "Simultaneous etching and deposition processes during the etching of silicon with a $Cl_2/O_2/Ar$ inductively coupled plasma," Plasma Process. Polym. **8**, 490 (2011).
172) S. Tinck, W. Boullart, and A. Bogaerts, "Investigation of etching and deposition processes of $Cl_2/O_2/Ar$ inductively coupled plasmas on silicon by means of plasma-surface simulations and experiments," J. Phys. D: Appl. Phys. **42**, 095204 (2009).
173) S. Tinck, W. Boullart, and A. Bogaerts, "Modeling $Cl_2/O_2/Ar$ inductively coupled plasmas used for silicon etching: effects of SiO_2 chamber wall coating," Plasma Source **20**, 045012 (2011).
174) N. Kuboi, T. Tatsumi, S. Kobayashi, J. Komachi, M. Fukasawa, T. Kinoshita, and H. Ansai, "Numerical simulation method for plasma-induced damage profile in SiO_2 etching," Jpn. J. Appl. Phys. **50**, 116501 (2011).
175) N. Kuboi, T. Tatsumi, S. Kobayashi, J. Komachi, M. Fukasawa, T. Kinoshita, and H. Ansai, "Modeling and simulation of plasma-induced damage distribution during hole etching of SiO_2 over Si substrate by fluorocarbon plasma," Appl. Phys. Express **5**, 126201 (2012).
176) N. Kuboi, T. Tatsumi, T. Kinoshita, T. Shigetoshi, M. Fukasawa, J. Komachi, and H. Ansai, "Prediction of plasma-induced damage distribution during silicon nitride etching using advanced three-dimensional voxel model," J. Vac. Sci. Technol. A **33**, 061308 (2015).
177) N. Kuboi, T. Tatsumi, H. Minami, M. Fukasawa, Y. Zaizen, J. Komachi, and T. Kawamura, "Influence of hydrogen in silicon nitride films on the surface reactions during hydrofluorocarbon plasma etching," J. Vac. Sci. Technol. A **35**, 061306 (2017).
178) N. Kuboi, T. Tatsumi, J. Komachi, and S. Yamakawa, "Insights into different etching properties of continuous wave and atomic layer etching processes for SiO_2 and Si_3N_4 films using voxel-slab model," J. Vac. Sci. Technol. A **37**, 051004 (2019).
179) P. Vanraes, S. P. Venugopalan, and A. Bogaerts, "Multiscale modeling of plasma-surface interaction-General picture and a case study of Si and SiO_2 etching by fluorocarbon-based plasmas," Appl. Phys. Rev. **8**, 041305 (2021).
180) K. Denpoh, P. Moroz, T. Kato, and M. Matsukuma, "Multiscale plasma and feature profile simulations of plasma-enhanced chemical vapor deposition and atomic layer deposition processes for titanium thin film fabrication," Jpn. J. Appl. Phys. **59**, SHHB02 (2020).
181) S. Hamaguchi and S. M. Rossnagel, "Simulations of trench-filling profiles under ionized magnetron sputter metal deposition," J. Vac. Sci. Technol. B **13**, 183 (1995).
182) S. M. Rossnagel, C. Nichols, S. Hamaguchi, D. Ruzic, and R. Turkot, "Thin, high atomic weight refractory film deposition for diffusion barrier, adhesion layer, and seed layer applications," J. Vac. Sci. Technol. **14**, 1819 (1996).

© 2022 The Author(s). Published on behalf of The Japan Society of Applied Physics by IOP Publishing Ltd

183) S. Hamaguchi and S. M. Rossnagel, "Liner conformality in ionized magnetron sputter metal deposition processes," J. Vac. Sci. Technol. B **14**, 2603 (1996).
184) A. A. Mayo, S. Hamaguchi, J. H. Joo, and S. M. Rossnagel, "Across-wafer nonuniformity of long throw sputter deposition," J. Vac. Sci. Technol. B **15**, 1788 (1997).
185) D. Sung, L. Wen, H. Tak, H. Lee, D. Kim, and G. Yeom, "Investigation of SiO_2 etch characteristics by $C_6F_6/Ar/O_2$ plasmas generated using inductively coupled plasma and capacitively coupled plasma," Material **15**, 1300 (2022).
186) C. Cho, K. You, S. Kim, Y. Lee, J. Lee, and S. You, "Characterization of SiO_2 etching profiles in pulse-modulated capacitively coupled plasmas," Material **14**, 5036 (2021).
187) K. Hattori, T. Ohta, A. Oda, and H. Kousaka, "Noncontact measurement of substrate temperature by optical low-coherence interferometry in high-power pulsed magnetron sputtering," Jpn. J. Appl. Phys. **57**, 01AC03 (2018).
188) D. H. Im, T.-W. Yoon, W.-S. Min, and S.-J. Hong, "Fabrication of planar heating chuck using nichrome thin film as heating element for PECVD equipment," Electronics **10**, 2535 (2021).
189) J.-H. Kim, Y. Koo, W. Song, and S. J. Hong, "On-wafer temperature monitoring sensor for condition monitoring of repaired electrostatic chuck," Electronics **11**, 880 (2022).
190) D. H. Im, W. S. Min, and S. J. Hong, "Planar heating chuck to improve temperature uniformity of plasma processing equipment," Jpn. J. Appl. Phys. **59**, SJJD01 (2020).
191) H. J. Lee and S. H. Lee, "Numerical evaluation on surface temperature uniformity of multi-zone and single-zone ceramic heaters with the electrostatic chuck," J. Mech. Sci. Technol. **35**, 3763 (2021).
192) T. Watanabe, T. Kitabayashi, and C. Nakayama, "Relationship between electrical resistivity and electrostatic force of alumina electrostatic chuck," Jpn. J. Appl. Phys. **32**, 864 (1993).
193) S. Benkadda, S. Hamaguchi, M. Muraglia, and D. O'Connell, "Preface to special topic: invited papers from the 2nd international conference on data-driven plasma science," Phys. Plasmas **28**, 030401 (2021).
194) S. Hamaguchi, "Plasma informatics – application of data driven science to plasmas," J. Plasma Fusion Res. **95**, 535 (2019).
195) S. L. Brunton and J. N. Kutz, *Data-Driven Science and Engineering: Machine Learning, Dynamical Systems, and Control* (Cambridge University Press, Cambridge, 2019).
196) A. Agrawal and A. Choudhary, "Perspective: materials informatics and big data: realization of the "fourth paradigm" of science in materials science," APL Mater. **4**, 053208 (2016).
197) P. W. Hatfield et al., "The data-driven future of high-energy-density physics," Nature **593**, 351 (2021).
198) J. Degrave et al., "Magnetic control of tokamak plasmas through deep reinforcement learning," Nature **602**, 414 (2022).
199) S. Koubaa and A. T. Azar, *Deep Learning for Unmanned Systems* (Springer, Berlin, 2022).
200) T. Chen and C. Guestrin, "XGBoost: a scalable tree boosting system," Proc. of the 22nd ACM SIGKDD Int. Conf. on KDD, p. 785, 2016.
201) G. Ke, Q. Meng, T. Finley, T. Wang, W. Chen, W. Ma, Q. Ye, and T. Liu, "LightGBM: a highly efficient gradient boosting decision tree," Proc. of the 31st Int. Conf. on NeurIPS, p. 3149, 2017.
202) N. Srivastava, G. Hinton, A. Krizhevsky, I. Sutskever, and R. Salakhutdinov, "Dropout: a simple way to prevent neural networks from overfitting," J. Mach. Learn. Res. **15**, 1929 (2014).
203) R. D. White, R. E. Robson, S. Dujko, P. Nicoletopoulos, and B. Li, "Recent advances in the application of Boltzmann equation and fluid equation methods to charged particle transport in non-equilibrium plasmas," J. Phys. D: Appl. Phys. **42**, 194001 (2009).
204) P. J. Drallos and J. M. Wadehra, "Exact time-dependent evolution of electron-velocity distribution functions in a gas using the Boltzmann equation," Phys. Rev. A **40**, 1967 (1989).
205) K. Maeda and T. Makabe, "Time-dependent RF swarm transport by direct numerical procedure of the boltzmann equation," Jpn. J. Appl. Phys. **33**, 4173 (1994).
206) H. Sugawara, "Configuration of propagator method for calculation of electron velocity distribution function in gas under crossed electric and magnetic fields," Plasma Sci. Technol. **21**, 094001 (2019).
207) G. E. Karniadakis, I. G. Kevrekidis, L. Lu, P. Perdikaris, S. Wang, and L. Yang, "Physics-informed machine learning," Nat. Rev. Phys. **3**, 422 (2021).
208) A. G. Baydin, B. A. Pearlmutter, A. A. Radul, and J. M. Siskind, "Automatic differentiation in machine learning: a survey," J. Mach. Learn. Res. **18**, 1 (2018), https://jmlr.org/papers/v18/17-468.html.
209) S. Kawaguchi, K. Takahashi, H. Ohkama, and K. Satoh, "Deep learning for solving the Boltzmann equation of electrons in weakly ionized plasma," Plasma Sources Sci. Technol. **29**, 025021 (2020).
210) S. Kawaguchi and T. Murakami, "Physics-informed neural networks for solving the Boltzmann equation of the electron velocity distribution function in weakly ionized plasmas," Jpn. J. Appl. Phys. **61**, 086002 (2022).
211) S. Wang, Y. Teng, and P. Perdikaris, "Understanding and mitigating gradient flow pathologies in physics-informed neural networks," SIAM J. Sci. Compt. **43**, A3055 (2021).
212) D. P. Kingma and J. Ba, "Adam: a method for stochastic optimization," (2014), arXiv:1412.6980.
213) M. Ichikawa, K. Ikuse, K.-L. Chen, J.-S. Wu, and S. Hamaguchi, "Construction of a surrogate model for low-temperature plasma simulation using machine learning," Presented at 69th Japan Society of Applied Physics (JSAP) Spring Meeting 2022 (March 22–26, 2022, Sagamihara, Japan & online).
214) O. Sakai, K. Nobuto, S. Miyagi, and K. Tachibana, "Analysis of weblike network structures of directed graphs for chemical reactions in methane plasmas," AIP Adv. **5**, 107140 (2015).
215) Y. Mizui, T. Kojima, S. Miyagi, and O. Sakai, "Graphical classification in multi-centrality-index diagrams for complex chemical networks," Symmetry **9**, 309 (2017).
216) M. J. Kushner, "A model for the discharge kinetics and plasma chemistry during plasma enhanced chemical vapor deposition of amorphous silicon," J. Appl. Phys. **63**, 2532 (1988).
217) K. Tachibana, M. Nishida, H. Harima, and Y. Urano, "Diagnostics and modelling of a methane plasma used in the chemical vapour deposition of amorphous carbon films," J. Phys. D **17**, 1727 (1984).
218) T. Murakami and O. Sakai, "Rescaling the complex network of low-temperature plasma chemistry through graph-theoretical analysis," Plasma Sources Sci. Technol. **29**, 115018 (2020).
219) E. W. Dijkstra, "A note on two problems in connexion with graphs," Numeri. Math. **1**, 269 (1959).
220) M. Jacomy et al., "Gephi: an open source software for exploring and manipulating networks," Proc. of Int. AAAI Conf. on Web and Social Media, 2009, Graphi (https://gephi.org/) last accessed on August 1, 2022).
221) D. T. Holmes, R. H. Rothman, and W. B. Zimmerman, "Graph theory applied to plasma chemical reaction engineering," Plasma Chem. Plasma Process. **41**, 531 (2021).
222) O. Sakai, S. Kawaguchi, and T. Murakami, "Complexity visualization, dataset acquisition, and machine-learning perspectives for low-temperature plasma: a review," Jpn. J. Appl. Phys. **61**, 070101 (2022).
223) E. Pfender, "Fundamental-studies associated with the plasma spray process," Surf. Coat. Technol. **34**, 1 (1988).
224) T. A. Choudhury, N. Hosseinzadeh, and C. C. Berndt, "Artificial neural network application for predicting in-flight particle characteristics of an atmospheric plasma spray process," Surf. Coat. Technol. **205**, 4886 (2011).
225) T. A. Choudhury, C. C. Berndt, and Z.-H. Man, "An extreme learning machine algorithm to predict the in-flight particle characteristics of an atmospheric plasma spray process," Plasma Chem. Plasma Process. **33**, 993 (2013).
226) T. A. Choudhury, C. C. Berndt, and Z.-H. Man, "Modular implementation of artificial neural network in predicting in-flight particle characteristics of an atmospheric plasma spray process," Eng. Appl. Artif. Intell. **45**, 57 (2015).
227) M. Liu, Z. Yua, Y. Zhang, H. Wu, H. Liao, and S. Deng, "Prediction and analysis of high velocity oxy fuel (HVOF) sprayed coating using artificial neural network," Surf. Coat. Technol. **378**, 88 (2019).
228) K. Hartz-Behrend, J. Schaup, J. Zierhut, and J. Schein, "Controlling the twin wire arc spray process using artificial neural networks (ANN)," J. Therm. Spray Technol. **25**, 21 (2016).
229) J. Ramshaw and C. Chang, "Computational fluid dynamics modeling of multicomponent thermal plasmas," Plasma Chem. Plasma Process. **12**, 299 (1992).
230) C. Chang and J. Ramshaw, "Numerical simulation of nonequilibrium effects in an argon plasma jet," Phys. Plasmas **1**, 3698 (1994).
231) R. C. Batra and U. Taetragool, "Numerical techniques to find optimal input parameters for achieving mean particles' temperature and axial velocity in atmospheric plasma spray process," Sci. Rep. **10**, 21482 (2020).
232) J. Zhu, X. Wang, L. Kou, L. Zheng, and H. Zhang, "Prediction of control parameters corresponding to in-flight particles in atmospheric plasma spray employing convolutional neural networks," Surf. Coat. Technol. **394**, 125862 (2020).
233) J. Zhu, X. Wang, L. Kou, L. Zheng, and H. Zhang, "Application of combined transfer learning and convolutional neural networks to optimize plasma spraying," Appl. Surf. Sci. **563**, 150098 (2021).

© 2022 The Author(s). Published on behalf of The Japan Society of Applied Physics by IOP Publishing Ltd

234) M. Liu, H. Wu, Z. Yu, H. Liao, and S. Deng, "Description and prediction of multi-layer profile in cold spray using artificial neural networks," J. Therm. Spray Technol. **30**, 1453 (2021).
235) U. M. R. Paturi, S. Cheruku, and S. R. Geereddy, "Process modeling and parameter optimization of surface coatings using artificial neural networks (ANNs): state-of-the-art review," Mater. Today Proc. **38**, 2764 (2021).
236) G. Mauer and C. Moreau, "Process diagnostics and control in thermal spray," J. Therm. Spray Technol. **31**, 818 (2022).
237) K. Malamousi, K. Delibasis, B. Allcock, and S. Kamnis, "Digital transformation of thermal and cold spray processes with emphasis on machine learning," Surf. Coat. Technol. **433**, 128138 (2022).
238) B.-Y. Han, W.-W. Xu, K.-B. Zhou, H.-Y. Zhang, W.-N. Lei, M.-Q. Cong, W. Du, J.-J. Chu, and S. Zhu, "Performance analysis of plasma spray Ni60CuMo coatings on a ZL109 via a back propagation neural network model," Surf. Coat. Technol. **433**, 128121 (2022).
239) X. Gao, C. Li, X. Han, X. Chen, and X. Zhao, "Numerical simulation and parameter sensitivity analysis of multi-particle deposition behavior in HVAF spraying," Surf. Coat. Technol. **441**, 128569 (2022).
240) L. Mao, J. Xiao, G. Sun, X. Wei, D. Wu, P. Cao, and C. Zhang, "Microstructure and wear behaviors of Cr_2O_3-Al_2O3 composite coatings deposited by atmospheric plasma spraying," Surf. Coat. Technol. **444**, 128619 (2022).
241) J. Liu, C. Ma, H. Gui, and S. Wang, "Transfer learning-based thermal error prediction and control with deep residual LSTM network," Knowl.-Based Syst. **237**, 107704 (2022).
242) K. Bobzin, W. Wietheger, H. Heinemann, S. R. Dokhanchi, M. Rom, and G. Visconti, "Prediction of particle properties in plasma spraying based on machine learning," J. Thermal Spray Tech., **30**, 1751 (2021).
243) D. Y. Yang, Y. Kim, M. Y. Hur, H. J. Lee, Y. J. Kim, T. S. Lim, K. B. Kim, and S. Yang, "Control of the nano-particle weight ratio in stainless steel micro and nano powders by radio frequency plasma treatment," Metals **5**, 2058 (2015).
244) J. M. Park, K. S. Kim, T. H. Hwang, and S. H. Hong, "Three-dimensional modeling of arc root rotation by external magnetic field in non-transferred thermal plasma torches," IEEE Trans. Plasma Sci. **32**, 479 (2004).
245) C. Cheon, M. Y. Hur, H. J. Kim, and H. J. Lee, "Effects of quenching gas feeding on silver nanoparticle synthesis by the inductively coupled plasma torch," IEEE Trans. Plasma Sci. **49**, 4022 (2021).
246) S. Yoshimura, Y. Otsubo, A. Yamashita, and K. Ishikawa, "Insights into normothermic treatment with direct irradiation of atmospheric pressure plasma for biological applications," Jpn. J. Appl. Phys. **60**, 010502 (2021).
247) D. Gidon, B. Curtis, J. A. Paulson, D. B. Graves, and A. Mesbah, "Model-based feedback control of a kHz-excited atmospheric pressure plasma jet," IEEE Transaction on Radiat. Plasma Med. Sci. **2**, 129 (2018).
248) D. Gidon, X. Pei, A. D. Bonzanini, D. B. Graves, and A. Mesbah, "Machine learning for real-time diagnostics of cold atmospheric plasma sources," IEEE Trans. Radiat. Plasma Med. Sci. **3**, 597 (2019).
249) Software library developed by Google, (2022), TensorFlow (https://tensorflow.org) last accessed on August 1, 2022.
250) Python library, (2022), scikit-learn (https://scikit-learn.org) last accessed on August 1, 2022.
251) A. Mesbah and D. B. Graves, "Machine learning for modeling, diagnostics, and control of non-equilibrium plasmas," J. Phys. D: Appl. Phys. **52**, 30LT02 (2019).
252) Z. Ghahramani, "Probabilistic machine learning and artificial intelligence," Nature **521**, 452 (2015).
253) D. Gidon, D. B. Graves, and A. Mesbah, "Spatial thermal dose delivery in atmospheric pressure plasma jets," Plasma Sources Sci. Technol. **28**, 025006 (2019).
254) D. Gidon, D. B. Graves, and A. Mesbah, "Predictive control of 2D spatial thermal dose delivery in atmospheric pressure plasma jets," Plasma Sources Sci. Technol. **28**, 085001 (2019).
255) Y. Lyu, L. Lin, E. Gjika, T. Lee, and M. Keidar, "Mathematical modeling and control for cancer treatment with cold atmospheric plasma jet," J. Phys. D: Appl. Phys. **52**, 185202 (2019).
256) I. V. Schweigert, A. L. Alexandrov, and D. E. Zakrevsky, "Self-organization of touching-target current with ac voltage in atmospheric pressure plasma jet for medical application parameters," Plasma Sources Sci. Technol. **29**, 12LT02 (2020).
257) M. Witman, D. Gidon, D. B. Graves, B. Smit, and A. Mesbah, "Sim-to-real transfer reinforcement learning for control of thermal effects of an atmospheric pressure plasma jet," Plasma Sources Sci. Technol. **28**, 095019 (2019).
258) D. Rodrigues, K. J. Chan, and A. Mesbah, "Data-driven adaptive optimal control under model uncertainty: an application to cold atmospheric plasmas," to be published in IEEE Trans. Control Systems Technol. (2022).
259) K. Shao, X. Pei, D. B. Graves, and A. Mesbah, "Active learning-guided exploration of parameter space of air plasmas to enhance the energy efficiency of NO_x" production," Plasma Sources Sci. Technol. **31**, 055018 (2022).
260) A. D. Bonzanini, K. Shao, A. Stancampiano, D. B. Graves, and A. Mesbah, "Perspectives on machine learning-assisted plasma medicine: toward automated plasma treatment," IEEE Trans. Radiat. Plasma Med. Sci. **6**, 16 (2022).
261) A. D. Bonzanini, J. A. Paulson, D. B. Graves, and A. Mesbah, "Toward safe dose delivery in plasma medicine using projected neural network-based fast approximate NMPC," IFAC Papers On Line **53**, 5279 (2020).
262) A. D. Bonzanini, D. B. Graves, and A. Mesbah, "Learning-based SMPC for reference tracking under state-dependent uncertainty: an application to atmospheric pressure plasma jets for plasma medicine," IEEE Trans. Control Systems Technol. **30**, 611 (2022).
263) D. B. Graves and R. Brault, "Molecular dynamics for low temperature plasma–surface interaction studies," J. Phys. D: Appl. Phys. **42**, 194011 (2009).
264) H. Ohta and S. Hamaguchi, "Classical interatomic potentials for Si–O–F and Si–O–Cl systems," J. Chem. Phys. **115**, 6679 (2001).
265) S. Hamaguchi, H. Ohta, and H. Yamada, "On interatomic potential functions for molecular dynamic (MD) simulations of plasma-wall interactions," J. Plasma Fusion Res. **6**, 80 (2004).
266) E. J. C. Tinacba, T. Ito, K. Karahashi, M. Isobe, and S. Hamaguchi, "Molecular dynamics simulation for reactive ion etching of Si and SiO_2 by SF5+ ions ," J. Vac. Sci. Technol. B **39**, 043203 (2021).
267) J. Behler, "Constructing high-dimensional neural network potentials: a tutorial review," Int. J. Quantum Chem. **115**, 1032 (2015).
268) L. Chen, I. Sukuba, M. Probst, and A. Kaiser, "Iterative training set refinement enables reactive molecular dynamics via machine learned forces," RSC Adv. **10**, 4293 (2020).
269) Y. Yamamura and H. Tawara, "Energy dependence of ion-induced sputtering yields from monatomic solids at normal incidence," At. Data Nucl. Data Tables **62**, 149 (1996).
270) H. Kino, K. Ikuse, H.-C. Dam, and S. Hamaguchi, "Characterization of descriptors in machine learning for data-based sputtering yield prediction," Phys. Plasmas **28**, 013504 (2021).
271) GPR-based sputtering yield prediction, (http://camt.eng.osaka-u.ac.jp/hamaguchi/SY/) last accessed on April 3, (2011).
272) Y. Okuyama and T. Ohmori, "Deep learning-based automated measurement method for cross-sectional SEM images in semiconductor devices," Microsc. Microanal. **26**, 698 (2020).
273) R. Girshick, J. Donahue, T. Darrel, and J. Malik, "Rich feature hierarchies for accurate object detection and semantic segmentation," Computer Vision and Pattern Recognition (CVPR), 2014, p. 580.
274) R. Girshick, J. Donahue, T. Darrel, and J. Malik, "Region-based convolutional networks for accurate object detection and segmentation," IEEE Trans. Pattern Anal. Mach. Intell. **38**, 142 (2016).
275) Y. Midoh and K. Nakamae, "Image quality enhancement of a CD-SEM image using conditional generative adversarial networks," Proc. SPIE **10959**, 109590B (2019).
276) T. Xiao, Z. Wu, P. D. Christofides, A. Armaou, and D. Ni, "Recurrent neural-network-based model predictive control of a plasma etch process," Ind. Eng. Chem. Res. **61**, 638 (2022).
277) T. Q. Xiao and D. Ni, "Multiscale modeling and neural network model based control of a plasma etch process," Chem. Eng. Res. Design. **164**, 113 (2020).
278) T. Q. Xiao and D. Ni, "Multiscale modeling and recurrent neural network based optimization of a plasma etch process," Processes **9**, 151 (2021).
279) S. Yun, M. Tom, J. Luo, G. Orkoulas, and P. D. Christofides, "Microscopic and data-driven modeling and operation of thermal atomic layer etching of aluminum oxide thin films," Chem. Eng. Res. Design. **177**, 96 (2022).
280) F. Abdullah, Z. Wu, and P. D. Christofides, "Sparse-identification-based model predictive control of nonlinear two-time-scale processes," Comp. Chem. Eng. **153**, 107411 (2021).
281) F. Abbullah, Z. Wu, and P. D. Christofides, "Data-based reduced-order modeling of nonlinear two-time-scale processes," Chem. Eng. Res. Des. **166**, 1 (2021).
282) A. Dodhia, Z. Wu, and P. D. Christofides, "Machine learning-based model predictive control of diffusion-reaction processes," Chem. Eng. Res. Des. **173**, 129 (2021).
283) Z. Wu, R. Anh, D. Rincon, and P. D. Christofides, "Machine learning-based predictive control of nonlinear processes. Part I: theory," AlChE J. **65**, e16729 (2019).

© 2022 The Author(s). Published on behalf of The Japan Society of Applied Physics by IOP Publishing Ltd

284) Z. Wu, R. Anh, D. Rincon, and P. D. Christofides, "Machine-learning-based predictive control of nonlinear processes: II. Computational implementation," AIChE J. **65**, e16734 (2019).
285) Y. Y. Ding, Y. C. Zhang, Y. M. Ren, G. Orkoulas, and P. D. Christofides, "Machine learning-based modeling and operation for ALD of SiO_2 thin-films using data from a multiscale CFD simulation," Chem. Eng. Res. Des. **151**, 131 (2019).
286) Y. C. Zhang, Y. Y. Ding, and P. D. Christofides, "Multiscale computational fluid dynamics modeling of thermal atomic layer deposition with application to chamber design," Chem. Eng. Res. Des. **147**, 529 (2019).
287) Y. Y. Ding, Y. C. Zhang, and P. D. Christofides, "Microscopic modeling and optimal operation of thermal atomic layer deposition," Chem. Eng. Res. Design **145**, 159 (2019).
288) Y. C. Zhang, Y. Y. Ding, and P. D. Christofides, "Integrating feedback control and run-to-run control in multi-wafer thermal atomic layer deposition of thin films," Processes **8**, 18 (2020).
289) C. H. Qu, Y. Sakiyama, P. Agarwal, and M. J. Kushner, "Plasma-enhanced atomic layer deposition of SiO_2 film using capacitively coupled Ar/O_2 plasmas: A computational investigation," J. Vac. Sci. Technol. A **39**, 052403 (2021).
290) S. Yun, Y. Y. Ding, Y. C. Zhang, and P. D. Christofides, "Integration of feedback control and run-to-run control for plasma enhanced atomic layer deposition of hafnium oxide thin films," Comp. Chem. Eng. **148**, 107267 (2021).
291) Y. Y. Ding, Y. C. Zhang, H. Y. Chung, and P. D. Christofides, "Machine learning-based modeling and operation of plasma-enhanced atomic layer deposition of hafnium oxide thin films," Comp. Chem. Eng. **144**, 107148 (2021).
292) Y. C. Zhang, Y. Y. Ding, and P. D. Christofides, "Multiscale computational fluid dynamics modeling and reactor design of plasma-enhanced atomic layer deposition," Comp. Chem. Eng. **142**, 107066 (2020).
293) Y. Y. Ding, Y. C. Zhang, G. Orkoulas, and P. D. Christofides, "Microscopic modeling and optimal operation of plasma enhanced atomic layer deposition," Chem. Eng. Res. Des. **159**, 439 (2020).
294) L. Zhyang, P. Corkery, D. T. Lee, S. Lee, M. Kooshkbaghi, Z. L. Xu, G. C. Gance, I. G. Kevrekidis, and M. Tsapatsis, "Numerical simulation of atomic layer deposition for thin deposit formation in a mesoporous substrate," AIChE J. **67**, e17305 (2021).
295) A. Marcato, G. Boccardo, and D. Marchisio, "A computational workflow to study particle transport and filtration in porous media: coupling CFD and deep learning," Chem. Eng. J. **417**, 128936 (2021).
296) R. Dallaev, "Investigation of hydrogen impurities in PE-ALD AlN thin films by IBA methods," Vaccum **193**, 110533 (2021).
297) N. Sharma and A. Liu, "A hybrid science-guided machine learning approach for modeling chemical processes: a review," AIChE J. **68**, e17609 (2022).
298) M. S. Alhajeri, Z. Wu, D. Rincon, F. Albalawi, and P. D. Christofides, "Machine-learning-based state estimation and predictive control of nonlinear processes," Chem. Eng. Res. Des. **167**, 268 (2021).
299) N. H. Paulson, A. Yanguas-Gil, O. Y. Abuomar, and J. W. Elam, "Intelligent agents for the optimization of atomic layer deposition," ACS Appl. Mater. Interfaces **13**, 17022 (2021).
300) N. Cheimarios, D. To, G. Kokkoris, G. Memos, and A. G. Boudouvis, "Monte carlo and kinetic monte carlo models for deposition processes: a review of recent works," Front. Phys. **9**, 631918 (2021).
301) N. Cheimarios, G. Kokkoris, and A. G. Boudouvis, "Multiscale modeling in chemical vapor deposition processes: models and methodologies," Arch. Comput. Method. Eng. **28**, 637 (2021).
302) M. A. Albao and S. Co-mediated, "island-edge decoration in Co/Cu(001): a kinetic Monte Carlo study," J. Vac. Sci. Technol. A **39**, 063201 (2021).
303) M. A. Albao and A. A. B. Padama, "CO adsorption on W(100) during temperature-programmed desorption: a combined density functional theory and kinetic Monte Carlo study," Appl. Surf. Sci. **396**, 1282 (2017).
304) M. Crose, W. Q. Zhang, A. Tran, and P. D. Christofides, "Run-to-run control of PECVD systems: Application to a multiscale three-dimensional CFD model of silicon thin film deposition," AIChE J. **65**, e16400 (2019).
305) M. Crose, W. Q. Zhang, A. Tran, and P. D. Christofides, "Multiscale three-dimensional CFD modeling for PECVD of amorphous silicon thin films," Comp. Chem. Eng. **113**, 184 (2018).
306) J. Kurokawa, H. Kondo, T. Tsutsumi, K. Ishikwa, M. Sekine, and M. Hori, "Effects of deposition precursors of hydrogenated amorphous carbon films on the plasma etching resistance based on mass spectrometer measurements and machine learning analysis," Vacuum **205**, 111351 (2022).
307) H. Kwon and S. J. Hong, "Use of optical emission spectroscopy data for fault detection of mass flow controller in plasma etch equipment," Electronics **11**, 253 (2022).
308) P. L. Stephan Thamban, J. Hosch, and M. J. Goeckner, "Controllable optical emission spectroscopy diagnostic system for analysis of process chemistries," Rev. Sci. Instrum. **81**, 013502 (2010).
309) S. J. Hong, W. Y. Lim, T. Cheong, and G. S. May, "Fault detection and classification in plasma etch equipment for semiconductor manufacturing e-diagnostics," IEEE Trans. Semicond. Manuf. **25**, 83 (2011).
310) B. Kim, S. Im, and G. Yoo, "Performance evaluation of CNN-based end-point detection using in-situ plasma etching data," Electronics **10**, 49 (2020).
311) D. H. Kim and S. J. Hong, "Use of plasma information in machine-learning-based fault detection and classification for advanced equipment control," IEEE Trans. Semicond. Manufact. **34**, 408 (2021).
312) S. H. Kim, C. Y. Kim, D. H. Seol, J. E. Choi, and S. J. Hong, "Machine learning-based process-level fault detection and part-level fault classification in semiconductor etch equipment," IEEE Trans. Automat. Sci. Technol. **35**, 174 (2022).
313) J. E. Choi, H. Park, Y. Lee, and S. J. Hong, "Virtual metrology for etch profile in silicon trench etching with SF_6/O_2/Ar plasma," IEEE Trans. Semicond. Manufact. **35**, 128 (2022).
314) A. A. Osipov et al., "OES diagnostics as a universal technique to control the Si etching structures profile in ICP," Sci. Rep. **12**, 5287 (2022).
315) C. Zhang, X. Gao, Y. Li, and L. Feng, "Fault detection strategy based on weighted distance of k nearest neighbors for semiconductor manufacturing processes," IEEE Trans. Semicond. Manufact. **32**, 75 (2019).
316) S.-K. S. Fan, C.-Y. Hsu, D.-M. Tsai, F. He, and C. C. Cheng, "Data-driven approach for fault detection and diagnostic in semiconductor manufacturing," IEEE Trans. Automat. Sci. Technol. **17**, 1925 (2020).
317) A. Zhakov, H. Zhu, A. Siegel, S. Rank, T. Schmidt, L. Fienhol, and S. Hummel, "Application of ANN for fault detection in overhead transport systems for semiconductor fab," IEEE Trans. Semicond. Manufact. **33**, 337 (2020).
318) A. Salimian, A. Aminishahsavarani, and H. Upadhyaya, "Artificial neural networks to predict sheet resistance of indium-doped zinc oxide thin films deposited via plasma deposition," Coatings **12**, 225 (2022).
319) S.-K. S. Fan, C.-Y. Hsu, D.-M. Tsai, M. C. Chou, C.-H. Jen, and J.-H. Tsou, "Key feature identification for monitoring wafer-to-wafer variation in semiconductor manufacturing," IEEE Trans. Automat. Sci. Technol. **19**, 1530 (2022).
320) O. Kwon, N. Lee, and K. Kim, "Improvement of virtual diagnostics performance for plasma density in semiconductor etch equipment using variational auto-encoder," IEEE Trans. Semicond. Manufact. **35**, 256 (2022).
321) S. Lee, H. Jang, Y. Kim, S. J. Kim, and H. Chae, "Sensitivity enhancement of SiO_2 plasma etching endpoint detection using modified Gaussian mixture model," IEEE Trans. Semicond. Manufact. **33**, 252 (2020).
322) H. Mazumdar, T. H. Kim, J. M. Lee, E. Kum, S. Lee, S. Jeong, and B. G. Chung, "Sequential and comprehensive algorithm for fault detection in semiconductor Sensors," Appl. Sci. **11**, 10419 (2021).
323) S. Yasuda, T. Tanaka, M. Kitabata, and Y. Jisaki, "Chamber and recipe-independent FDC indicator in high-mix semiconductor manufacturing," IEEE Trans. Semicond. Manufact. **34**, 301 (2021).
324) T. Tsuda, S. Inoue, A. Kayahara, S. Imai, T. Tanaka, N. Sato, and S. Yasuda, "Advanced semiconductor manufacturing using big data," IEEE Trans. Semicond. Manufact. **28**, 229 (2015).
325) J. Moyne, J. Samantaray, and M. Armacost, "Big data capabilities applied to semiconductor manufacturing advanced process control," IEEE Trans. Semicond. Manufact. **29**, 283 (2016).
326) N. G. Orji et al., "Metrology for the next generation of semiconductor devices," Nat. Electron. **1**, 532 (2018).
327) S. Hamaguchi, Jpn. Plasma Fusion Res. **95**, 560 (2019).
328) K. Rajan, "Materials informatics," Mater. Today **8**, 38 (2005).
329) T. Ueno, H. Hino, A. Hashimoto, Y. Takeichi, M. Sawada, and K. Ono, "Adaptive design of an X-ray magnetic circular dichroism spectroscopy experiment with Gaussian process modelling," npj Comput. Mater. **4**, 4 (2018).
330) Y. K. Wakabayashi, T. Otsuka, Y. Taniyasu, H. Yamamoto, and H. Sawada, "Improved adaptive sampling method utilizing Gaussian process regression for prediction of spectral peak structures," Appl. Phys. Express **11**, 112401 (2018).
331) Y. K. Wakabayashi, T. Otsuka, Y. Krockenberger, H. Sawada, Y. Taniyasu, and H. Yamamoto, "Machine-learning-assisted thin-film growth: Bayesian optimization in molecular beam epitaxy of $SrRuO_3$ thin films," APL Mater. **7**, 101114 (2019).
332) H. Yamamoto, Y. Krockenberger, and M. Naito, "Multi-source MBE with high-precision rate control system as a synthesis method *sui generis* for multi-cation metal oxides," J. Cryst. Growth **378**, 184 (2013).
333) Y. K. Wakabayashi, Y. Krockenberger, N. Tsujimoto, T. Boykin, S. Tsuneyuki, Y. Taniyasu, and H. Yamamoto, "Ferromagnetism above 1000 K in a highly cation-ordered double-perovskite insulator Sr_3OsO_6," Nat. Commun. **10**, 535 (2019).

© 2022 The Author(s). Published on behalf of The Japan Society of Applied Physics by IOP Publishing Ltd

334) G. Koster, L. Klein, W. Siemons, G. Rijnders, J. S. Dodge, C.-B. Eom, D. H. A. Blank, and M. R. Beasley, "Structure, physical properties, and applications of $SrRuO_3$ thin films," Rev. Mod. Phys. **84**, 253 (2012).
335) K. Takiguchi et al., "Quantum transport evidence of Weyl fermions in an epitaxial ferromagnetic oxide," Nat. Commun. **11**, 4969 (2020).
336) S. K. Takada, Y. K. Wakabayashi, Y. Krockenberger, S. Ohya, M. Tanaka, Y. Taniyasu, and H. Yamamoto, "Thickness-dependent quantum transport of Weyl fermions in ultra-high-quality $SrRuO_3$ films," Appl. Phys. Lett. **118**, 092408 (2021).
337) S. K. Takada et al., "Quantum limit transport and two-dimensional Weyl fermions in an epitaxial ferromagnetic oxide," (2021), arXiv:2106.03292.
338) Y. K. Wakabayashi, S. K. Takada, Y. Krockenberger, K. Takiguchi, S. Ohya, M. Tanaka, Y. Taniyasu, and H. Yamamoto, "Structural and transport properties of highly Ru-deficient $SrRu_{0.7}O_3$ thin films prepared by molecular beam epitaxy: comparison with stoichiometric $SrRuO_3$," AIP Adv. **11**, 035226 (2021).
339) Y. K. Wakabayashi et al., "Wide-range epitaxial strain control of electrical and magnetic properties in high-quality $SrRuO_3$ films," ACS Appl. Electron. **3**, 2712 (2021).
340) Y. K. Wakabayashi et al., "Single-domain perpendicular magnetization induced by the coherent O 2p-Ru 4d hybridized state in an ultra-high-quality $SrRuO_3$ film," Phys. Rev. Mater. **5**, 124403 (2021).
341) Y. K. Wakabayashi, Y. Krockenberger, T. Otsuka, H. Sawada, Y. Taniyasu, and H. Yamamoto, "Intrinsic physics in magnetic Weyl semimetal $SrRuO_3$ films addressed by machine-learning-assisted molecular beam epitaxy," Jpn. J. Appl. Phys. **62**, SA0801 (2023).
342) T. Onishi, T. Kadohira, and I. Watanabe, "Relation extraction with weakly supervised learning based on process-structure-property-performance reciprocity," Sci. Technol. Adv. Mater. **19**, 649 (2018).
343) M. Cohen, "Unknowables in the essence of materials science and engineering," Mater. Sci. Eng. **25**, 3 (1976).
344) M. E. Deagen, L. C. Brinson, R. A. Vaia, and L. S. Schadler, "The materials tetrahedron has a 'digital twin'," MRS Bull. **47**, 379 (2022).
345) R. S. Geiger, D. Cope, J. Ip, M. Lotosh, A. Shah, J. Weng, and R. Tang, "'Garbage in, garbage out' revisited: what do machine learning application papers report about human-labeled training data?," Quant. Sci. Stud. **2**, 795 (2021).
346) T. Toyao, Z. Maeno, S. Takakusagi, T. Kamachi, I. Takigawa, and K. Shimizu, "Machine learning for catalysis informatics: recent applications and prospects," ACS Catal. **10**, 2260 (2020).
347) E. Stolterman and A. C. Fors, "Information technology and the good life," *IFIP International Federation for Information Processing* (Springer, Berlin, 2004) Information Systems Research, Vol. 143, Chap. 45, p. 697.

© 2022 The Author(s). Published on behalf of The Japan Society of Applied Physics by IOP Publishing Ltd